



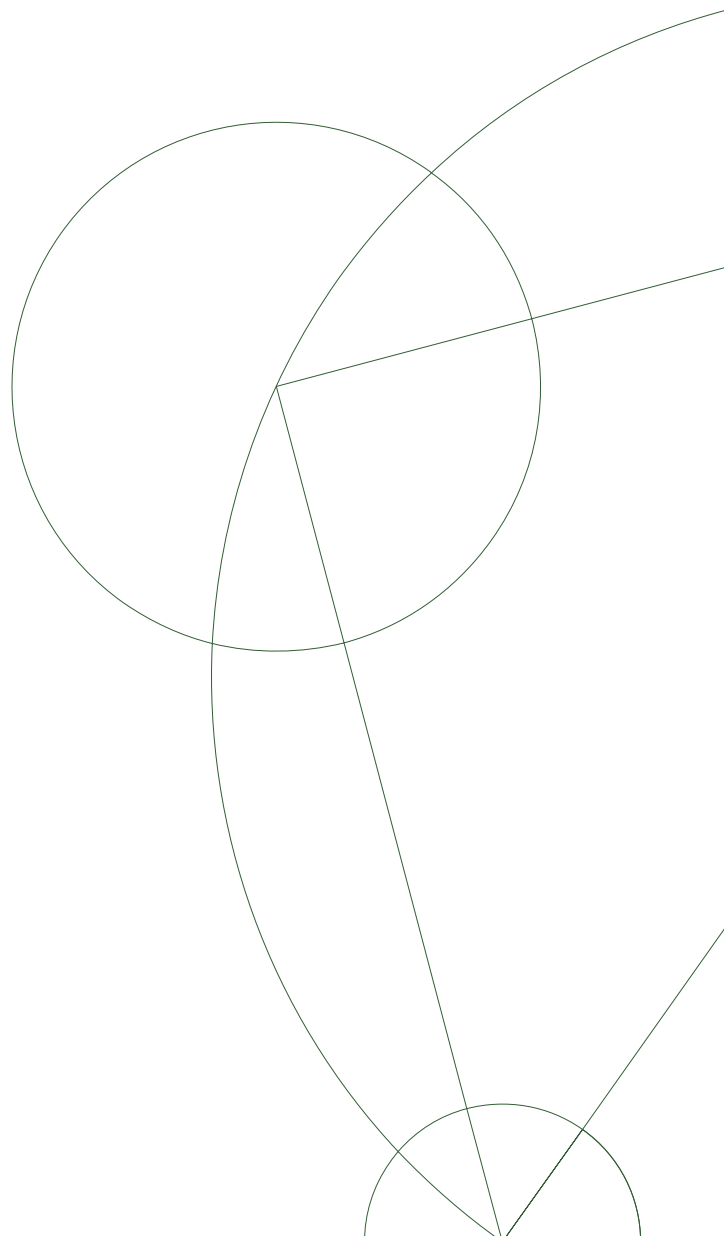
Cand. Scient. Thesis

The Effect of Arachidonic Acid on Endothelial Cell Motility

By:
Ninna Struck Rossen

Niels Bohr Institute
January 21, 2010

Supervisors:
Lene Oddershede and
Christine Selhuber-Unkel



Summary

Endothelial cell spreading and migration play an important role in angiogenesis, the formation of new blood vessels. Angiogenesis plays a part in many pathologies, e.g., as a prerequisite for malignant tumor growth. Amphiphilic compounds influence cell migration, possibly through their incorporation into the cellular membrane, and propose a novel non-receptor specific regulation of angiogenesis. This thesis investigates the effect of the amphiphilic compound arachidonic acid and shows that it has an effect on endothelial cell spreading and migration. This thesis's investigation of arachidonic acid's effect on the spreading of adhering endothelial cells shows that arachidonic acid enhances spreading of adhering cells at low concentrations (20 μM) and inhibits spreading of adhering cells at high concentrations (60-80 μM). Previous literature on cell adhesion has shown adhesion contact area versus time traces display either two or three distinct phases of spreading, each phase being governed by a separate scaling law. The adhesion assay data presented here can be treated to fit both the two and the three phase models. In this thesis, a general analysis method, which introduces a lag-time variable, is proposed. It reconciles the three phase model with the two phase model, such that it agrees with the two state model. This thesis also investigates the migration of endothelial cells using a razor wound assay. The migration traces of individual cells were followed continuously for 24 hours. When arachidonic acid is present in the cells' media, the leading cells lose their sense of direction, and their traces become less directed and more random than in the control assay.

Resume

Endotelcellers spredning og migration spiller en vigtig rolle i angiogenese, som er dannelsen af nye blodkar. Angiogenese spiller en rolle i mange patologier, f.eks. er det en forudsætning for væksten af maligne tumorer. Amphifile stoffer influerer celle migration, muligvis gennem deres inkorporering i cellens membran, og udgør en ny ikke-receptor specifik regulering af angiogenese. Dette speciale undersøger effekten af det amphifile stof arakidonsyre, og viser at tilstedeværelsen af arakidonsyre påvirker endotelcellernes spredning og migration. Specialets undersøgelser af arakidonsyres effekt på adhererende cellers spredning viser at arakidonsyre fremskynder spredningen af adhererende celler ved lave koncentrationer (20 μM) og bremser spredningen af adhererende celler ved høje koncentrationer (60-80 μM). Tidligere litteratur omhandlende cellespredning viser at cellens adhesionskontaktareal som funktion af tid udviser enten to eller tre faser, hvor hver fase styres af hver deres skaleringslov. De eksperimentelle data for adhesionsassays kan behandles så det passer med både to og tre fase modellen. I dette speciale fremføres en generel analysemetoder, hvori der introduceres en tidsforskydnings variable, som kan få tre fase modellen til at stemme overens med to fase modellen. Endotelcellers migration undersøges også i specialet ved hjælp af razor wound assays. De enkelte cellers migration blev fulgt nøje over 24 timer. Når arakidonsyre er tilstede i cellernes medie, så mister de førende celler deres retningsans og deres spor bliver mindre retningsorienteret, og mere tilfældige end i de tilsvarende kontrolforsøg der ikke havde arakidonsyre i cellernes medie.

Contents

1	Introduction	1
1.1	Thesis Outline	3
2	Angiogenesis	5
2.1	Angiogenesis's Role in Cancer	7
2.2	A Short History of Angiogenesis Research	8
3	Eukaryotic Cell Migration	13
3.1	The Cytoskeleton	14
3.2	The Steps in Cell Migration	17
3.2.1	Receiving the signal	18
3.2.2	Extending pseudopodial protrusions from the leading edge	18
3.2.3	Attachment of the pseudopodial extensions	19
3.2.4	Translocation of the cell	21
3.2.5	Dissociating the trailing edge	21
3.3	Motility phenotypes	22
3.4	The Membrane	23
4	Inspiration	29
4.1	Arachidonic Acid	33
5	Viability Assays with Arachidonic Acid	35
5.1	Previous Viability Assays with Arachidonic Acid	36
5.2	Viability Assays: Materials and methods	36
5.3	Viability Assay Data	37
5.4	Results	37

6	Endothelial Cell Adhesion	41
6.1	Models for Endothelial Cell Adhesion	43
6.1.1	The three phase model	43
6.1.2	The two phase model	46
6.1.3	A mathematical model without phases	56
6.1.4	The reconciled model	57
6.2	Adhesion Assays: Materials and methods	61
6.3	Adhesion Assay Data for Regular Endothelial Cell Adhesion	66
6.4	Toxicity Assay of the 514 nm Laser Illumination	67
6.5	The Three-Dimensional Shape of Regularly Spreading Endothelial Cells . . .	69
6.6	Standard for Regularly Adhering Endothelial Cells	71
6.7	Arachidonic Acid's Effect on Endothelial Cell Adhesion	77
6.8	Conclusion to Endothelial Cell Adhesion	82
7	Endothelial Cell Migration	83
7.1	Previous Studies of Endothelial Cell Migration	84
7.2	Migration Assays: Materials and methods	90
7.3	Migration Assay Data	91
7.4	Collective Migration Behavior	94
7.5	Single Cell Tracking	98
7.6	Conclusion to Endothelial Cell Migration	108
8	Conclusion	111

Chapter 1

Introduction

This thesis investigates the effect of arachidonic acid on endothelial cell motility.

Angiogenesis is the creation of new blood vessels. Blood vessels are constituted of endothelial cells, and new vessels are formed when endothelial cells in existing blood vessels migrate into the surrounding tissue. After embryonic development, few new blood vessels are created, and the main creation of new blood vessels in adults occurs as a response to inflammation and during wound healing. Angiogenesis is also a prerequisite for malign cancerous tumor growth, as the tumor growth is halted until new blood vessels have been formed to provide the tumor with its own blood supply. A disruption in the mechanisms that regulate angiogenesis plays a part in many pathologies. Since angiogenesis is mediated by endothelial cell migration, angiogenesis regulation is essentially the regulation of endothelial cell migration. Due to its significant role in a variety of pathologies, there is a large incentive to investigate, understand and regulate endothelial cell migration.

Some receptor-specific drugs have secondary pharmacologies. That means that at very small concentrations they bind to and regulate a specific receptor, but at larger concentrations, the drug may regulate a variety of membrane proteins in a non-specific manner. These drugs are mostly amphiphilic and have a hydrophobic and a hydrophilic end. When amphiphilic compounds are present in an aqueous solution, they will spontaneously incorporate themselves into a membrane to shield their hydrophobic ends from the aqueous solution. This incorporation alters the composition of the membrane and thereby also its physical properties, such as stiffness or viscosity. The diverse regulation of membrane proteins found in the secondary pharmacology of amphiphilic drugs could be caused by the incorporation of these drugs into the cell's membrane. This suggests that the lipid bilayer in the membrane may be a regulatory mechanism for the membrane proteins.

Many amphiphilic compounds have been shown to change endothelial cell migration in a way that highly correlates with the induced changes in the physical properties of the cells' membranes. Such correlation between the change in physical properties of the membrane and the observed change in migration suggests that amphiphilic compounds affect the cells by their incorporation into the membrane and not by binding to specific receptors. Endothelial cell migration may be regulated through non-receptor-specific treatments by amphiphilic compounds. Receptor-specific drugs that enhance or inhibit angiogenesis exist, but the possibility of regulating angiogenesis through non-receptor-specific means is novel.

Most of the investigated amphiphilic compounds are only able to inhibit the migration of endothelial cells. Arachidonic acid is an amphiphilic compound that can both enhance and inhibit endothelial cell migration depending on its concentration in the cells' surroundings. Arachidonic acid has been shown to enhance cell migration at low concentrations and inhibit cell migration at high concentrations. The dual regulating properties of arachidonic acid make it an interesting subject for further study. The main focus of this thesis is the effect that arachidonic acid has on endothelial cell migration, which will be investigated in adhesion and migration assays with different concentrations of arachidonic acid.

Endothelial cell migration is a complex process which involves both the actions of the individual cell and its interactions with neighboring cells and the environment. Collective cell migration can often be simplified by examining the migration of a single cell. Unfortunately, single cell studies are not relevant to endothelial cells, since endothelial cells are never found as single cells in healthy physiology. Endothelial cells constitute the blood vessels which form a continuous barrier of cells between the blood lumen and the tissue that must remain unbreached to function. These cells need to maintain complete cell-cell contact at all times, even during migration, when creating a new blood vessel.

This thesis simplifies the complex process of migration by examining individual cell adhesion. Endothelial cell adhesion occurs naturally post-mitosis. Mitosis is the only time when the complete cell-cell contact is breached in healthy pathology. The endothelial tissue is never actually breached since the cells surrounding the dividing cell maintain cell-cell contact. An individual endothelial cell's independence during mitosis can be mimicked *in vitro* in adhesion assays. Adhesion assays observe a cell in suspension as it makes contact with, adheres to and spreads out on a substrate. A cell is able to spread by remodeling its cytoskeletal structure to accommodate a new spread out shape. An adhesion assay is not only able to isolate the behavior of a single cell but also the remodeling of the cytoskeleton of that single cell as it spreads out onto a substrate.

Adhesion and migration are two types of endothelial cell motility, both of which are investigated in this thesis. The aim of this thesis is two-fold:

- To investigate the effect of arachidonic acid on endothelial adhesion. In particular to investigate the effect of arachidonic acid on the rate of cytoskeletal remodeling as evinced by the rate at which the cell is able to spread out on a substrate.
- To investigate the effect of arachidonic acid on endothelial cell migration, both the collective dynamics of the cells and the motility at the individual cell level within the collective of cells.

The rate of cytoskeletal remodeling has an impact on the rate of cell adhesion and migration. The incorporation of arachidonic acid into the cells' membranes can regulate a variety of membrane proteins in a non-specific manner. This regulation may affect endothelial cell adhesion and migration in an unambiguous manner that will shed light on both the regulatory mechanisms of the cell membrane and how it relates to cytoskeletal remodeling. A better understanding of how cytoskeletal remodeling is regulated will aid the development of new angiogenesis-regulating treatments.

1.1 Thesis Outline

This thesis describes nine months of experimental work for the degree of Cand.Scient. in Biophysics performed in the Optical Tweezer group at the Niels Bohr Institute, Faculty of Science, University of Copenhagen. The outline of the thesis is as follows:

Chapter 2, “Angiogenesis”, will introduce the mechanisms behind the creation of new blood vessels. The creation of new blood vessels, or lack thereof, are implicated in many pathologies, one of which is cancer. The treatment of cancer can be aided through the inhibition of angiogenesis, and angiogenesis inhibiting drugs are used as a supplement to traditional chemotherapy in the treatment of colon cancer. The treatment of cancer provides a current example of applied angiogenesis regulation, so the first chapter is primarily focused on angiogenesis’s role in cancer treatment, though the regulation of angiogenesis may provide or aid the treatment of several other pathologies. Developments in angiogenesis research have historically been closely linked with cancer research, and the last section in Chapter 2 will provide a short overview of the history of angiogenesis research.

The migration of cells is a complex process, so an entire chapter has been devoted to describing it. The migration of cells is mediated through the remodeling of the cytoskeleton. The first section in Chapter 3, “Eukaryotic Cell Migration”, describes the cytoskeleton’s role in migration. The next section then proceeds to describe the five-step cycle of cell migration in more detail. The cell displays many different motility phenotypes when migrating, and these have been listed in a separate section to provide an easy overview. Arachidonic acid’s effect on cells is hypothesized to stem from its incorporation into the cell membrane. Such an incorporation has been witnessed many times before for other drugs and has been related to a non-specific regulation of several proteins called secondary pharmacology. The last section of Chapter 3 will describe the cells membrane and provide a possible explanation for the secondary pharmacology.

Chapter 4, “Inspiration”, describes two previous studies of amphiphilic compound’s effect on endothelial cell migration, which is essentially angiogenesis. These two studies have been the main inspiration for the investigation and experiments in this thesis. They describe the regulating effect of amphiphilic compounds on endothelial cell migration. The regulatory effect of amphiphilic compounds is hypothesized to rely on the amount of incorporated amphiphilic molecules in the cells’ membranes, which is dependent on the initial concentration of amphiphilic molecules around the cells. Such dependencies were observed and described in these two studies. One study described a particularly interesting dependency on the amphiphilic compound arachidonic acid, which can both enhance and inhibit endothelial cell migration. When arachidonic acid was present in low concentrations, it enhanced endothelial cell migration, and in high concentrations, it inhibited endothelial cell migration. This thesis further investigates the dual regulatory property of arachidonic acid, so a section of Chapter 4 briefly describes arachidonic acid.

Before the findings of this thesis are presented, a small study which tests the toxicity of arachidonic acid is reported in Chapter 5, “Viability Assay”. The viability assay ensures that arachidonic acid does not harm the cells or alter their proliferation rate at the concentrations used in the experiments. The proliferation rate is a good measure of how stressed the cells are, since stressed cells are forced to deal with the stressing factor in the environment before

they can proceed with their cell cycle. The viability assay concludes that concentrations of arachidonic acid up to 82.11 μM are not harmful to the cells, so any effects observed in the experiments are due to arachidonic acid's harmless presence and not the pathologies of stressed or dying cells.

The first aim of this thesis is treated in Chapter 6, "Endothelial Cell Adhesion", which investigates the effect of arachidonic acid on endothelial cell adhesion through *in vitro* experiments. The adhesion of cells are accommodated through the remodeling of the cytoskeleton. Adhesion assays are simplified versions of migration assays, which focus on the regulation of cytoskeletal remodelling. Many such assays have been performed previously, though, to my knowledge, none have specifically investigated the effect of an amphiphilic compounds incorporation into the membrane. Some of the previous studies have proposed models for the adhesion process, and these are described and discussed in a section in Chapter 6. The model description is substantial because I do not agree with some of the assumptions in the models. I have proposed an alternative model which I find more biologically and physically relevant. There are some discrepancies in the previously proposed models, and to facilitate the analysis of the adhesion assays, a reconciliation of the previous models is necessary. Since, to my knowledge, these models have not been reconciled previously in the literature I have devoted a section to reconciling the models based on an investigation of the different approaches. The reconciled models culminate in an analysis method which is subsequently used throughout the chapter. The alternative model and the reconciled model are both fitted to the experimental data presented here, and I conclude that the reconciled model better describes the data. Using the reconciled model to describe data, it is possible to compare the different adhesion assays. Through the comparison of adhesion assays, this chapter concludes that arachidonic acid regulates the rate of endothelial cell adhesion, i.e., the rate of the cytoskeletal remodeling, similarly to the way arachidonic acid has regulated cell migration in previous studies: arachidonic acid enhances endothelial cell adhesion at low concentrations, whereas it inhibits cell adhesion at high concentrations.

The second aim of this thesis is treated in Chapter 7, "Endothelial Cell Migration", in which the effect of arachidonic acid on endothelial cell migration is investigated through *in vitro* experiments. The collective behavior of migrating endothelial cells is analyzed and compared to the previous results of Jensen and his collaborators presented in Chapter 4. The individual behavior of the cells within the monolayer are also analyzed through the tracking and analysis of their motion. Such motion analysis have, to my knowledge, not been performed on individual cell within a monolayer before, and the the presence of arachidonic acid is shown to make the motion of the cells at the edge less directed; the higher the concentration of arachidonic acid is, the more diffusive the motion of the cells.

Finally a general conclusion of the adhesion and migration assays is provided in Chapter 8, "Conclusion".

Chapter 2

Angiogenesis

Blood vessels can be formed in three different ways through:

- Vasculogenesis, which is the formation of vascular structures from endothelial stem cells (angioblasts). This form is mostly seen during embryonal development of the vascular system.
- Intussusception, in which the capillary wall extends into the lumen of the blood vessel, thereby splitting a single vessel into two.
- *Angiogenesis*, the process in which new vessels sprout from existing vessels.

Vasculogenesis is only relevant in embryonic development. Once the fetus has developed, new blood vessels will mostly be formed through angiogenesis, which is the sprouting of new blood vessels from existing ones.

Blood vessels are primarily constituted of *endothelial cells*. Apart from endothelial cells, larger blood vessels also contain smooth muscle cells. The contraction of the smooth muscle cells regulates the blood flow in the larger vessels, enabling the regulation of blood pressure. Fully developed blood vessels also contain a basement membrane, which is a specialized, sheet-like structure of the extracellular matrix. The basement membrane's primary functions are to anchor the endothelial cells to connective tissues and to act as a barrier between the vessel and the tissue, e.g., to prevent malignant cells from invading the deeper tissue.

Angiogenic sprouting is an ordered series of events. It occurs in response to the emission of angiogenic growth factors by cells that are trying to recruit new blood vessels. The angiogenic growth factors bind to specific receptors on the endothelial cells of the nearby blood vessels, thereby signaling the cells to start proliferating and activating their production of *proteolytic molecules*. The proteolytic molecules dissolve the basement membrane, providing a breach through which the endothelial cells can migrate into the deeper tissue. The migrating cells also produce additional enzymes (matrix metalloproteinases) to dissolve the tissue in front of the budding vessel, creating a pathway. A new blood vessel is created as the endothelial cells migrate out into the tissue. Sprouting endothelial cells form a blood vessel tube and individual blood vessels connect to form loops that can circulate blood [1]. The angiogenic sprouting process is illustrated in Figure 2.1. The creation of new blood vessels is mediated

by the migration of endothelial cells from existing blood vessels, and the study of angiogenesis is therefore essentially the study of endothelial cell migration. Chapter 3 will describe the process of eukaryotic cell migration in detail.

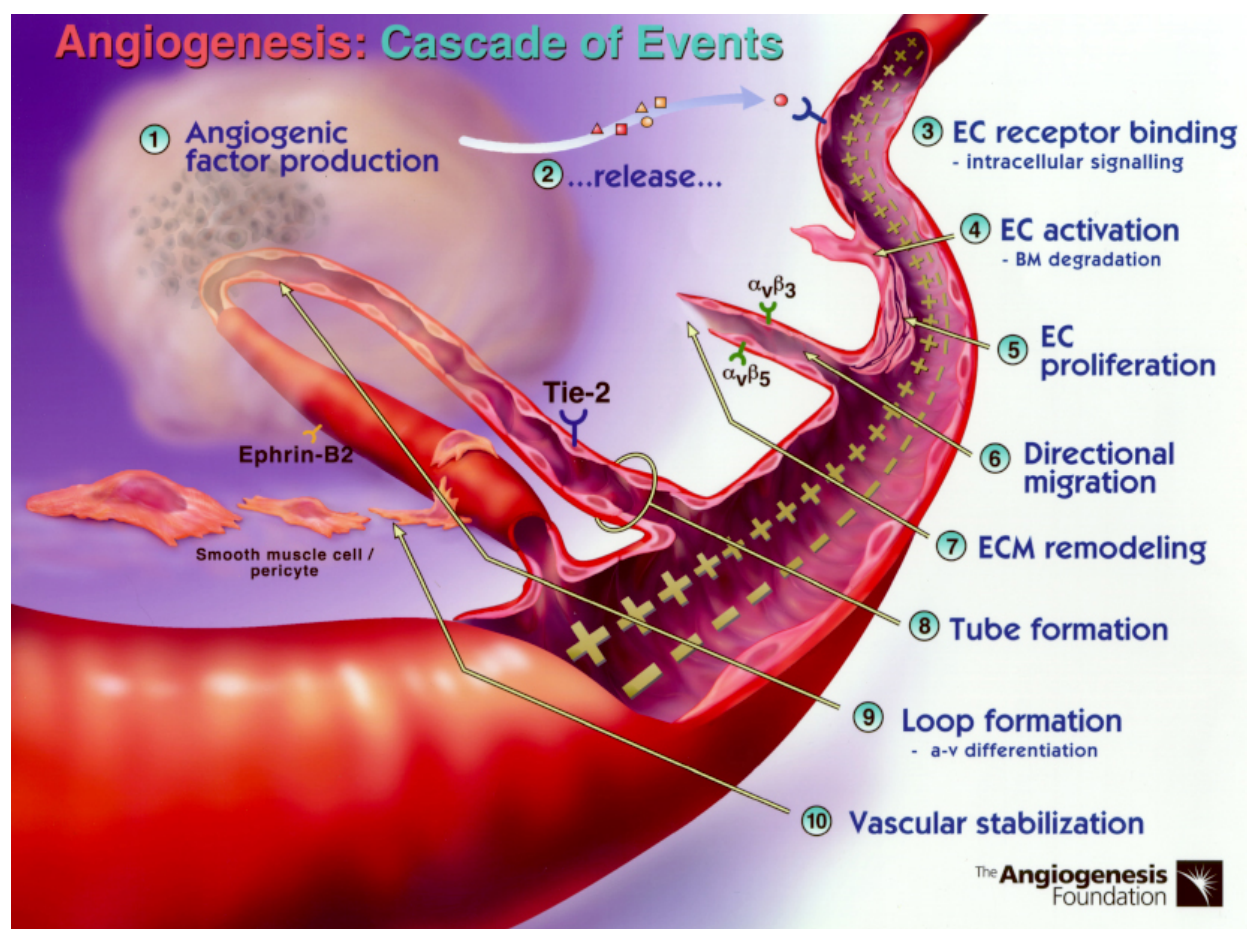


Figure 2.1: A schematic of angiogenesis (kindly provided by The Angiogenesis Foundation).

In healthy adults, the process of angiogenesis is carefully balanced by angiogenic stimulating and inhibiting factors. If the balance between these factors is affected, a pathology may develop. The creation of blood vessels can in such cases be either benign or malign. Pathologies such as impaired wound healing or limb ischemia can be treated through the stimulation of angiogenesis [2, 3]. Pathologies such as rheumatoid arthritis, age-related macular degeneration, pathologic diabetic blindness, malignant neoplasia or cancer, are due to (or worsened by) the creation of new blood vessels. An inhibition of angiogenesis would treat (or relieve) the pathology in such cases [4].

Due to its role in a variety of pathologies, it is important to investigate, understand and possibly regulate angiogenesis. Its role in cancer has merited particular interest the last 50 years. The following section will provide a brief description of angiogenesis role in cancer. Then Section 2.2 will provide a more elaborate summary of the historical research that led to the general description in the following section.

2.1 Angiogenesis's Role in Cancer

The development of a cancerous tumors begins with a small population of cells that does not respond to the normal regulation of cell division and death. The cancerous cells divide uncontrollably, growing in size and will eventually create a tumor. The size to which the tumor can grow is only limited by the amount of nutrients and oxygen that the tumor receives from the nearest blood vessels through the surrounding tissue [5]. The limited size to which the tumor can grow when it is dependent on diffusion from the nearest blood vessels through the surrounding tissue for nutrients and oxygen, is around 1-2 mm³ depending on the type of cancer [6]. If the tumor does not have a direct blood supply, it becomes *dormant* when it reaches its limiting size. Dormant tumors are not able to grow in size, but they are still viable [7]. It is widely accepted that tumors can obtain a direct blood supply through the sprouting angiogenesis from nearby blood vessels. Normal cells can survive up to 100 μm away from vessels [8], and the vascularization of normal tissue reflects this dependency, so the nearest blood vessels from a tumor are never that far away.

The cancerous cells on the periphery of a dormant tumor still receive oxygen and nutrients via passive diffusion through the surrounding tissue, but the cells in the middle of the tumor will lack oxygen and undergo *necrosis*. Necrosis is different form the natural, programmed cell death, *apoptosis*. When cells go through apoptosis, they are degraded in an orderly and controlled manner. When they go through necrosis, the cells swell and burst, thereby spreading their intracellular content among the surrounding cells and causing inflammation. The necrotic parts of the tumor induce a strong inflammatory response in the adjacent tissue. One response to inflammation is an increase in vascular endothelial growth factor (VEGF), and this is highly expressed in the tissue adjacent to necrotic cells [9]. VEGF is considered to be “the master switch of the angiogenic cascade”, since VEGF expression is one of the first steps in the angiogenic process. The adjacent tissue of a necrotic tumor core is effectively recruiting new blood vessels to the area through their expression of VEGF. Due to VEGF's strong angiogenic effect and specificity for endothelium, VEGF is considered to be the most important signaling molecule in tumor angiogenesis [10].

The cancerous tumor becomes dormant when it is no longer able to support its entire cell mass on the diffusion of nutrients and oxygen through the surrounding tissue, i.e., when the inner cells become necrotic. The tumor's growth is restricted as long as it remains dormant, and it can only resume growth when it has obtained a direct blood supply [11]. The necrosis of cells causes inflammation. The tissue surrounding the necrotic cells will respond to inflammation by emitting VEGF to recruit new blood vessels to the area. The natural response of the surrounding tissue thus aids the cancerous tumor in gaining a direct blood supply.

Since tumors are dependent on a direct blood supply in order to grow above a certain size, prevention of angiogenesis should stop further growth of the tumor or its metastases. Pre-clinical studies have shown that inhibition of angiogenesis decreases mean vascular diameter and arrests tumor growth [12], and is already used in combination with regular chemotherapy. Inhibition of angiogenesis can keep the tumor from growing and metastazing while the chemotherapy attacks the cancer itself.

In adults, it is mainly the tumor's recruitment of endothelial cells and wound healing that

are responsible for angiogenesis. Anti-angiogenesis treatment has the potential to be more specifically directed towards cancerous tumors than chemotherapy and radiation. Endothelial cells are also in direct contact with the bloodstream, so drug-delivery would be persistent. Concerns have been raised that reducing the blood supply to the tumor would also compromise drug delivery. Fortunately, this was not the case, and anti-angiogenic therapies can actually increase sensitivity to both chemotherapy and radiation [13, 14]. The details of this synergistic effect remain to be elucidated.

2.2 A Short History of Angiogenesis Research

The term “angiogenesis” was coined in 1794 when British surgeon John Hunter used it to describe the growth of blood vessel in reindeer antlers [15]. Some 70 years later, angiogenesis was put into the context of cancerous tumor growth by German doctor Rudolph Virchow. He drew attention to the huge number of blood vessels that was to be found in a tumor mass. He also recognized that the connective tissue of tumors had a distinct capillary network [16].

Another 40 years passed before the studies of blood vessels in tumors were conducted more systematically. This work was undertaken by Goldman in 1907 [17] when he started injecting bismuth in oil into the arteries of rats. He found that “the normal blood vessels of the organs in which the tumor is developing are disturbed by chaotic growth. There is a dilation and spiraling of the affected vessels, marked capillary budding and new vessel formation, particularly at the advancing border”. The chaotic growth of blood vessels in the organs in which the tumor is developing was confirmed by Lewis in 1927 [18] when he was studying the vasculature, i.e., the blood vessels, of several tumors that occur spontaneously in rats. He found the vascular architecture of each tumor to be different and concluded that the tumor’s environment has a significant influence of the growth and morphological characteristics of the developing blood vessels [18].

Up until 1928 research on tumors was conducted *in vitro* or by autopsy, but in March 1928 Sandison [19] introduced an approach that accelerated angiogenesis research. Sandison successfully inserted a transparent chamber into a rabbit’s ear, which allowed for microscopic observations of the living tissue underneath a glass coverslip. During the 1930s, this approach was perfected by Clark and his collaborators [20, 21, 22], so morphological characteristics of blood and lymphatic vessels could be studied *in vivo* through the use of contrast media. With this new transparent chamber technology, Ide and his collaborators [23] investigated the growth of cancerous tumors that had been transplanted into the ears of healthy rabbits and their correlation with vascular supply. Not only did their experiments confirm that tumor growth is accompanied by rapid and extensive formation of new blood vessels, they also found that if blood vessel growth did not occur, the transplanted tumor failed to grow [23]. Ide and his collaborators were the first to suggest that tumors release specific factors that are capable of stimulating the growth of blood vessels [16].

The idea that tumors were releasing specific factors capable of stimulating blood vessels growth, i.e., angiogenesis, resonated within the scientific community, and several groups of researchers joined the hunt for these factors. In 1941, Green [24] demonstrated that rabbit carcinomas transplanted into guinea pigs did not recruit new blood vessels and failed to

grow, suggesting that certain factors could be species specific. These same tumors would vascularize and expand when they were re-implanted into their original hosts - rabbits.

A quantitative approach to assess blood vessel growth was introduced in 1945, when Algire and Chalkley performed daily counts of blood vessels and compared them to the tumor size [25]. They found that the rate of blood vessel formation induced by implanted tumors was more substantial than that induced by a simple wound or the implantation of non-tumor tissue. This confirmed that the implanted cancerous tissue was somehow responsible for the release of specific angiogenesis stimulating factors. They also concluded that the growth of the tumor is closely connected with the development of an intrinsic vascular network. This conclusion defined a possible method to stop the autonomous growth of cancerous cells.

It had been noted that the intensity of the angiogenic response seemed to be influenced by the distance between the implant and the host's vessel [26], so scientists speculated that the angiogenesis stimulating factor was diffusible. This was experimentally verified in 1968 when Greenblatt and Shubik [27] made use of *Millipore chambers* when implanting tumor fragments into a hamster's cheek pouch. A Millipore chamber is a small chamber consisting of porous walls with a pore size of $0.45\ \mu\text{m}$. The size of the pores makes the Millipore chamber permeable to fluids and signaling molecules but impermeable to cells. A dramatic creation of new blood vessels was induced both when the tumor fragment was in direct apposition to the hamsters cheek pouch membrane and when the tumor fragment was separated from the membrane by a Millipore chamber wall. The signaling molecules were thus not hindered by the walls of the millipore chamber, indicating that they must be diffusible and smaller than $0.45\ \mu\text{m}$. Control materials in the Millipore chambers did not induce neovascularization, so Greenblatt and Shubik concluded that, as previously suspected, a diffusible factor was responsible for the development of new blood vessels. Similar results were found in chick embryos by Ehrman and Knoth later the same year [16].

The idea that tumor growth would be halted if the tumor was deprived of blood supply was first proposed by Folkman in 1971. The idea is now widely accepted due to the convincing research performed by Folkman and his collaborators. Folkman discovered that when cancerous mouse cells were injected into canine thyroid glands tiny tumors developed. However, due to the difference in species, the small tumors never vascularized and stopped growing when they reached a size of 1-2 mm in diameter. The tiny tumors were only in a "dormant" state and still viable, so when the 1 mm tumors were transplanted into syngeneic mice, they rapidly vascularized and grew to more than 1000 times their original volume [7]. This supported the species specific factors' hypothesis, but, more importantly, it was the first evidence to show that the absence of neovascularization correlated with severe restriction of tumor growth. In 1971 Folkman published the hypothesis that tumor growth is angiogenesis-dependent and that inhibition of angiogenesis could be therapeutic [5].

Since 1971 many experimental studies and clinical observations have supported Folkman's hypothesis, and it is now generally accepted that tumor growth is angiogenesis-dependent and that without the continuous recruitment of new capillary blood vessels the tumor cannot grow beyond the microscopic size of $1\text{-}2\ \text{mm}^3$, as seen in Figure 2.2.

Tumors can lie dormant in the absence of vascularization. Folkman's student, Gimbrone, continued the study of dormant tumor cells in close collaboration with Folkman. They made use of the aqueous humor of the anterior chamber in a rabbit's eye to investigate how close

a dormant tumor had to be to a blood supply before it began growing actively again. The aqueous humor is too far removed from the iris to support any vascularization of the tumors (these tumors did induce neovascularization of the iris vessels, but they were too remote from the iris for the tumors to invade [28]). As a result, the tumors remained of a limited size of less than 1 mm^3 . Gimbrone and his collaborators were able to observe the tumors for up to 6 weeks, when the tumors remained viable. When they were re-implanted contiguous to the iris, the tumors vascularized and grew rapidly, reaching 16,000 times their original size within two weeks, see Figure 2.2. They observed that tumor growth proceeds slowly at a linear rate, but after vascularization, tumor growth is exponential [28]. This can also be seen in Figure 2.2. Tumors grow through the proliferation of cancerous cells. The proliferation rate of tumor cells decreases with increased distance from the blood vessels. This provides direct evidence that diffusion of oxygen and nutrients from the blood vessels nearby is a rate-limiting step in tumor cell growth.

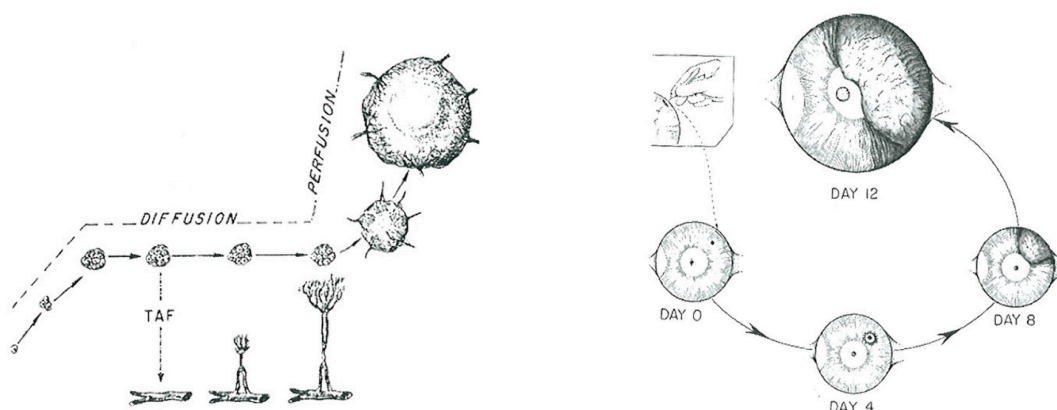


Figure 2.2: Left: Schematic drawing showing that most solid tumors may exist early as tiny cell populations living by simple diffusion in the extracellular space. Further growth requires neovascularization, and a tumor angiogenesis factor (TAF) may be the mediator of neovascularization (from Folkman *et al.* 1971 [5]). Right: The patterns of development of two simultaneous implants of Brown-Pearce tumor in the rabbit's eye, one in the anterior chamber and one in the iris. The anterior chamber implant remains avascular, while the iris implant vascularizes and grows progressively (from Gimbrone *et al.* 1972 [28]).

Gimbrone formed the hypothesis that prior to vascularization the cancerous cells get their oxygen and nutrients through extracellular diffusion. Histological analysis shows that dormant tumors develop a necrotic core surrounded by a layer of viable cells [29]. Again, they made use of the aqueous humor of the anterior chamber in a rabbit's eye. They suspended tumors at various distances from the iris vessels and observed that moving the distant, dormant tumors closer to the iris's vessels jump started the growth of these vessels. In Gimbrone's rabbit-eye experiments, dormancy was brought about by a lack of blood supply and not by cell cycle arrest or immune control [16].

Preventing the cancerous tumors from getting their own blood supply rendered them dormant. The tumors recruit the new blood vessels to its location, i.e., angiogenesis, through the emission of diffusible angiogenesis stimulating factors. In 1989 the first angiogenesis

stimulating factor known as vascular endothelial growth factor (VEGF), was identified and isolated by Ferrara [30]. The discovery of other factors, such as basic fibroblast growth factor (bFGF), soon followed.

The first successful animal trials for anti-angiogenic treatments were conducted four years later when Ferrara and his colleagues demonstrated that by preventing the angiogenesis stimulating factor VEGF from transmitting its angiogenesis stimulating signal, angiogenesis could be inhibited and tumor growth suppressed *in vivo* [31]. The first clinical trial was published in 1996 by Isner. He and his research team successfully used VEGF to treat 156 patients with critical limb ischemia [32], a disease in which the limb has a pathological deprivation of blood supply.

These successful trials led to the clinical development of bevacizumab, better known as Avastin. Avastin is a humanized anti-VEGF monoclonal antibody that binds to VEGF, thereby making the angiogenesis stimulating factor unable to bind to its specific receptor. In 2001 at least 20 angiogenesis inhibiting drugs were in clinical trials, including angiostatin and endostatin - the first two angiogenesis inhibiting factors. In 2003 the number of angiogenesis inhibiting drugs in clinical trials had risen to 65, and the year after, the American Food and Drug Agency (FDA) approved Avastin as the first in a class of cancer drugs called angiogenesis inhibitors. Today, Avastin is routinely used in the treatment of colon/colorectal cancer [33]. The halting of angiogenesis is not a cure in and of itself; it is used in combination with regular chemotherapy. Avastin keeps the tumor from growing and metastasizing, while traditional chemotherapy attacks the cancer itself [33].

Today, there are three recognized approaches to halting angiogenesis: ¹)by altering the angiogenesis stimulating factor's shape through the binding of antibodies, so it is unable to bind to its specific receptor, thereby preventing the factors from transmitting their signal, ²)by blocking the receptors for angiogenesis stimulating factor with the binding of another body, thereby preventing the factors from transmitting their signal, and ³)by releasing angiogenesis inhibiting factors, which upon binding to their specific receptors on the cells' membrane signal a halt in angiogenesis. All three approaches are receptor-specific, and all anti-angiogenic drugs approved for cancer treatment have been receptor specific.

The latest development within angiogenesis research is the realization that angiogenesis can be regulated through non-receptor-specific treatments. In 2002 Ghosh and his collaborators showed that chemical compounds that change the microviscosity of the cells' membranes also change the angiogenic process. Depending on the concentration of these chemical compounds, angiogenesis can be enhanced or inhibited *in vitro* [34]. Jensen and his collaborators elaborated on these results in 2007 when they tested a multitude of chemical compounds that all induced changes in the cells' membranes stiffness. All of these compounds regulated angiogenesis in a way that was highly correlated with the change they had induced in the microviscosity of the cells' membranes [35]. The different structures of the compounds made it impossible for them to be regulating angiogenesis through receptor-specific binding [35]. The chemical compounds were all amphiphilic, i.e., they had both hydrophobic and hydrophilic ends, just like the lipids that constitute the cells' membranes. The amphiphilic compounds' regulatory effect on angiogenesis is hypothesized to stem from their incorporation into the membrane, which changes the microviscosity of the membrane.

Chapter 3

Eukaryotic Cell Migration

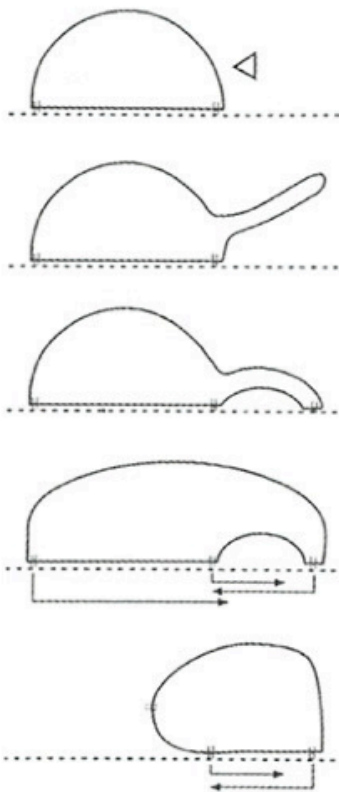
Cells migrating across a surface represent a basic form of cell locomotion. Examples include the crawling of amoebas, the migration of embryonic cells during development, the invasion of tissues by white blood cells to fight infection, the migration of cells involved in wound healing, the spread of cancer cells during the metastasis of malignant tumors, and the creation of new blood vessels (angiogenesis) [36].

Eukaryotic cell migration results from the coordinated remodeling of the cell's cytoskeleton and adhesion structures. The cytoskeleton is a network of protein filaments extending throughout the cytoplasm. The cytoskeleton provides a structural framework for the cell, serving as a scaffold that determines the shape of the cell and the general organization of the cytoplasm. In addition to playing this structural role, the cytoskeleton is also responsible for cell movements. These movements include not only the movement of the entire cell, but also the internal transport of organelles and other structures through the cytoplasm [36]. In short, the cytoskeleton is a dynamic structure that is continually remodeled as the cell moves and changes shape. Section 3.1 will go into the details of this remodeling.

The coordinated remodeling of the cell's cytoskeleton and adhesion structures gives rise to the movement of the cell and is a periodically repeated sequence involving several stages [37].

1. The cell receives a signal.
2. Pseudopodial protrusions are extended from the leading edge.
3. The pseudopodial extensions attach to suitable surroundings.
4. The cell translocates to its new position
5. The trailing edge is dissociated from the substrate and retracted into the cell body.

The schematic illustrations below were borrowed from Thomas Pollard's book "Cell Motility: From Molecules to Organism" [38]. Each of these steps will be elaborated on after the following short introduction to the cytoskeleton of eukaryotic cells. The main reference for the following sections is Geoffrey Copper and Robert Hausman's book "The Cell: A Molecular Approach, third edition" [36]. Any unreferenced statements may be found in their book.



The cell receives a signal that prompts it to initiate the remodeling of the cytoskeleton.

Protrusions form and extend from the leading edge. These protrusions can be lamellipodial (sheet-like), filopodial (thin rod-like) or, as is most often the case, pseudopodial (larger rod-like). First, protrusions such as pseudopodia, lamellipodia or filopodia must be extended from the leading edge of the cell.

Some of these extensions attach to the substratum across which the cell is migrating and create an adhesion signal.

The cell reacts to the adhesion signal by translocating in the direction of the new attachment sites. This translocation is accomplished through a contractible part of the cytoskeleton and the exertion of tension forces.

Finally the attachment of the cell at the trailing edge must dissociate from the substratum and retract into the cell body.

3.1 The Cytoskeleton

In eukaryotic cells, the cytoskeleton is composed of three principal types of protein filaments: ¹)microtubules (diameter of about 25 nm), ²)intermediate filaments (diameter of about 10 nm), and ³)actin filaments (diameter of about 7 nm) [36]. These protein filaments are held together and linked to subcellular organelles and the plasma membrane by a variety of accessory proteins.

Microtubules help determine cell shape and are involved in a variety of movements within the cell, e.g., the transportation of organelles, and in the separation of chromosomes during mitosis [36]. The intermediate filaments are, unlike actin filaments and microtubules, not directly involved in cell movement. Instead, they appear to play a basic structural role by providing mechanical strength to cells and tissues [36]. Actin filaments are particularly interesting for the subject of this thesis, as they form the network that provides mechanical support, determines cell shape, and allows movement of the cell surface. Through the actions of the actin filaments, cells are able to migrate, engulf particles, and divide. Some cell movements, such as the migration of cells in wound healing, can be served by the actin cytoskeleton alone in the absence of microtubules and intermediate filaments [39]. Since some cell movements can be served by the actin cytoskeleton alone, this section will mainly focus on the actin composition of the cytoskeleton and its role in cell migration.

Actin filaments account for 5-10% of the total protein in all types of eukaryotic cells and are most abundant in the supporting structure just beneath the plasma membrane. Actin

filaments are composed of subunits assembled into thin fibres that can reach lengths of up to several micrometers. The subunits are called actin monomers, and they polymerize in head-to-tail arrays, giving the filaments a polar structure with two distinct ends [36], see Figure 3.1. This polarity of the filaments is important both in their assembly and in establishing a directional movement along the filaments. The “plus end” of the filaments has a higher affinity for polymerization and grows faster than the “minus end”. Because actin polymerization is reversible, filaments can depolymerize by the dissociation of actin subunits, allowing actin filaments to be broken down when necessary [36].

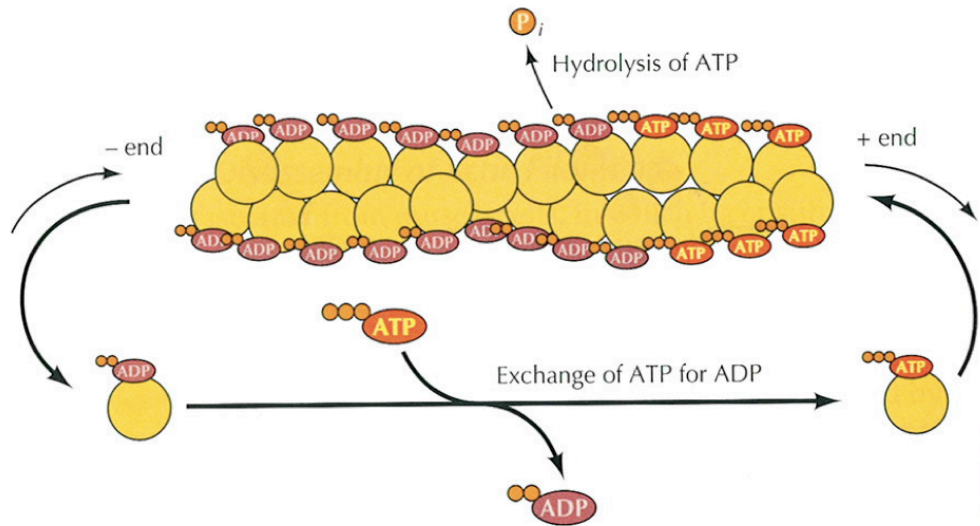


Figure 3.1: An actin filament composed of actin monomers. The higher affinity for polymerization of the plus end makes it possible for the actin filament to “treadmill”, i.e., have dissociation occurring at the minus end at the same rate as association at the plus end (from Cooper and Hausman’s “The Cell” [36]).

Within the cell, the individual actin filaments are organized into higher-order structures forming bundles or three-dimensional networks. There are three general types of these higher-order structures: ¹⁾actin networks, ²⁾close actin bundles and ³⁾contractible actin bundles. These structures play different roles in the cell. The shape and nature of these structures are determined by the shape and size of the crosslinking proteins, as can be seen in Figure 3.2.

In **actin networks**, the actin filaments are crosslinked by large flexible proteins that can crosslink perpendicular filaments in orthogonal arrays to form three-dimensional meshworks with the properties of a semisolid gel. Networks support the whole membrane, whereas bundles support more rigid protrusions of the plasma membrane [36].

In **close actin bundles**, the actin filaments are crosslinked by small rigid proteins that force the filaments to align closely with one another. In these close bundles, all the filaments have the same polarity with their rapidly growing “plus ends” adjacent to the plasma membrane, so any extensions of the filaments will push out on the membrane. The closely-packed parallel arrays create stiff rods that can support projections of the plasma membrane, such as pseudopodia and filopodia [36].

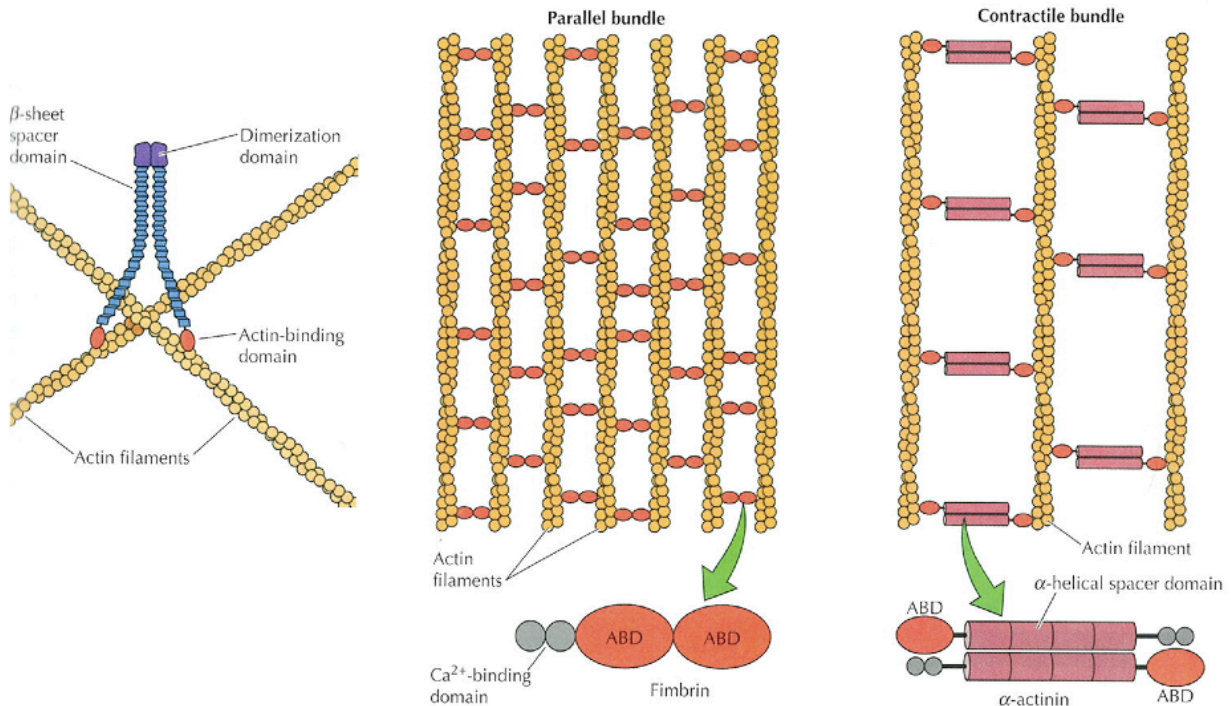


Figure 3.2: Left: An actin network crosslink by a large flexible protein that binds the two filaments orthogonally. Multiple such crosslinks will lead to a three-dimensional meshwork with the properties of a semisolid gel. Middle: A close actin bundle crosslinked by small rigid proteins to form stiff rods. Right: A contractible actin bundle crosslinked by larger rigid proteins to form stiff, yet contractible rods (all from Cooper and Hausman’s “The Cell” [36]).

In **contractible actin bundles**, the actin filaments are crosslinked by larger rigid proteins that also align the filaments but with more space in between. The increased spacing between filaments allows the motor protein myosin to interact with the actin filaments in these bundles, which enables the bundles to contract [36]. These bundles interlace most actin networks, and their contraction creates the movement of the cell.

The crosslinking of actin filaments into bundles and networks are regulated by a variety of actin-binding proteins, which are critical components of the actin cytoskeleton. The assembly and disassembly of the actin filaments are likewise regulated by a variety of actin-binding proteins (see Figure 3.3), of which the most important are:

Arp2/3: This complex binds to the side of an existing actin filament near the plus end and forms a new branch. The construction of such branches and their subsequent elongation pushes the plasma membrane under cell movement, creating lamellipodia.

ADF/cofilin: This protein binds to the minus end of actin filaments and enhances the rate of dissociation of actin. ADF/cofilin prefers to stay bound to the actin monomers after dissociation and can thereby prevent their reincorporation into filaments.

Prolifin: This protein can dissociate ADF/cofilin from the actin monomers and stimulate the incorporation of actin monomers into filaments.

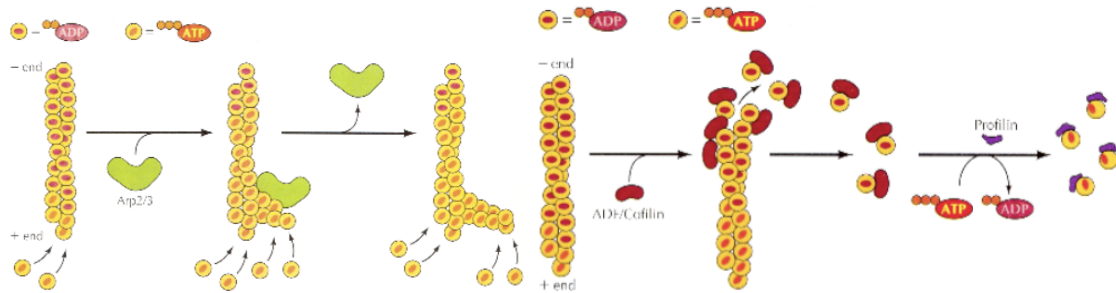


Figure 3.3: Left: A schematic illustrating the way Arp2/3 protein affects actin filaments by creating branching. Right: A schematic illustrating the way ADF/cofilin and profilin proteins affect actin filaments by enhancing dissociation and stimulate association of actin monomers respectively (both from Cooper and Hausman’s “The Cell” [36]).

Through the regulation of these actin-binding proteins, the polymerization of actin filaments can be finely tuned to respond appropriately to environmental stimuli. Arp2/3, ADF/cofilin and profilin, as well as other actin-binding proteins, can act together to promote the rapid turnover of actin filaments and remodeling of the actin cytoskeleton that is required for changes in cell shape and movement. Changing the shape of the cell is a major undertaking and, in some cell types, actin filament assembly and disassembly are responsible for half the cell’s energy consumption, i.e. half the hydrolysis and turnover of ATP [36].

3.2 The Steps in Cell Migration

Despite the complexity of the external stimuli and the types of locomotory responses, the general model for cell motility regulation, as it emerges from the studies of the last 15 years, is surprisingly uniform. The actin cytoskeleton is responsible for the migrating movements of cells across a surface, which appear to be driven directly by actin polymerization and actin-myosin interactions. The remodeling of the cytoskeleton involved in migration is a five-step, periodically repeated process:

1. The cell receives a signal.
2. Pseudopodial protrusions are extended from the leading edge.
3. The pseudopodial extensions attach to suitable surroundings.
4. The cell translocates to its new position
5. The trailing edge is dissociated from the substrate and retracted into the cell body.

3.2.1 Receiving the signal

The process of locomotion is costly for the cell and is not initiated needlessly. A cell will not move unless it is somehow forced or signaled to do so. These signals can come from both external and internal sources. External signals do not signal directly to the actin assembling and disassembling mechanism, instead they signal to an integrated translation system based mainly on small guanine nucleotide-binding proteins (G-proteins) [40]. Each specific stimulus is “translated” into a specific combination of activities and localizations of the small G-proteins. The G-proteins then initiate cascades of events that lead to cytoskeletal reorganization and ultimately to alterations in adhesion and locomotory behavior [41, 42, 43]. The cellular machinery involved in the coordinated remodeling of the cytoskeleton and adhesion structures is very complex and includes many regulatory loops. These loops and the translation system provide the proper coordination between different structural components and enable the cell to respond correctly to a variety of external stimuli.

One of the external stimuli that can affect cell motility is chemotactic signalling, which can both attract and repel. *Chemoattractants* activate two parallel signalling pathways: one promotes actin polymerization locally by creating new barbed ends, and one stabilizes existing filaments. If the cell does not receive any positive signals for actin assembly, the whole system runs down automatically, and the cell stops migrating. The rate of actin filament decay will be determined by the rate of GTP hydrolysis. Actin networks in unstimulated parts of the cells are predicted to disassemble in tens of seconds, perhaps faster if it is hurried by the active ADF/cofilin [44]. *Chemorepellents* also make the cell move, possibly also by promoting actin polymerization and stabilizing existing filaments, but on the other side of the cell, the one facing away from the repellent. The external signals from chemotactic attractants and repellents guide actin filament assembly both temporally and spatially. In seconds cells can re-orientate toward a new source of attractant or turn away from repellents [45, 46].

The major types of internal signals affecting cell motility are the cell’s contacts with other cells and its contact with the extracellular matrix. These contact regions generate signals that determine the character of cell motility, its direction, velocity and persistence [47, 48]. Once the cell has received a directional signal, it will initiate cytoskeleton remodeling to accommodate this signal.

3.2.2 Extending pseudopodial protrusions from the leading edge

The leading edge is the edge closest to the direction in which the cell initiates movement. The cell’s movement begins with a *pseudopodial* sensing of the area in front of the leading edge. Pseudopodia are extensions of moderate width made of the stiff, rod-like actin filament bundles with the membrane wrapped around it. The actin filament is embedded in the three-dimensional actin filaments network of the supporting cytoskeleton in one end, see Figure 3.4. Many cells also extend filopodia, thinner projections of the plasma membrane also supported by actin bundles. The formation and retraction of these structures is based on the regulated assembly and disassembly of actin filaments. These extensions are transient structures that form in response to environmental stimuli. If they, in sensing the area in

front of the leading edge, find a region suitable for adhesion, they attach to it creating either “focal adhesion” or “adherens junctions”.

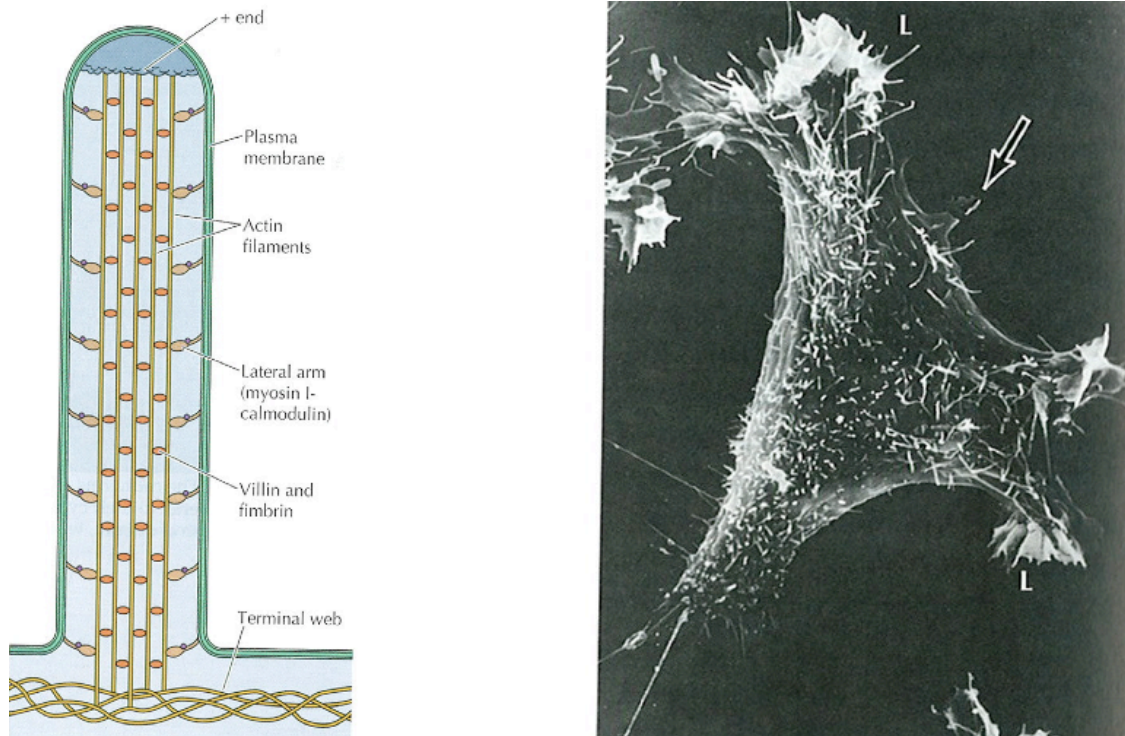


Figure 3.4: Left: A schematic of the formation of a pseudopod with a stiff, rod-like close actin bundle embedded in the supporting cytoskeleton made of the three-dimensional actin network. Right: A cell with fluorescently marked actin bundles. The arrow points to a pseudopod, and lamellopodial sheets are marked with an “L” (both from Cooper and Hausman’s “The Cell” [36]).

3.2.3 Attachment of the pseudopodial extensions

Most cells have specialized discrete regions of the plasma membrane that form contacts with adjacent cells, tissue components, or other substrates, such as the surface of a culture dish. These regions differ depending on their purpose. The cellular attachment region to an extracellular matrix is called a *focal adhesion*, whereas a cell’s attachment region to another cell is called an *adherens junction*.

In **focal adhesions**, the attachment of the cell is mediated by the binding of transmembrane proteins (called integrins) to the extracellular matrix. The protein integrin has one hydrophilic end on the exterior of the cell that can attach to the extracellular matrix, a hydrophobic region that transcends the membrane and another hydrophilic end in the interior cell that can form complexes that attach to actin filaments, as can be seen in Figure 3.5. Other proteins found at focal adhesions also participate in the attachment of actin filaments, and a combination of these interactions may be responsible for the linkage of actin filaments

to the plasma membrane. Focal adhesions are mostly found at the cell's edge where the pseudopods are actively establishing them, but they are also found throughout the contact area between the cell and the substrate, see Figure 3.6, where the focal adhesions have been fluorescently marked in red.

In **adherens junctions**, the attachment of the cell to another cell is mediated by trans-membrane proteins called cadherins. The protein cadherin also has one hydrophilic end on the exterior of the cell that can attach to the cadherins of other cells, a hydrophobic region that transcends the membrane and another hydrophilic end in the interior cell that can attach to actin filaments through forming a complex with the cytoplasmic proteins called catenins [36]. A schematic of the adherens junction can be found in Figure 3.5, and Figure 3.6 shows the progression of adhesion junctions over time as two cells attach to each other. The adherens junctions have been fluorescently marked in these black-and-white images.

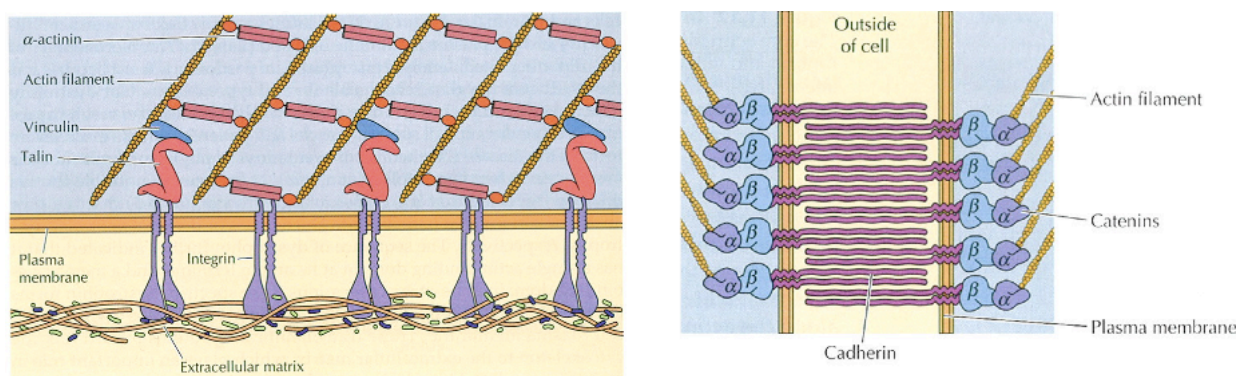


Figure 3.5: Left: A schematic of a focal adhesion of a cell attached to a substrate with integrins. Right: A schematic of an adherens junction of a cell attached to another cell with cadherins (both from Cooper and Hausman's "The Cell" [36]).

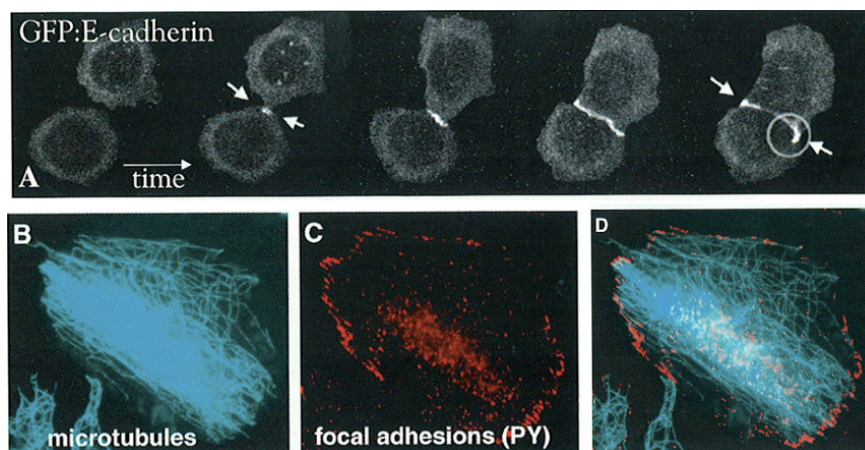


Figure 3.6: Top (A): A cell attached to another cell with fluorescently marked adherens junction (white). Bottom (B)-(D): A cell attached to a substrate with fluorescently marked focal adhesion (red) (both from Ridley, Peckham and Clark's "Cell Motility" [40]).

The plasma membrane is not only linked to the cytoskeleton at focal adhesions and adherens junctions, but also distributed throughout the surface by transmembrane ERM proteins (Ezrin/Radixin/Moesin proteins). Like integrins and cadherins, the transmembrane protein ERM has a local hydrophobic section, which anchors the protein in the lipid bilayer, bracketed by two hydrophilic sections. The intracellular, hydrophilic part of the ERM protein attaches to the general actin filament network of the cytoskeleton, pinning the stretched membrane to the supportive cytoskeleton. [36]

Once focal adhesions or adherens junctions have been formed at the end of pseudopodia reaching out from the leading edge, the leading edge is pushed forward to these focal adhesions. The cell membrane is pushed forward by the growth of the supportive actin filament network immediately below it. The resulting broad, actin network-containing, sheet-like extensions are called lamellipodia, which can be seen in Figure 3.4. [36]

Lamellipodia are sheet-like membrane protrusions supported by the actin network. When extending lamellipodia, the major part of the actin assembly occurs in a narrow band just behind the membrane, which is less than $1\ \mu\text{m}$ wide. Any actin filament disassembly occurs in a broader zone behind the assembling band at the leading edge¹. If a cell is extending its leading edge at $0.2\ \mu\text{m/s}$, the network of branches must be remodeled in less than 5 s [40].

3.2.4 Translocation of the cell

Once the lamellipodia have caught up to the newly established focal adhesions at the end of the probing pseudopodia, the cytoskeleton is anchored to these focal adhesion regions and rearranged through the tension exerted by the contractile bundles. The contraction of actin bundles by *myosin* motors produces tension across the cell, allowing the cell to pull on the substrate or the neighboring cells to which it is anchored, thereby pulling the cytoskeleton mass toward the location of the focal adhesion or adherens junction. Myosin is the prototype of a molecular motor - a protein that converts chemical energy in the form of ATP to mechanical energy, thus generating force and movement [36]. Focal adhesion assembly is induced by tension either resulting from internally myosin-driven cell contractility or applied externally. Thus, focal adhesions can function as mechanosensors, “reporting” to the cell information about the physical properties of the surrounding environment [40]. The actin cytoskeleton is anchored to adherens junctions (cell-cell contact), just as it is to focal adhesions (cell-substrate contact). In sheets of endothelial cells, these adherens junctions can form a continuous beltlike structure, called an adhesion belt, around each cell in which an underlying contractile bundle of actin filaments is linked to the plasma membrane.

3.2.5 Dissociating the trailing edge

The final stage of cell migration, the retraction of the trailing edge, involves the action of small GTP-binding proteins of the ADP Ribosylation Factors (ARF) family. These proteins break down existing focal adhesion at the trailing edge of the cell. Once the focal adhesions

¹The actin filament assembly and disassembly both happen deeper in the cytoplasm as well but not to any significant extent.

have been broken down, the trailing edge is pulled forward by the contraction of actin bundles [36]. The turnover of adhesion contact regions, both focal adhesions and adherens junctions, is not an unusual property. It is essential for cell migration. Adhesion is too often viewed as a static property, but it obviously is not. If it were, cells would not exchange neighbors or migrate as they do [39].

3.3 Motility phenotypes

During migration eukaryotic cells display a wide variety of motility phenotypes, some of which were mentioned above. When a cell is stationary, it is said to display *quiescence*. This means that the assembly and disassembly of actin filaments balance each other out, and the net amount of actin is the same and structured in approximately the same way. Once a cell starts migrating, it displays several different motility phenotypes, such as pseudopodial protrusion and retraction, filopodial protrusion and retraction, lamellipodial protrusion and retraction, retraction of the trailing edge and sometimes blebbing.

Pseudopodial protrusion occurs primarily during the cell's initial testing of its surroundings. Pseudopods are stiff rod-like protrusions of the membrane, supported by a close actin bundle, which cannot contract. The minus end of the actin bundle is embedded in the main actin network of the cytoskeleton, and the plus end is directed outwards. This means that as actin monomers assemble on the plus end, the closed bundle will lengthen outward, pushing the cell's membrane further and further. The membrane wraps around the newly created support of the closed actin bundle. The proteins embedded in the membrane will enable the pseudopod to attach with both focal adhesions and adherens junctions if the cell finds its surroundings suitable.

Pseudopodial retraction occurs if the surroundings of the cell were not found suitable. The minus end embedded in the main actin network of the cytoskeleton has a higher affinity for actin monomer dissociation, so the pseudopod degrades from this end. As the actin filaments of the closed bundle degrade, the pseudopod is retracted.

Filopodial protrusion is much like pseudopodial protrusion, only for thinner closed actin bundles. They also occur primarily during the testing of the surroundings and can also attach with both focal adhesions and adherens junctions.

Filopodial retraction occurs if the surroundings of the cell were not found suitable, as in pseudopodial retraction. The filopod also degrades from the network embedded minus end, thereby retracting the filopod.

Lamellipodial protrusion usually follows the successful attachment of a pseudo- or filopod. The lamellipodium is a broad sheet-like protrusion of the membrane supported by an actin network. The already existing actin filaments constituting the main actin network of the cytoskeleton have most of their plus ends oriented outwards. The lamellipodia is created by polymerizing, branching and lengthening part of the already existing actin network. The creation of lamellipods are really just an extension and relocation of the cytoskeleton. The actin binding protein Arp2/3 binds to the actin

filaments and induces branching. The multiple branches provide a better scaffold to support the membrane that is wrapped around the broad sheet-like protrusions and future pseudo- or filopodial protrusions. The actin polymerization occurs right beneath the membrane, providing the force with which the membrane is pushed forward. Lamellipodia are usually seen near the leading edge of the cell, and the contraction of contractile actin bundles within the lamellipodia creates the tension with which a cell translocates itself.

Lamellipodial retraction occurs primarily as part of the retraction of the the trailing edge but can also occur before the cell relocates. The lamellipod is attached through either focal adhesions or adherens junctions or both, and these need to be broken down before the lamellipod can be retracted. The lamellipod also degrades from the minus end, i.e., towards the center of the cell. The front is retracted through the contraction of contractile actin bundles, and the network is disassembled in an orderly fashion in the more central parts of the cell.

Retraction of the trailing edge is a special kind of lamellipodial retraction that occurs when a cell has relocated itself.

Blebbing is mostly seen when cells go through apoptosis, but it can also be seen during cell adhesion. Blebs are unsupported protrusions of the membrane and do not need actin assembly or disassembly, so the time scale on which blebbing happens can be much faster than the other motility phenotypes. Blebbing resembles a flopping or bubbling membrane.

3.4 The Membrane

The majority of migration studies investigates either the role of actin in the cytoskeletal regulation or the role of the substrate's composition. Sandwiched between these two entities lies the cell's membrane, which has received less attention in the literature. In the last decade, two interesting studies have been published which have investigated the influence of the membrane's physical properties on endothelial cell migration. A summary of these two studies will follow in Chapter 4. In this section, the physical composition of the membrane will be described.

Cells are critically dependent on their membranes not only to separate the interior of the cell from its environment but also to conduct signals to and from the cell's immediate environment and to transport different molecules across the membrane. All cell membranes share a common structural organization, a lipid bilayer with *integral membrane proteins*. Integral membrane proteins are proteins which are embedded directly into the membrane. Most of these proteins are *transmembrane* proteins, which span the entire bilayer and have portions exposed on both sides, e.g., integrins, cadherins and ion channels. The integral membrane proteins control and facilitate the selective transport of different molecules across the cell membrane, transduce the external signals to allow the cell to respond to them, control the interactions between cells of a multicellular organism, and participate in electron transport and oxidative phosphorylation [36].

Proteins are attributed for carrying out the specific functions of the membrane, but the basic structure of all biological membranes is the lipid bilayer, which is composed of different types of *phospholipids*. Phospholipids are *amphiphilic* molecules which consists of two hydrophobic fatty acid chains linked to a phosphate-containing hydrophilic head group. The term amphiphilic refers to the molecule's dual property; one end is hydrophilic, and the other is hydrophobic. Because of their hydrophobic fatty acid tails, phospholipids are poorly soluble in aqueous solutions. Instead, they spontaneously form bilayers (or vesicles), which only expose their hydrophilic headgroups to the aqueous solution on both sides of the bilayer, shielding their hydrophobic tails in the interior of the membrane, see Figure 3.7. Lipids constitute about 50% of the mass in most cell membranes, although this proportion varies depending on membrane and cell type. In endothelial cells, it is approximately half. Several types of phospholipids can constitute the lipid bilayer, and the lipid composition also depends on cell type.

Lipid bilayers behave as two dimensional fluids in which molecules (both proteins and lipids) are free to rotate and move in lateral directions, see Figure 3.7. The *fluidity* is a critical property of membranes and is determined by both temperature *and* the lipid composition of the bilayer [36]. Fluidity is a measure of the degree to which molecules are able to move within the membrane: the higher the fluidity, the more mobile the molecules. There is another measure for molecule mobility in membranes called *microviscosity*, which relates to fluidity as $\text{microviscosity} = 1/\text{fluidity}$. That means that the higher the fluidity of the membrane, the less microviscous it is and the more mobile the molecules within the membrane are [35].

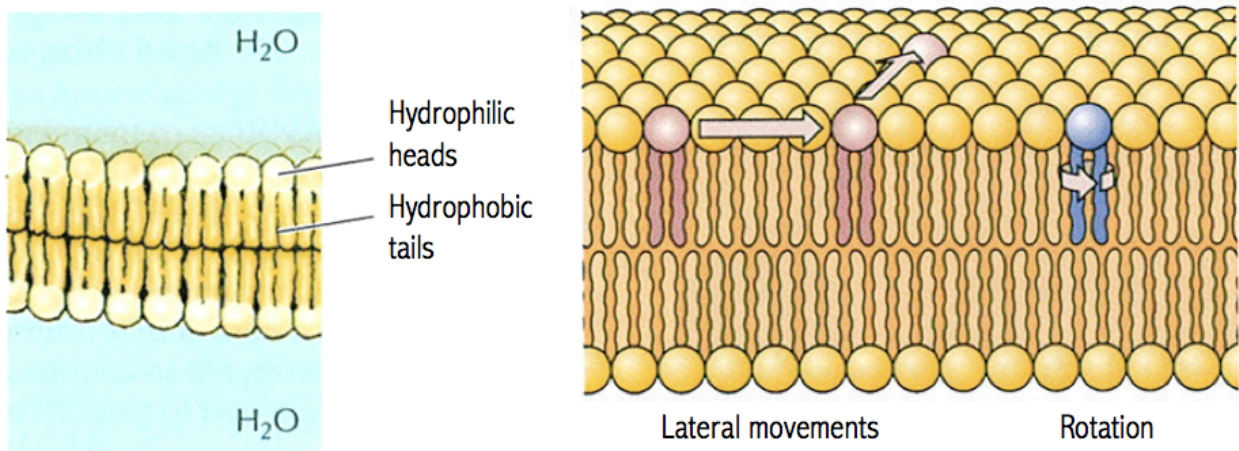


Figure 3.7: A schematic of a lipid bilayer membrane. Left: The amphiphilic lipids arrange themselves spontaneously into a bilayer membrane in aqueous solutions to shield their hydrophobic tails. Right: A lipid bilayer behaves as a two dimensional fluid in which molecules are free to rotate and move in lateral directions (both from Cooper and Hausman's "The Cell" [36]).

As mentioned before, the fluidity of the membrane is determined by both temperature and the lipid composition of the bilayer. If the bilayer consists mainly of lipids with short fatty acid chains, the membrane will appear less *stiff* and remain fluid at lower temperatures [36]. *Membrane stiffness* is the degree to which the membrane resists deformation. The stiffer

the membrane, the more energy is required to deform it [49]. There is a correlation between membrane fluidity and stiffness, but it has not been elucidated quantitatively [50]. In general the stiffer the membrane, the less fluid. The interactions between short fatty acid chains are weaker than those between long chains, so the membrane composed of phospholipids with fatty acid chains will have a higher fluidity. Lipids containing saturated fatty acids will have a lower membrane fluidity because the presence of double bonds introduces kinks in the fatty acid chains and makes them more difficult to pack together [36].

Since the lipid composition determines the membrane's physical properties, such as stiffness or fluidity (i.e., microviscosity), the incorporation of molecules into the membrane not only changes the composition of the lipid bilayer but also the physical properties of the membrane. A common example is the incorporation of cholesterol in membranes. Because of cholesterol's amphiphilic structure, it incorporates into the membrane spontaneously to shield its hydrophobic end from the aqueous solution, see Figure 3.8. This incorporation plays a complex role in determining the membrane fluidity of cells. The rigid hydrocarbon rings of cholesterol interact with the regions of the fatty acid chains nearest the membrane exterior. This interaction decreases mobility of the outer portions of the fatty acid chains, making the exterior part of the membrane more rigid. On the other hand, the incorporation of cholesterol also interferes with the normal interactions between the fatty acid chains, thereby maintaining membrane fluidity at lower temperatures [36]. Cholesterol's effect on membrane fluidity is due to its incorporation into the membrane, and the resulting effect is highly depending on the amount of cholesterol that has been incorporated, i.e., the concentration with which cholesterol was present in the first place. Similar effects are seen with the membranous incorporation of other amphiphilic compounds such as arachidonic acid [50, 51].

Many pharmaceutical studies have remarked on the *secondary pharmacology* of tested drugs [52]. Secondary pharmacologies are the non-specific manners in which a drug can regulate a variety of membrane proteins. At pico- or nanomolar concentrations, most pharmaceutical drugs function through a high-affinity binding to their cognate receptor. However, when the drug concentration is increased to micromolar concentrations, some drugs begin to display a secondary pharmacology. It has been shown that drugs at these concentrations can alter a number of parameters for the physical properties of the cell's membrane [49, 53]. A number of studies have focused on the role of the bilayer's "fluidity", but the mechanisms whereby the fluidity of a bilayer might regulate membrane function have never been clear. Fluidity correlates with other parameters for the physical properties of the membrane, such as stiffness, so it can still be used as a decent measure for change in the physical properties of the membrane.

In 1972 Seeman remarked that many amphiphilic drugs modulated membrane protein function in an apparently non-specific manner. He proposed that the modulation of membrane protein function could be due to the change in the cell membrane's physical properties, but a possible causal relation or mechanism was not identified at that time. The diverse regulation of membrane proteins found in the secondary pharmacology of these drugs, could be caused by the incorporation of drugs into the cell's membrane. Similarly, a given protein may be regulated by a number of structurally different compounds [49]. This suggests that the lipid bilayer in the membrane may be a regulatory mechanism for the membrane proteins. In 2006 Lundbæk and his collaborators provided a quantitative approach to characterize

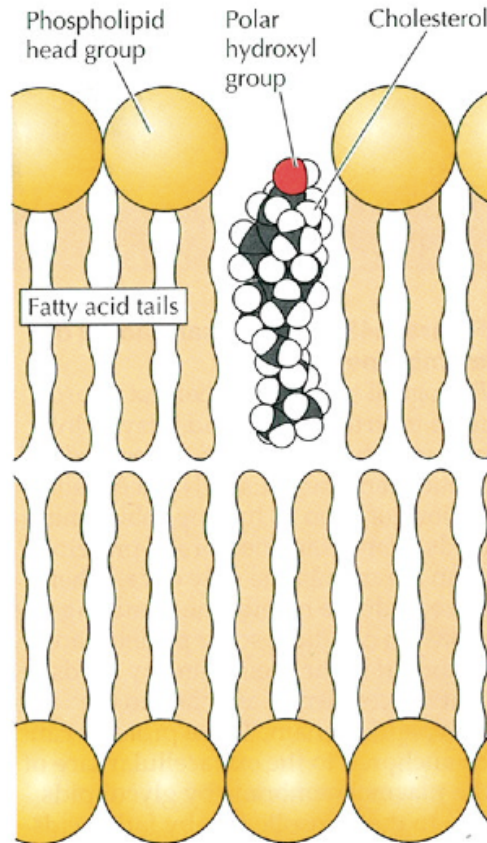


Figure 3.8: A schematic of a cholesterol molecule’s incorporation into a lipid bilayer membrane (from Cooper and Hausman’s “The Cell” [36]).

this non-specific regulation mechanism using the well-described transmembrane ion channel *gramacidin A*.

A transmembrane protein conformational change causes a local bilayer deformation, as can be seen in Figure 3.9. The *hydrophobic length* of the membrane compresses or extends to accommodate a change in the hydrophobic exterior part of the transmembrane protein. The hydrophobic length of a membrane is the length of the hydrophobic transmembrane segment. A decrease in the hydrophobic length causes a local perturbation or thinning of the bilayer. Both the change in free energy intrinsic to the protein when conforming ($\Delta G_{\text{protein}}$) and the change in bilayer perturbation energy ($\Delta\Delta G_{\text{bilayer}}$) contribute to the free energy difference between the conformational states of the transmembrane protein (ΔG_{total}) [50],

$$\Delta G_{\text{total}} = \Delta G_{\text{protein}} + \Delta\Delta G_{\text{bilayer}}.$$

Cause and effect are interchangeable in this case, so, though a conformational change in the protein causes a local deformation of the membrane, a general deformation or change in the membrane can cause a change in the protein’s functionality. This is seen in the equation above in which a change in the physical properties of the bilayer that affects the magnitude of $\Delta\Delta G_{\text{bilayer}}$ also affects the protein’s conformational equilibrium ΔG_{total} , and thereby its functionality. The hydrophobic coupling mechanism (HCM) for an ion channel, when

the channels opening involves a thinning of the bilayer, depends on the energetic cost of deforming the bilayer. Lundbæk describes the hydrophobic coupling mechanism as

$$\ln \left(\frac{n_2}{n_1} \right) = -(\Delta G_{\text{protein}} + \Delta\Delta G_{\text{bilayer}})/RT,$$

where $\frac{n_2}{n_1}$ describes the equilibrium distribution between the number of molecules in each state, R is the gas constant, and T is the absolute temperature. Lundbæk and his collaborators have experimentally verified the equation above for gramicidin A ion channels [49, 50]. Using the gramicidin A ion channel, it has also been shown that the presence of arachidonic acid can alter the membrane bilayer stiffness of living cells [51], which is of great importance to the migration studies presented here.

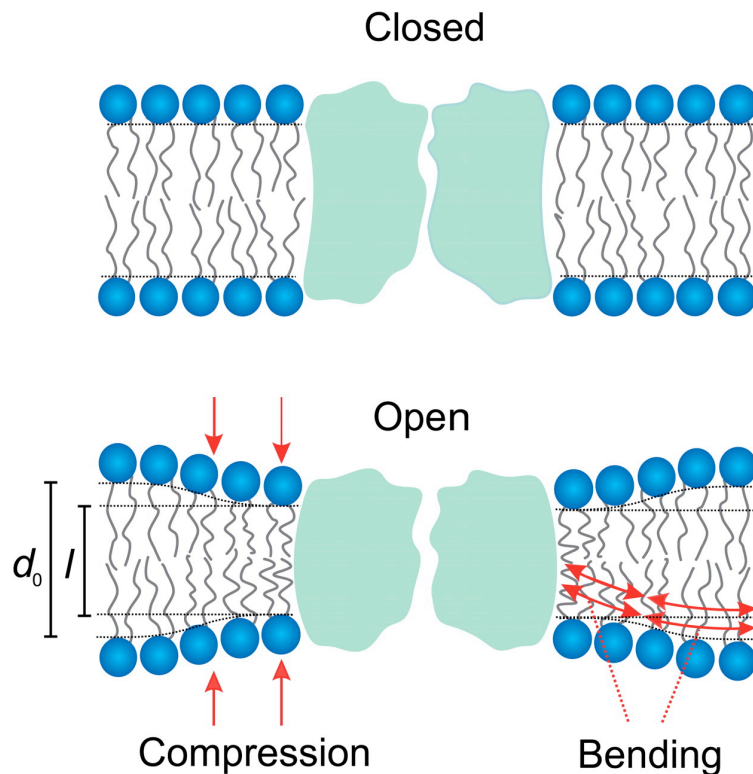


Figure 3.9: A schematic of the hydrophobic coupling between a transmembrane protein and the thickness of the lipid bilayer. The protein's conformational change causes a local bilayer deformation (from Andersen and Koeppe 2007 [53]).

Chapter 4

Inspiration

The main inspiration for the experiments presented in this thesis comes from two papers: “Membrane microviscosity regulates endothelial cell motility” by Ghosh *et al.* from 2002 [34] and “Regulation of endothelial cell migration by amphiphiles - are changes in cell membrane physical properties involved?” by Jensen *et al.* from 2007 [35]. Both of these papers address regulation of endothelial cell motility, which is essentially the regulation of angiogenesis. Angiogenesis is involved in a series of different pathologies (see Chapter 2), so there is much incentive to develop means of regulating endothelial cell migration.

It has been possible to follow the process of angiogenesis and thereby the migration of endothelial cells *in vivo* since 1928 when transparent chambers were introduced by Sandison (see Section 2.2). However, most migration assays are presently done *in vitro* using *razor wound assays*, as they offer a higher degree of control of the experimental set-up. In razor wound assays, the cells are grown in a monolayer on a surface suitable for microscopic investigation, such as a glass slide or a transparent petri dish. The cells are grown until confluence, i.e., to such a density that there are no vacant spaces between the cells. When confluence is reached, the cells are in approximately the same state as *in vivo* [54]. In razor wound assays, half the cells are carefully removed when the cells have reached confluence. This is done by gently pressing a sterile razor blade down to the glass and sweeping the monolayer of cells off to one side, thereby vacating a large space into which the remaining untouched cells can migrate. The progress of the cells’ migration is then recorded through microscopic observations, as has been done by Ghosh, Jensen and their respective collaborators.

Razor wound assays are conventionally used to study cell migration. In the two papers, the migration of endothelial cells was recorded as the number of cells that crossed the *demarcation line* in 24 hours. The demarcation line is the line from which half the cells were removed, i.e., where the razor blade was gently pressed down. The number of migrated cells (NMC) in a given assay was compared to the number of migrated cells in a control assay, and any effect on endothelial cell migration was interpreted from the difference in the number of migrated cells (NMC) between the given assay and the control [35]. Figure 4.1 shows the observations and the data from such razor wound assays as presented in Jensen *et al.* 2007.

The papers by Ghosh [34] and Jensen [35] report that adding amphiphilic compounds to the cell’s media in *in vitro* experiments affects the migration of endothelial cells. This is clearly

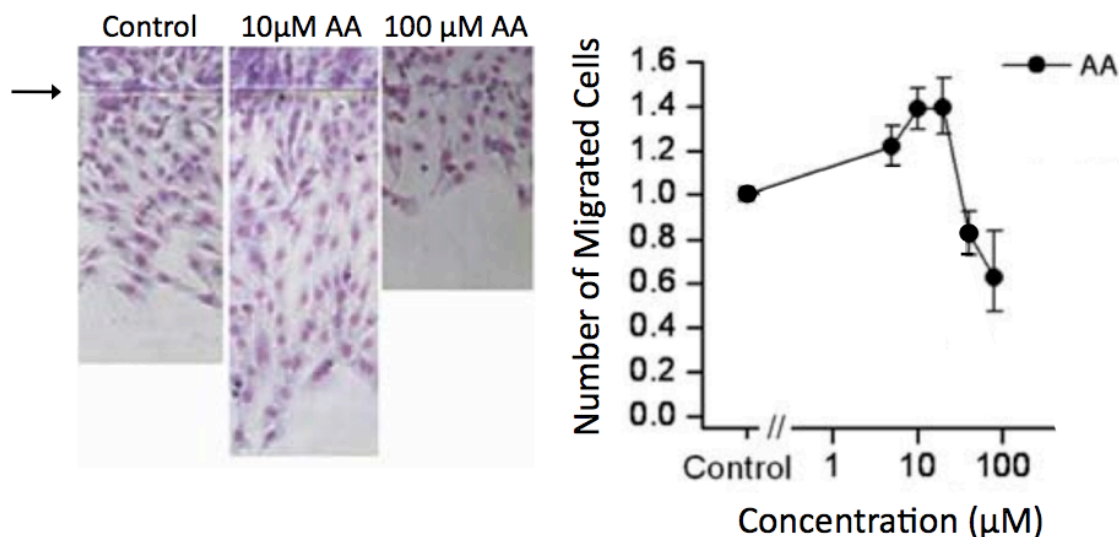


Figure 4.1: Left: Exemplary razor wound assays observed by Jensen *et al.*, both of a control assay and after adding 10 and 100 μM arachidonic acid (AA) to the media of the cells. The cells have been fixed and stained after 24 hours of migration. Right: The number of migrated cells (NMC) when compared to the control razor wound assays as a function of the concentration of arachidonic acid (AA) added to the migration media (from Jensen *et al.* 2007 [35]). Arachidonic acid (AA) is an amphiphilic compound, and its ability to both promote migration at low concentrations and inhibit migration at higher concentrations is clearly seen.

seen in Figure 4.1, which shows data from the paper by Jensen *et al.* [35]. Amphiphilic compounds have a hydrophobic and a hydrophilic end to them, just like the lipids that constitute the cellular membrane. Amphiphilic molecules will spontaneously incorporate themselves into the membrane to shield their hydrophobic ends, minimizing the free energy of the system. The incorporation of amphiphilic compounds into the membrane will not only change the composition of the membrane but also its physical properties. The observed effect on migration is speculated to relate to the change in physical properties [34, 35].

The changes in physical properties induced by the incorporation of amphiphilic compounds into the membrane will change many parameters, two of which are the membrane's stiffness and microviscosity. Membrane stiffness can be measured using the gramicidin A ion channel's lifetime¹ [49, 50, 53], and membrane microviscosity can be measured using the fluorescence anisotropy² of membrane-embedded 1,6-diphenyl-1,3,5-hexatriene (DPH) [55]. Ghosh and

¹The gramicidin A ion channel's lifetime is the duration of time when the channels are open for ion passage.

²Microviscosity is 1/fluidity of a lipid bilayer and refers to the rate of molecular motion within the bilayer. The rate of molecular motion is higher in a membrane with low microviscosity than in a membrane with high microviscosity. Microviscosity can be evaluated from the fluorescence anisotropy of membrane-embedded 1,6-diphenyl-1,3,5-hexatriene (DPH). The membrane embedded DPH aligns parallel to the fatty acyl chain axis of the bilayer as a probe and is photobleached in a small area. The fluorescence recovery after this bleaching is used as a measure for the membrane's microviscosity. The faster the fluorescence is recovered by the diffusion of unbleached DPH probes from the surroundings of the photobleached area,

his collaborators showed that the change in number of migrating endothelial cells correlates particularly well with the change in the *microviscosity* of the membrane [34] (as can be seen in Figure 4.2), and Jensen *et al.* showed a similar correlation between changes in the membrane stiffness and changes in the number of migrated endothelial cells (see Figure 4.3).

The high correlation between endothelial cell migration and the change in two parameters describing the physical properties of the membrane suggests that it is the incorporation of amphiphilic compounds into the membrane that regulates endothelial cell migration. The correlation between microviscosity and migration is “biphasic” to use Ghosh *et al.*’s terminology. By biphasic they mean that there is an optimal microviscosity for cell migration and that the migration will be slower for any microviscosity removed from this optimum. The microviscosity of normal (control) cells is slightly lower than this optimum, which lies at around 110% microviscosity compared to the normal (control) cells, see Figure 4.2. It is therefore possible to enhance endothelial cell migration, i.e., angiogenesis, beyond the normal rate. Adding amphiphilic or other microviscosity altering compounds to the cells’ media will affect their migration [34]. Changing the microviscosity to values lower than that of the control ($< 100\%$) will inhibit the migration of endothelial cells. If the microviscosity is changed to lie between 100% and 120% of that of normal (control) cells, it is closer to the optimal value for microviscosity, and migration is enhanced. If the microviscosity is increased more than 120% of normal (control) cells, the microviscosity will be further removed from its optimal value, and the effect will again be inhibitory (just like when the microviscosity is lower than that of the control), see Figure 4.2.

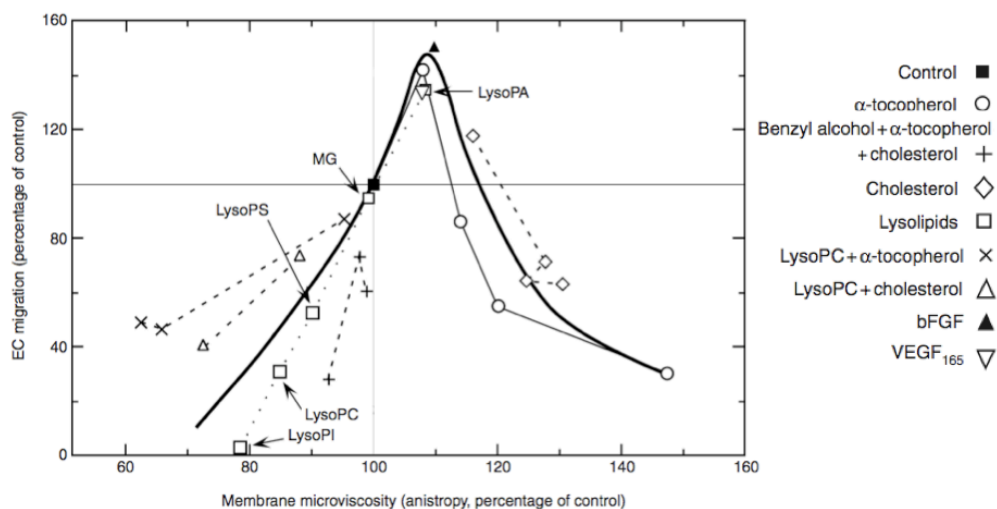


Figure 4.2: Endothelial cell migration plotted as a function of membrane microviscosity measured through membrane anisotropy. Several membrane-active agents were used, as indicated. All experiments were compared to the control experiments at (100%, 100%). The estimated fit for the biphasic relation between migration and microviscosity is shown as a broad solid line (from Ghosh *et al.* 2002 [34]).

the faster the molecular motion is within the lipid bilayer and the lower the microviscosity. Membrane anisotropy measured by this method reflects a combination of rotational and axial motion of the DPH probe and is directly related to membrane microviscosity [55].

Jensen and his collaborators [35] tested the effect of many different types of amphiphilic compounds on endothelial cell migration: lysophospholipids, Triton X-100, octyl- β -glucoside, arachidonic acid (AA), docosahexaenoic acid, eicosatetraenoic acid (ETYA) and capsaicin. These compounds are all amphiphilic but structurally different. All of these amphiphilic compounds could affect the migration of endothelial cells, and their effect correlated quantitatively with their effect on the membranes' stiffness as measured through gramicidin A ion channels [35, 49, 50], see Figure 4.3. The close correlation between the effect on membrane stiffness and migration suggests that amphiphilic compounds affect the cell through their incorporation into the membrane.

The structural differences between all the amphiphilic compounds that induced similar effects on the migration, membrane microviscosity and membrane stiffness further support the claim of regulation of endothelial cell migration through amphiphilic membrane incorporation and not through receptor-specific binding. The use of amphiphilic compounds establishes a novel non-receptor specific approach to regulating endothelial cell migration.

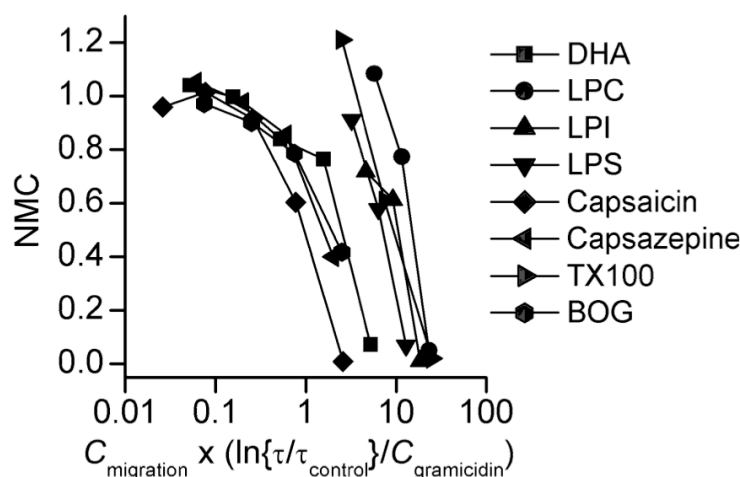


Figure 4.3: The relation between the effects of the amphiphiles on the number of migrated cells (NMC) and on lipid bilayer stiffness measured using gramicidin channels. The lipid bilayer stiffness is expressed as $C_{\text{migration}} \cdot (\ln(\tau/\tau_{\text{control}})) \cdot C_{\text{gramicidin}}$, where $C_{\text{migration}}$ is the concentration of the amphiphilic compound in the migration experiments, and $\ln(\tau/\tau_{\text{control}})$ represents the change in gramicidin channel lifetime induced by a low amphiphile concentration, $C_{\text{gramicidin}}$ (from Jensen *et al.* 2007 [35]). Jensen *et al.* did not portray arachidonic acid (AA) in this graph, probably due to arachidonic acid's ability to either enhance or inhibit endothelial cell migration.

Regarding Figures 4.2 and 4.3, the addition of most amphiphilic compounds either decreases or increases the correlated physical properties of the cell's membrane (microviscosity or stiffness), thereby only enhancing or inhibiting the endothelial cell migration. Of all the amphiphilic compounds tested by Jensen *et al.*, only arachidonic acid (AA) could enhance as well as inhibit migration depending on the concentration with which it was present in the cells' media. At low concentrations, arachidonic acid enhances endothelial cell migration, whereas it inhibits migration at high concentrations [35], see Figure 4.1.

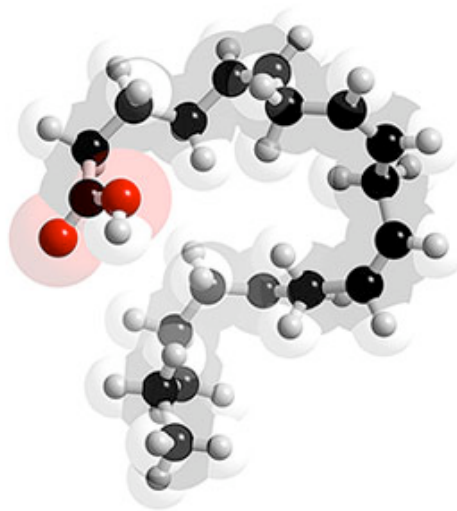


Figure 4.4: Space-filling model of Arachidonic Acid which has the molecular formula $C_{20}H_{32}O_2$. Key: Hydrogen = white, carbon = black, oxygen = red.

4.1 Arachidonic Acid

Arachidonic acid (AA) is a polyunsaturated fatty acid (PUFA) and can be seen in Figure 4.4. Arachidonic acid occurs naturally within cells. It is freed from a phospholipid molecule by the enzyme phospholipase A_2 , which cleaves it off fatty acids [56]. Arachidonic acid is both a signaling intermediate and a constituting part of the cell's membrane. Arachidonic acid acts as an intermediary in inflammation signaling and constitutes part of the phospholipids in cells' membranes, particularly in muscle and brain cells [57]. Arachidonic acid is one of the most abundant fatty acids in the brain, accounting for 10% of its fatty acid content [58], and neurological health is dependent on sufficient levels of arachidonic acid. Among other things, arachidonic acid protects the brain from oxidative stress and helps to maintain hippocampal cell membrane fluidity [59].

Jensen *et al.* conducted a series of experiments in which the metabolism of arachidonic acid was blocked [35]. The effect of arachidonic acid on migration in such experiments was similar to those of other, structurally different polyunsaturated fatty acids (PUFAs) in that it only inhibited migration and the higher the concentration is, the stronger the inhibitory effect. Migration must therefore be enhanced by a mechanism involving the metabolic products of arachidonic acid [35]. These metabolic products' influence is only observable for a low concentration of arachidonic acid, possibly because the inhibiting influence of arachidonic acid incorporation into the membrane drowns out the metabolic products' effect at high concentrations.

Arachidonic acid has a regulating influence on endothelial cell migration since it can both promote and inhibit the migration and not just block it. The dual regulating properties of arachidonic acid make it an interesting subject for further study. The following chapters investigate arachidonic acid's effect on endothelial cell motility, both adhesion and migration.

Chapter 5

Viability Assays with Arachidonic Acid

Previous studies by Ghosh, Jensen and their respective collaborators suggest that arachidonic acid regulates the migration of endothelial cells. To investigate the effect of arachidonic acid on endothelial cell motility, arachidonic acid will be added to the medium of adhering and migrating endothelial cells as part of the investigations in this thesis. Arachidonic acid is hypothesized to regulate endothelial cell migration through the spontaneous incorporation of amphiphilic compounds into lipid bilayers, which changes the physical properties of the cells' membranes.

A change in the physical properties of the cell's membrane, particularly in its stiffness, may alter the functionality of several transmembrane proteins [49, 50]. The incorporation will change the physical properties of the membrane, which in turn may change the function of proteins embedded in the membrane. Such an induced change in the functions of several proteins may prove toxic to the cell. It is paramount to ensure that the concentration of arachidonic acid used in the subsequent adhesion and migration experiments is not harmful to the cell. Otherwise, any observed change in adhesion or migration could be due to the pathology of a stressed cell, apoptosis, or necrosis. An assay that tests the harmfulness of certain conditions is called a *viability assay*. A viability assay tests the harmfulness of a condition by comparing the proliferation rate of cells under that condition to the proliferation rate of normal cells. If the condition is harmful and stresses the cells, the cells are forced to respond to the stressing factor before continuing their proliferation cycle. A cell's proliferation cycle culminates with the division of the cell into two daughter cells, and harmful conditions affect the rate at which this happens. Through viability assays, this section will establish that any observed change in the endothelial cells' adhesion or migration is due to the harmless presence of arachidonic acid in the cells media and *not* to the pathology, apoptosis, or necrosis of stressed cells.

5.1 Previous Viability Assays with Arachidonic Acid

The previous studies by Jensen *et al.* which involved the effect of arachidonic acid on endothelial cell migration also tested the toxicity of arachidonic acid. They concluded that arachidonic acid in concentrations of less than 100 μM in the media is not toxic to endothelial cells [35]. The concentrations used in the subsequent experiments and tested here are all less than 100 μM , so a similar result is expected for the viability assay.

The toxicity of arachidonic acid was tested on the cellular level by Jensen *et al.*, but it has also been tested on the level of the entire organism. Arachidonic acid is one of the essential fatty acids required by most mammals; and it is usually acquired through diet. Dietary supplements of arachidonic acid have been shown to be harmless to humans in clinical trials [60, 61, 62, 63]. Daily supplements of 1,000-1,500 mg arachidonic acid for 50 days have been well tolerated during several clinical studies, with no significant side effects reported. All common markers of health, including kidney and liver function [60], serum lipids [61], immunity [62], and platelet aggregation [63], appear to be unaffected with this level and duration of use. The actual concentration of arachidonic acid in the blood was not registered during these clinical trials.

5.2 Viability Assays: Materials and methods

Cell culture

The porcine aortic endothelial cells used in these experiments were from a strain that stably expresses the human VEGF receptor 2 and were a gift from Dr. Anker J. Hansen at Novo Nordisk A/S. The cells were grown at the bottom of plastic wells (Multidish 6 wells from NunclonTM Δ Surface) in a CO₂ dependent media consisting of D-MEM:F12 (1:1) + GlutaMAX medium supplemented with 10% heat inactivated fetal bovine serum (FBS), 100 U/mL penicillin and 100 $\mu\text{g}/\text{mL}$ streptomycin (all from Gibco, USA).

The cells were cultured in an ambient atmosphere with 5% CO₂ at 37°C and grown until confluence. When cells had reached confluence, they were passaged by gentle *trypsination*. Trypsination severs the integrin bonds with which the cells adhere to the bottom of the plastic wells. The trypsination is halted by diluting the trypsinated cells with medium (1 μL trypsin : 1 mL medium), which then brings the cells into suspension. The suspended cells can then be seeded in new plastic wells at any desired concentration by further dilution of the cells with medium. Trypsination, dilution and seeding of the cells to grow in a new well constitutes *one* passage. Cells lose a bit of their endothelial characteristics every time they are passaged and should only be used until their 30th passage.

Experimental samples

For the viability assays, cultured, confluent endothelial cells were gently trypsinated and brought into suspension in CO₂-dependent media. The CO₂-dependent media with the suspended endothelial cells were then transferred to a multiwell (from flexipermTM) attached

to a *Collagen IV* coated glass slide. Collagen IV is a protein found in abundance in the extracellular matrix of cells. The glass slides were coated with this extracellular matrix protein to mimic the endothelial cells' *in vivo* environment as closely as possible¹. For each viability assay, ten wells were filled with 100 μL of a 1:100 dilution of endothelial cells suspended in CO_2 -dependent media. The cells were then left to adhere to the glass slide in an ambient atmosphere with 5% CO_2 at 37°C for 24 hours.

After 24 hours, it is safe to assume that the cells are no longer stressed by the previous day's trypsination, and several "before" images were taken across each well using a regular bright field microscope with 10 \times magnification. The location of each frame was noted so that they could be replicated. Then arachidonic acid was added to eight of the ten wells, leaving the last two as controls. A stock solution of arachidonic acid was added to the eight wells, resulting in two wells with a concentration of 20.53 μM , two wells with 41.05 μM , two wells with 61.58 μM , and two wells with 82.11 μM arachidonic acid. The cells were then left to incubate in an ambient atmosphere with 5% CO_2 at 37°C for another 24 hours.

After the cells had incubated with 0, 20.53, 41.05, 61.58, or 82.11 μM of arachidonic acid for 24 hours, the "after" images were taken with each frame at the same approximate location as in the "before" picture, using the same regular bright field microscope with 10 \times magnification. The migration experiments presented later lasted 24 hours, during which arachidonic acid was present in the cells' media. The viability assay has to last for at least that long, too. The location of the wells with the different molarities was randomly chosen in each viability assay to ensure the results were unbiased with respect to the wells location in the flexipermTM multiwell.

5.3 Viability Assay Data

The proliferation rates of the cells with 20.53, 41.05, 61.58, and 82.11 μM arachidonic acid present in the media were subsequently compared to the proliferation rate of the control cells with no arachidonic acid present in the media.

The proliferation rate over 24 hours was found by comparing the number of cells in the "before" and "after" images for each frame,

$$\text{Proliferation rate} = \frac{\text{no. of cells in the "after" image}}{\text{no. of cells in the "before" image}}.$$

Figure 5.1 shows two exemplary frames' "before" and "after" images.

5.4 Results

In each viability assay, there were two wells with 0, 20.53, 41.05, 61.58, or 82.11 μM of arachidonic acid in the media. The viability assay was conducted three times, so in total

¹When left on their own, some cultured cells, such as fibroblasts or endothelial cells, will secrete extracellular matrix protein onto any surface to which they are attached [54]. In experimental adhesion studies, it is preferable to have the glass slides already coated with an extracellular protein, such as collagen IV, to facilitate the adhesion of cells and thereby minimize the amount of biological noise.

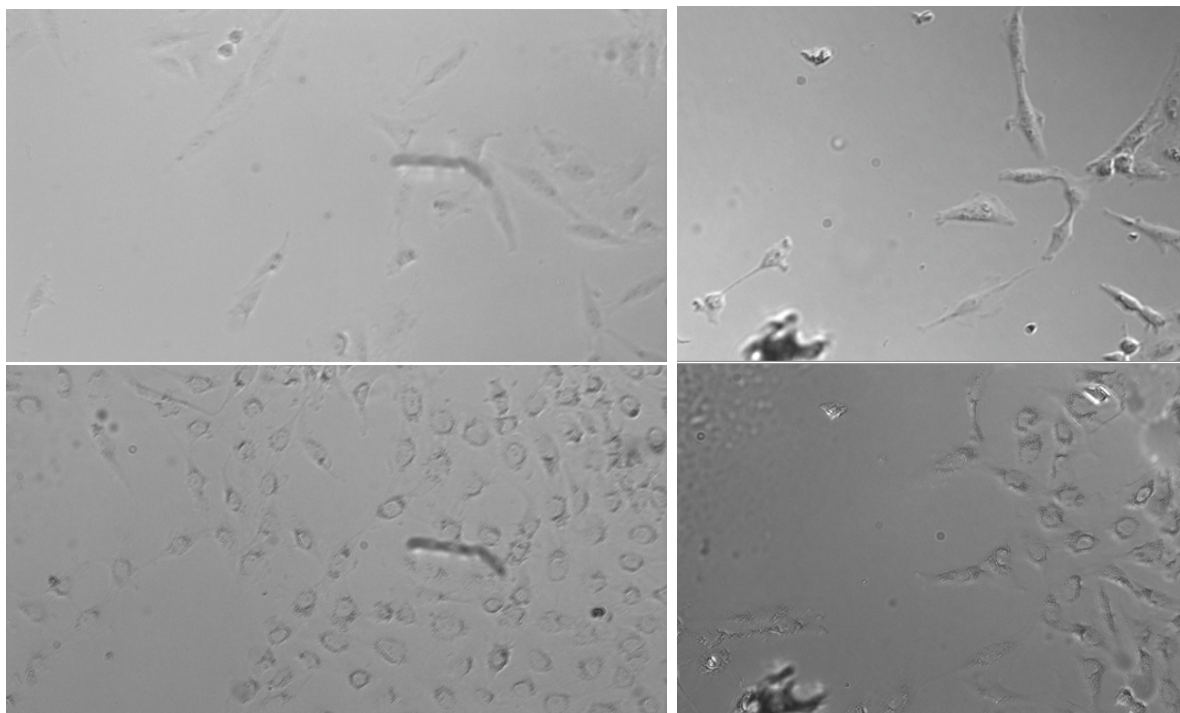


Figure 5.1: Exemplary viability assay data. Left top and bottom: Image of cell culture “before” addition of $41.05 \mu\text{M}$ arachidonic acid and “after” 24 hours of incubation with the amphiphilic compound. In this example, the proliferation rate is 2.83. Right top and bottom: Image of cell culture “before” addition of $82.11 \mu\text{M}$ arachidonic acid and “after” 24 hours of incubation with the amphiphilic compound. The proliferation rate is 2.29 in this example. Specks of dirt work as fiducial points in these images.

there were 6 independent well-observations for each concentration of arachidonic acid. In each of these wells, “before” and “after” images ($1016 \times 1016 \mu\text{m}^2$) were taken at 6 different locations across the well (8 mm diameter), amounting to a total of 36 measurements of the proliferation rates for each molarity. These proliferation rates are shown in Figure 5.2

The mean proliferation rates of the four molarities and the control lie between 2.4 and 2.8, see Figure 5.2. The mean proliferation rates show a slight trend toward lower proliferation rates for higher concentrations of arachidonic acid in the media. However, the trend is not statistically significant. This can be seen both in the p-values of student’s t-tests, none of which are remotely significant on a 5% level, < 0.05 , (Table 5.1) and in the overlapping standard deviations of the proliferation rates (Figure 5.2).

The proliferation rates in Figure 5.2 display a few outliers - a couple higher than 5 and a few lower than 1. For some of the pictures, there are specks of dirt on the glass slides which can be used as fiducial points to check the alignment of the “before” and “after” images, see Figure 5.1. Such fiducial points ensure that these images were taken at the same location, but not all frames contained specks of dirt, so the frames of some “before” and “after” images may not have been aligned exactly right. There is the possibility that outliers are due to a mismatch of “before” and “after” image frames. Mismatching the frames would

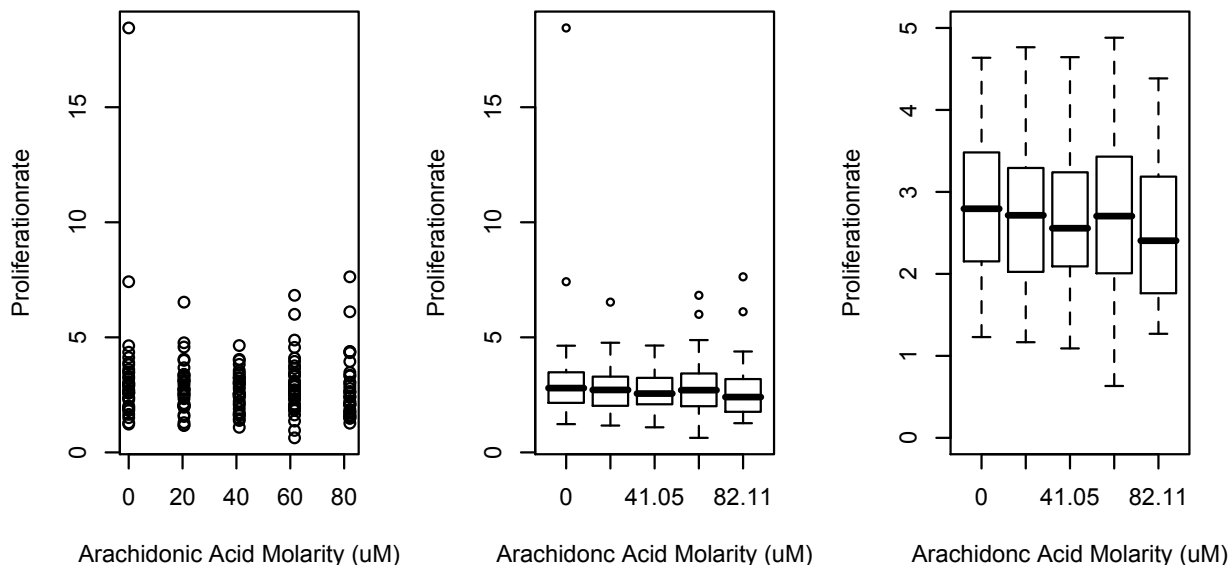


Figure 5.2: Proliferation Rate Results from the Viability Assay. Left: The 24 hour proliferation rates plotted as a function of the concentration with which arachidonic acid was present in the cells' media. Middle: A box-and-whiskers plot of the proliferation rates for the different molarities of arachidonic acid. The thick bar indicates the mean of the measurements, the box is the variance of the measurements and the whiskers are the standard deviation of the measurements. Right: A close-up of the box-and-whiskers plot.

p-values	control	20 μM AA	41 μM AA	62 μM AA	82 μM AA
control	-	0.307	0.195	0.417	0.262
20 μM AA	0.307	-	0.581	0.726	0.809
41 μM AA	0.195	0.581	-	0.379	0.831
62 μM AA	0.417	0.726	0.379	-	0.588
82 μM AA	0.262	0.809	0.831	0.588	-

Table 5.1: The p-values for a student's t-test comparing the proliferation rate for all concentrations. All p-values are > 0.05 , so none of the proliferation rates differ significantly from the control or from each other.

not matter as much if the cells were evenly scattered on the glass slides, but the cells adhere randomly to the glass slides when they are seeded, and they have a tendency to cluster. To limit the number of clusters in the viability assays, the cells were diluted 1:100 before being seeded on to the glass slides. Clusters would not only give distinct outliers in the proliferation measurement if frame locations were mismatched, they also have a naturally lower proliferation rate. A cluster is closer to confluence than scattered individual cells, and it has been noted that confluent cells produce a pressure that acts on the cells and results in signaling events that limit cell proliferation [64]. So, though the cells proliferate at a slower

rate in clusters, they are still healthy.

The endothelial cells could also migrate out of the frame's location within 24 hours. To take migration into account, the entire population of cells within each well would have to be counted. For the purpose of these viability assays, it can be assumed that the cells are seeded evenly enough that 6 frames ($1016 \times 1016 \mu\text{m}^2$) almost spanning the width of each well (8 mm) gives an accurate portrayal of the proliferation rate even if the cells do migrate in and out of the frames during the 24 hours between the "before" and "after" images.

Finally, another detail about arachidonic acid was tested. Arachidonic acid is acidic, and when added to the media, it may change the pH value of media. The pH value of the media was measured before and after the addition of arachidonic acid, and in both cases, it was 7.4 ± 0.1 . In concentrations of up to $82.11 \mu\text{M}$, arachidonic acid has no measureable effect on the pH value of the media, possibly due to the small amount of arachidonic acid or the buffer in the media.

The addition of $82.11 \mu\text{M}$ arachidonic acid or less has no statistically significant effect on the proliferation rate, and it can therefore be concluded that the cells will not be harmed by the addition of such small concentrations of arachidonic acid to the media. Any observed changes in the adhesion or migration of endothelial cells in the experiments presented here should therefore be due to the harmless presence of arachidonic acid in the media and *not* to the pathology, apoptosis, or necrosis of stressed cells.

Chapter 6

Endothelial Cell Adhesion

Endothelial cells can display a wide variety of motility at any given time during the complex process of migration. Chapter 3 described the five-step process of eukaryotic cell migration. Cell migration involves pseudopodial protrusion and retraction, filopodial protrusion and retraction, lamellipodial protrusion and retraction, blebbing, retraction of the trailing edge, and quiescence (see Section 3.3). The wide variety of motility makes it difficult to discern, analyze and understand the biophysical processes that give rise to cell migration. Biophysical and biochemical parameters are also difficult to measure on the individual cell level during migration because the migration process is so heterogeneous.

It is possible to simplify and isolate some of the cellular processes in migration in an *adhesion assay* [65]. An adhesion assay is an assay in which a cell in suspension is allowed to make contact with a substrate and subsequently adhere to and spread out across this substrate. For this reason, an adhesion assay is also called a *spreading assay*. When a cell spreads, it is the behavior of the cytoskeletal remodeling that is the most pronounced, so an adhesion assay isolates the cytoskeletal behavior from the myriad of other cellular processes that go on during migration [65].

When grown *in vitro*, cells are usually spread out in a monolayer. However, when a cell is going through mitosis, it will almost detach from the surface and ball up into a spherical configuration [66]. It is easier for a cell to organize itself in a spherical configuration, and balling up facilitates division. When mitosis is completed, the two daughter cells will adhere to and spread out onto the surface, see Figure 6.1. An adhesion assay is physiologically relevant since the adhesion and spreading of a cell occurs naturally post-mitosis. A non-post-mitosis cell *in vitro* can be detached and brought into suspension to mimic this naturally occurring phenomenon.

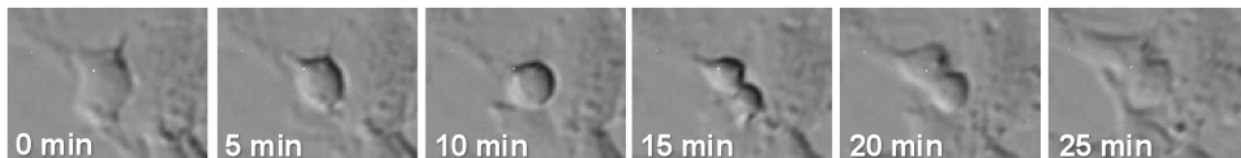


Figure 6.1: Images from own *in vitro* observation of an endothelial cell going through mitosis.

In suspension the cell has a spherical configuration. The process of a suspended cell making contact with, adhering to and spreading onto a substrate is illustrated in Figure 6.2. A cell in suspension usually initiates adhesion and spreading by extending filopodia which tests the substrate's adherence suitability. If the substrate is found suitable, the cytoskeleton will remodel to accommodate the spreading of the cell onto the surface [67], as seen in Figure 6.2. In order to mimic the *in vivo* environment as closely as possible, the substrates used in adhesion assays are usually proteins found in the extracellular matrix of cells.

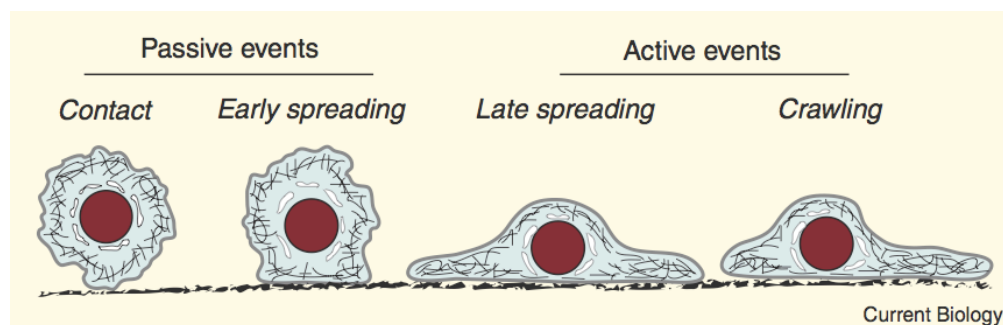


Figure 6.2: A schematic of a cell adhering to and spreading out on a surface over time from left to right (from McGrath 2007 [68]). The early stages of the spreading are characterized by passive processes since the cell is not required to expend metabolic energy, whereas the later stages of cell spreading and the subsequent motility (crawling of the cell) involve the active processes of actin polymerization and myosin contraction.

The adhesion area, i.e., the area of contact between a cell and the substrate as the cell spreads, is a widely used variable to establish the role a particular molecule or disease plays in cytoskeletal regulation [65, 69, 70, 71, 72, 73]. If a molecule or disease plays a noticeable role in cytoskeletal regulation, it will change the temporal development of the adhesion area, i.e., the adhesion area's enlargement as a function of time.

Amphiphilic compounds have been shown to have a regulating effect on the migration of endothelial cells [35], see Section 4. As previously mentioned, the process of migration is very complex, and the regulating effects of amphiphilic compounds may be more easily investigated in adhesion assays that simplify the process of migration. One amphiphilic compound, arachidonic acid (AA), is of particular interest since it has the ability to inhibit *or* to enhance endothelial cell migration depending on the concentration at which it is present in the cells' media (see Section 4).

The aim of this chapter is to establish what role the addition of arachidonic acid to the cells' media plays in cytoskeletal regulation. The analysis in this chapter will attempt to answer the question: Does arachidonic acid affect endothelial cell migration through a regulation of the cytoskeletal remodeling? Any arachidonic acid in the cells' media will be spontaneously incorporated into the cell's membrane. This incorporation will induce a change in the physical properties of the cells' membrane. Would changes in the physical properties of the cell membrane in endothelial cells induced by arachidonic acid change the adhesion process noticeably?

To answer such questions, it is important first to characterize the adhesion and spreading of

a regular cell in which no change has been induced, thereby establishing a standard to which possible induced changes, brought about by the harmless addition of arachidonic acid, can be compared.

6.1 Models for Endothelial Cell Adhesion

There are many adhesion assay studies in the literature, though not many specifically on endothelial cells and none (to my knowledge) involving the characterization of an induced change in the physical properties of the membrane. The temporal development of the adhesion area of mammalian cells in general has been characterized previously [65, 67, 74, 75, 69, 70, 71, 72, 73, 76, 77, 78]. The reported results have differed somewhat, both in their pre-analysis treatment of data and in the resulting proposed models. In the following, three proposed models will be presented and discussed: ¹⁾ the three phase model, ²⁾ the two phase model and ³⁾ a model without phases.

To date, nothing has been published that constructively investigates the differences between the proposed two and three phase models. Here, a reconciliation of the two and three phase model is proposed following the description of these models. The reconciliation of the two and three phase model will provide the basis on which the experimental data is analyzed. Because there are no similar analyses in the literature, the theoretical section of this chapter will be quite substantial.

6.1.1 The three phase model

In 2004 Döbereiner and his collaborators [67] published a model for the adhesion area's temporal development based on observations of adhering and spreading mouse embryonic fibroblasts on a fibronectin substrate. This model consisted of *three* well-defined and distinct spreading phases (see Figure 6.3):

- P0: The lag-phase is the phase with a slow increase in the adhesion area between the adhering cell and the substrate. During this phase, the cell is hypothesized to test the adhesion suitability of the substrate through filopodial sensing [67].
- P1: The middle, rapidly spreading phase is the phase in which the adhesion area between the adhering cell and the substrate increases rapidly.
- P2: The final, saturatingly spreading phase is the phase in which the adhesion area between the cell and the substrate increase less rapidly until the size of the adhesion area saturates. This phase is characterized by periodic protrusions and retractions of lamellipodia along the edge of the adhesion area. Periodic membrane retractions are a general phenomenon and have also been found in migrating fibroblasts, as well as in endothelial cells [67].

Three such phases have been observed and described in several detailed light- and electron-microscope studies [65, 67, 74, 75].

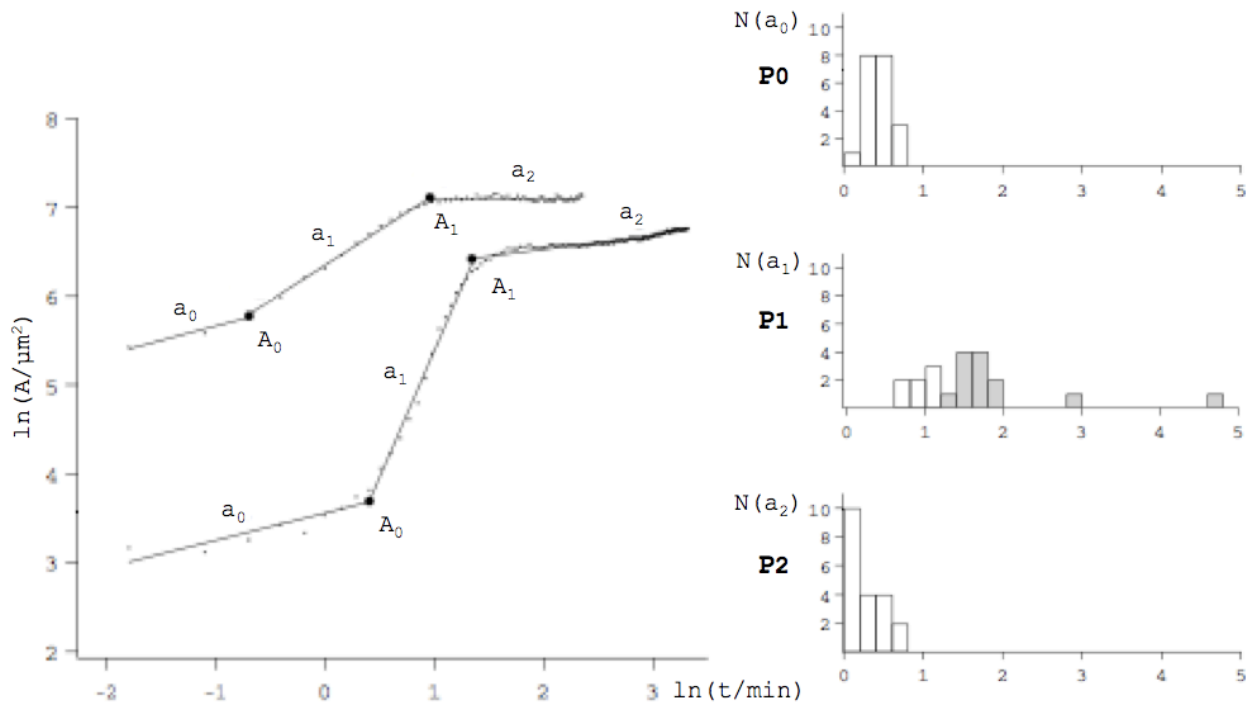


Figure 6.3: Adhesion in isotropically spreading fibroblasts increases with a scaling law in time, $A(t) \propto t^{a_i}$. Different but constant exponents a_i in the various phases of spreading area are evident in a double logarithmic plot as the slope of the linear sections. Left: The adhesion area plotted as a function of time on a double logarithmic plot for two adhering fibroblasts. The exponential constants in the scaling law have been determined by fitting a piecewise linear function to the data. Adhesion areas A_i at the transitions points are also indicated (A_0 and A_1). Right: Histograms of the exponential constants as obtained from the slopes of double logarithmic plots of adhesion area versus time, such as shown to the left. A total of 20 cells adhering and going through three phases (P0, P1 and P2) were analyzed. The middle phase, P1, with continuous spreading exhibits clustering corresponding to small (open bars) and large (solid bars) relative area growth during that phase, i.e., $A_1/A_0 < 5$ or $A_1/A_0 > 5$. (from Döbereiner *et al.* 2004 [67])

Döbereiner *et al.* [67] analyzed the adhesion area A over time in a double logarithmic plot where the three phases can be readily seen (see Figure 6.3). The adhesion area increases differently in each phase. These increases in area are described by scaling laws for the adhesion area, $A(t) \propto t^{\text{constant}}$. The scaling laws are distinctly different for each phase and show up as periods of linear growth in the double logarithmic plot. Denoting each phase by an index, $i = \{0, 1, 2\}$, the scaling laws are

$$A(t) \propto t^{a_i} \quad ,$$

$$\text{since } \ln(A(t)) \propto a_i \cdot \ln(t) \quad .$$

The slope in the double logarithmic plot has thus been used to express the exponential constant of the scaling law by Döbereiner *et al.*. However, there are pitfalls associated with analyzing data using a double logarithmic plot, as the slope does not always express the true

scaling law. This will be discussed in much more detail in Section 6.1.4.

The values for the exponential constant in the scaling laws for the increase in the adhesion area, a_i , found by Döbereiner and his collaborators in 2004 were:

Model:	a_0 (P0)	a_1 (P1)	a_2 (P2)
three phase	0.4 ± 0.2	1.6 ± 0.9	0.3 ± 0.2

These values were based on 20 experiments conducted on mouse fibroblasts on a fibronectin substrate and have since been confirmed by other publications from the same group using the same analysis [79, 67, 80, 65].

Figure 6.3 also shows histograms of the exponential constants, a_i , for the three phases as derived from the 20 adhesion assays in which single cells adhered and went through all three phases (P0, P1 and P2). The distributions of a_0 , a_1 and a_2 are distinct but rather broad. Particularly in the case of P1, where $a_1 = 1.6 \pm 0.9$. Döbereiner *et al.* propose a further grouping of the cells to rectify the large standard deviation. They separate the 20 cells into two groups according to the adhesion area's relative increase in the P1 phase. This relative increase is denoted, A_1/A_0 , where A_0 denotes the adhesion area at the transition from phase P0 to P1, and A_1 denotes the adhesion area at the transition from phase P1 to P2. With this discrimination, smaller increases in area ($A_1/A_0 < 5$) have an exponential growth of $a_1 = 0.9 \pm 0.2$, whereas larger increases in area ($A_1/A_0 > 5$) have an exponential growth of $a_1 = 1.6 \pm 0.2$ [67].

The adhering fibroblast in the 20 adhesion assays described above spread angularly isotropically [67], i.e., they spread out almost spherically. Döbereiner *et al.* also reported that 70 % of their cells from a different experiment spread angularly isotropically in medium lacking serum, compared to only 20 % in medium with the normal serum level of 10% fetal bovine serum (FBS) [67]. Fibroblasts are also prone to angular isotropic spreading, whereas endothelial cells are not.

Comments on the three phase model:

The three phase model proposed by Döbereiner and his collaborators cannot be verified as such since it is solely a statement of their observations and not derived mathematically from physical assumptions of the system. They do not offer any physical explanations of their results for the distinct exponential growth, though they try to limit the standard deviation of their results by further separating the cells into two groups based on their relative growth in phase P1. Though the deviations of the exponents are much smaller when discriminating cells with respect to their relative increase, A_1/A_0 , there is no apparent physiological reason for doing so. The relative increase could be closely correlated and even dependent on a_1 . For example, if the phase P1 had a certain duration, the exponential growth a_1 would dictate how much the cell's adhesion area grew in this phase, A_1/A_0 . Simply discriminating the cells at $A_1/A_0 = 5$ does not investigate any such relation, and without coming to any in depth conclusions, discriminating the cells at $A_1/A_0 = 5$ only serves to improve the statistics.

The data presented by Döbereiner *et al.* [67] is not treated or adjusted before being analyzed on a double logarithmic plot. Any conclusion based on unadjusted data may appear

stronger/more robust, but double logarithmic plots should be used with care, as Section 6.1.4 will show. The recording of data was initiated at arbitrary times compared to the spreading of the cell. The fact that data remain unadjusted for this arbitrariness may weaken their conclusions in the end.

The middle, rapidly spreading phase, P1, lasts only until the adhesion area reaches a certain size (around $\ln(A) = 7\mu\text{m}^2$ for the fibroblasts) and this may be the limit to which passive spreading can occur, i.e., where further spreading can only happen through actin-polymerization. In the final, saturatingly spreading phase, P2, the cell adhesion area increases less rapidly (a_2 is small). The last phase is characterized by periodic local protrusion and retractions of lamellipodia along the cell's edge [81]. These local protrusions and retractions require active spreading in the form of actin polymerization, i.e., active spreading, which is a slower process than passive spreading.

Classifying cellular behavior within well-defined phases can simplify the description of biophysical phenomena considerably. There are three phases, many fewer than in an enumeration of the concentration and activity levels of all molecular components of the cell that have an impact on cell adhesion and spreading. The conceptual advantage of such a classification is that one can characterize physical states (phases) of an adhering cell without a complete understanding of the complex signaling network that regulates it. Phase classification also enables a sensible comparison between different cellular phenotypes across genotypes. Döbereiner *et al.* appeal to researchers to use the classification of spreading motility into phases to serve as a paradigm to obtain a powerful general ordering principle in quantitative biology [67].

6.1.2 The two phase model

A comparison of adhesion assays across several genotypes was conducted in 2007 by Cuvelier and his collaborators [76], which showed that the temporal development of the adhesion area showed *two* distinct phases. They published data that supported a “universal” two phase model, which was derived from the physical assumptions of a simple cell model. The model claims to be “universal” because it contains no cell-type specific parameters, and it was experimentally verified with many different cell types, such as sarcoma murine, human HeLa and red blood cells and with many different types of substrates, such as fibronectin and polylysine [76]. The two phase model consist of only two phases, as opposed to the previous three phase model (see Figure 6.4):

P1 The early, rapidly spreading phase is the phase with a rapid increase in the adhesion area between the cell and the substrate.

P2 The later phase is the phase with a less rapid increase and a saturation of the adhesion area.

The notation P1 and P2 has been used again to illustrate the similarities and the overlap between the two and the three phase model.

Comparing the two phase model to the three phase model, it has an apparent lack of an early lag-phase. This lack may be explained by the pre-analysis treatment of the experimental

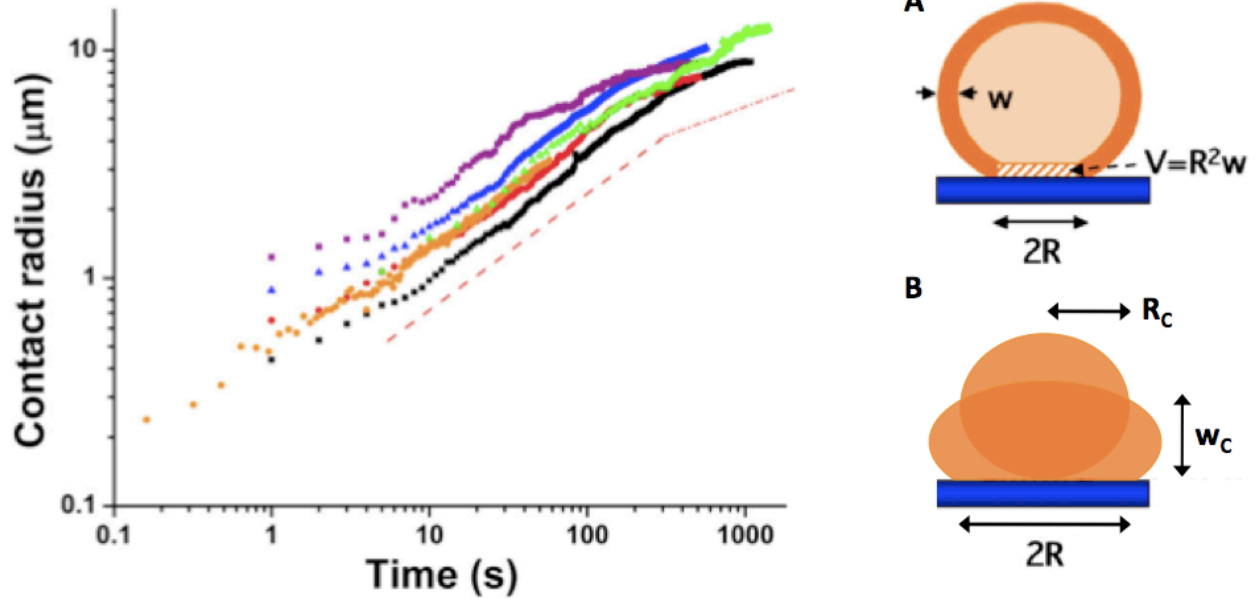


Figure 6.4: Left: The increase in the adhering cells' adhesion area during the early stages of spreading exhibits a universal power law that is independent of cell type, substrate, and adhesion receptors. Lag-times are subtracted so the time ≈ 1 corresponds to the onset of spreading. The average radius of the adhesion area increases initially as $t^{\frac{1}{2}}$ (the lower red dashed line in the middle indicates $R \propto t^{\frac{1}{2}}$) over more than three decades in time before slowing down (the upper red dash-dotted line to the right indicates $R \propto t^{\frac{1}{4}}$). The different curves are representative of a variety of experimental conditions corresponding to: HeLa cell on a fibronectin substrate (black square); E-cadherin expressing cells on a E-cadherin substrate (green triangle); filopodia inhibited cells on a fibronectin substrate (red circle); microtubule-disrupted HeLa cells on a fibronectin substrate (purple square); HeLa cells on a polylysine substrate (blue triangle); and biotinylated red blood cell on a streptavidin substrate (orange circle). Right: Schematic representations of the cell as modeled in the two phases (from Cuvelier *et al.* 2007 [76]). (A) In the early phase, P1, the cell is modeled as “a viscous shell enclosing a liquid”. The volume in which viscous dissipation is assumed to occur is shaded (from Cuvelier *et al.* 2007 [76]). (B) In the later phase, P2, the cell is modelled as “a homogeneous, viscous drop”. The viscous dissipation is assumed to occur within the entire drop (this schematic is made based on the description in Cuvelier *et al.* 2007 [76]).

data. Cuvelier *et al.* only address the dynamics of cell spreading after contact initiation and the onset of spreading, i.e., they have subtracted lag-times, t_0 's, from their data before analyzing it [76]. Two phases in cell adhesion have been observed in several studies [76, 77, 78]. In these studies, any possibly observed lag-times were either adjusted for or disregarded. Cuvelier and his collaborators even show that some of the data presented by Döbereiner *et al.* in 2004 supporting the three phase model does not contradict the two phase model when it has been adjusted for lag-times [76] (see Figure 6.5). Figure 6.4 shows the experimental data that supports the two phase model plotted on a double logarithmic plot. The linear

growth in the double logarithmic plot reveals the possibility of a distinct scaling law for each of the two phases.

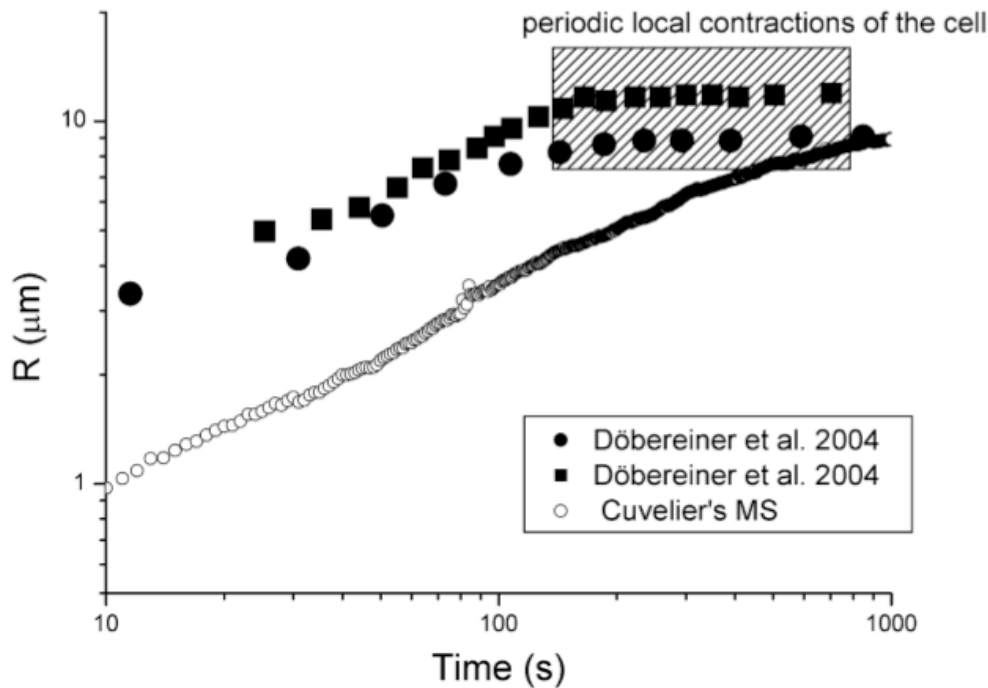


Figure 6.5: Some data from Döbereiner *et al.* lag-time adjusted by Cuvelier *et al.* to show that this data also supports the two phase model (from the supplemental discussion in Cuvelier *et al.* 2007 [76])

To mathematically derive the scaling laws of the phases, Cuvelier *et al.* use a simple model for the cell, modeling the cell either as “a membraneous, viscous shell enclosing a liquid” or as “an entirely viscous drop”. The cell is thus modeled differently in each of the two phases. Figure 6.4 shows schematic representations of these two different models for the cell. One is taken directly from Cuvelier *et al.* 2007, and the other is made based on their descriptions.

The approach to determining the temporal development of the adhesion area between a spreading cell and a substrate is the same in both phases and found by balancing the different powers believed to be exerted during cell spreading. The powers they believe to be exerted are: a dissipative power and an adhesive power. The spreading of a cell onto a substrate causes cell deformation and flattening, which leads to a viscous dissipative energy. During cell spreading, there is also an increase in the adhesion area between the cell and the substrate, to which the cell binds with both specific and non-specific interactions. This increases the adhesive energy of the cell. The power of these two types of energy is balanced,

$$P_{\text{dissipative}} = P_{\text{adhesive}} \quad .$$

The cell is in itself a source of energy that can and is used for remodeling the cell’s cytoskeleton to accommodate adhesion. In the two phase model, it is explicitly assumed that during the early stages of adhesion the spreading is passive (see Figure 6.2), and energy is

not directed explicitly at enhancing or reducing adhesion [76]. The early stage is defined as up until the time when the radius of the adhesion area, $R(t)$, exceeds the radius of the initial spherical cell in suspension, R_C , see Figure 6.4.

The early stage, P1, in the two phase model for $R(t) \leq R_C$

The early stage, P1, is defined as the stage of passive spreading, i.e., when the radius of the adhesion area is less than the radius of the initial cell in suspension $R(t) \leq R_C$. At this stage, the cell is modelled as a membraneous, viscous shell that encloses a liquid cytoplasm. The adhesion area is assumed to be of an angularly isotropic, disc-like shape. The rate of change for the adhesion area, $\frac{dA}{dt}$, can then be denoted using the radius of the adhesion area, R , as $\frac{dA}{dt} = 2\pi R \frac{dR}{dt}$, since $A = \pi R^2$.

The power of adhesive energy is

$$P_{\text{adhesive}} = J \frac{dA}{dt} = 2\pi R J \frac{dR}{dt} ,$$

if J is the adhesion energy per unit area, $J = (\text{areal density of adhesive bonds}) \cdot (\text{energy per bond})$.

The power of viscous, dissipative energy of the viscous flow within the shell on the affected volume is

$$P_{\text{dissipative}} = \int \eta (\nabla u)^2 dv = \eta \left(\frac{dR}{dt} \frac{1}{w} \right)^2 \cdot w\pi R^2 .$$

Here η is the viscosity of the membraneous, viscous shell, $\nabla u = \frac{dR}{dt} \frac{1}{w}$ is the characteristic strain rate¹, w is the width of the shell, and $w\pi R^2$ is the characteristic volume of the viscous shell in which the dissipation occurs according to this model. The flow of matter that enables the spreading of the model cell is assumed to happen in the membraneous, viscous shell and not in the cytoplasmic liquid within the cell. Furthermore, the actual adhesion area is assumed to be the part of the cell's membrane that accommodates the flow.

Balancing the two powers, the power of the viscous dissipative energy ($P_{\text{dissipative}}$) and the power of the adhesive energy of the cell (P_{adhesive}), the following scaling law for the temporal

¹The characteristic strain rate ∇u is supposedly induced by the shearing of cortical actin filaments within the membraneous shell [76]. These filaments are sheared as the shell deforms to adhere to the surface, and for short times the size of the contact area is comparable to the length of the cortical filaments in the cell [76]. The characteristic strain rate of this physical picture is of an order of $\nabla u = \frac{de}{dt} = \frac{1}{w} \cdot \frac{dR}{dt}$, where w is the width of the membraneous, viscous shell. An approximation has also been made with regards to the velocity vector u . Velocities vary from 0 in the middle of the contact zone to $\frac{dR}{dt}$ at the edge of the contact zone, but the characteristic velocity in the entire zone has been averaged to $\frac{dR}{dt} \frac{1}{w}$.

development of the contact area emerges:

$$\begin{array}{l}
\Downarrow \\
\Downarrow \\
\Downarrow \\
\Downarrow \\
\Downarrow
\end{array}
\begin{array}{l}
P_{\text{dissipative}} \propto P_{\text{adhesive}} \\
\eta \left(\frac{dR}{dt} \frac{1}{w} \right)^2 \cdot w \pi R^2 \propto \pi R J \frac{dR}{dt} \\
R \frac{dR}{dt} \propto \frac{Jw}{\eta} \\
\int R dR \propto \int \frac{Jw}{\eta} dt \\
R^2 \propto \left(\frac{Jw}{\eta} \right) t \\
R \propto \left(\frac{Jw}{\eta} \right)^{\frac{1}{2}} t^{\frac{1}{2}}, \quad \text{for } R \leq R_C.
\end{array}$$

The model's predictions for a scaling law for the rapid, early passive spreading of the cell (P1) becomes $R(t) \propto t^{\frac{1}{2}}$, when $R(t) \leq R_C$.

Comments on the early stage of the two phase model:

In the derivation above, the characteristic strain rate of the viscous dissipation only applies to the characteristic volume, which is assumed to be the part of the shell that constitutes the adhesion area between the cell and the substrate (Figure 6.4). This is a reasonable assumption if a cell is modeled as a simple, passive, membraneous, viscous shell that encloses a liquid cytoplasm. However, real cells adhere to a substrate actively through integrin bonds (see Section 3). Integrins are transmembrane proteins that span the membrane anchoring the cytoskeleton on the inside of the cell to the extracellularmatrix proteins constituting the substrate on the outside of the cell.

In my opinion, the anchoring of the cytoskeleton through the membrane would pin the membrane to the substrate. It would still be possible for the lipids and the membrane-embedded proteins to rotate and move laterally within the membrane but probably not as freely as the model's assumptions would suggest. I argue that when a cell adheres to a substrate, it is the cytoskeleton itself that adheres to the substrate, pinning down the membrane in the process (and not a passive, viscous shell adhering through non-specific interactions). If the membrane of the adhesion area is pinned down, it cannot flow as easily to accommodate the spreading of the cell. The viscous dissipation in the shell would instead occur at *the edge* of the adhesion area and the unattached part of the shell immediately adjacent to it. The characteristic volume, V , in which dissipation occurs should then be given as a circular band of breadth b with $V = w \cdot (\pi(R+b)^2 - \pi R^2) = w \cdot \pi(b^2 + 2Rb)$. The scaling law for the temporal development then becomes

$$\begin{array}{l}
\Downarrow \\
\Downarrow \\
\Downarrow \\
\Downarrow
\end{array}
\begin{array}{l}
P_{\text{dissipative}} \propto P_{\text{adhesive}} \\
\eta \left(\frac{dR}{dt} \frac{1}{w} \right)^2 w \cdot \pi(b^2 + 2Rb) \propto \pi R J \frac{dR}{dt} \\
\frac{b^2 + 2Rb}{R} \frac{dR}{dt} \propto \frac{Jw}{\eta} \\
\int \frac{b^2 + 2Rb}{R} dR \propto \int \frac{Jw}{\eta} dt \\
b^2 \ln |R| + 2bR \propto \left(\frac{Jw}{\eta} \right) t, \quad \text{for } R > R_C.
\end{array}$$

If the characteristic volume is a band at the edge of the adhesion area, rather than the part of the shell that constitutes the adhesion area, the resulting alternative "scaling law"

for $R \leq R_C$ as an expression of $R(t)$ is hard to derive analytically. However, the function $b^2 \ln |R| + 2bR = \left(\frac{Jw}{\eta}\right) t$ is continuous and has a positive derivative $\frac{dt}{dR} > 0$ for J, w, η and $R > 0$. This makes the function invertible, and any fitted solution to $t(R)$ will also be a solution to $R(t)$ for J, w, η and $R > 0$. It is thus possible to fit $R(t)$ to data despite the lack of an analytical expression for this function. The overall shape of the resulting alternative “scaling law” for the function $b^2 \ln |R| + 2bR \propto t$ is compared to $R \propto t^{\frac{1}{2}}$ in Figure 6.6.

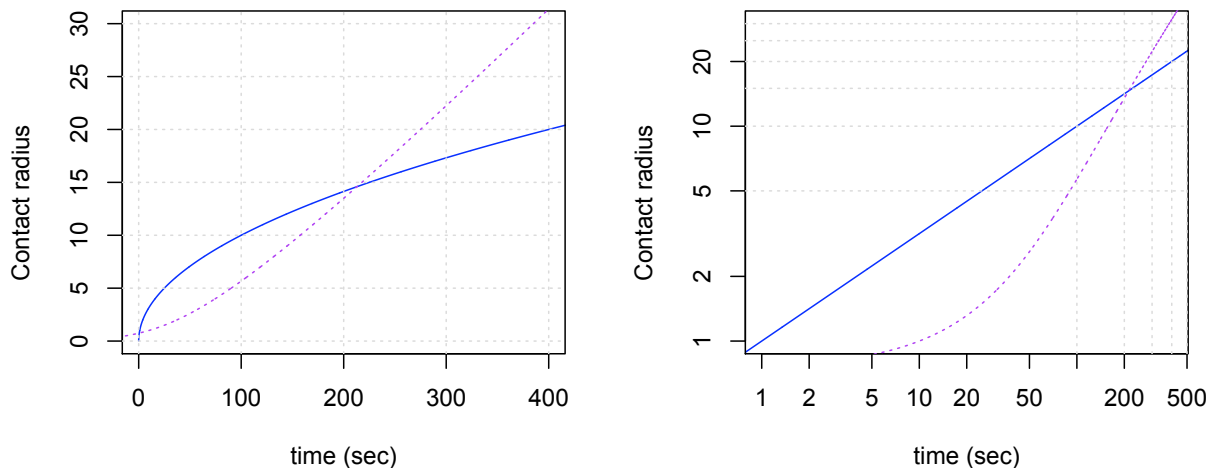


Figure 6.6: The shape of the alternative “scaling law” in the early stage, P1, in which the radius of the adhesion area is smaller than the radius of the initial cell in suspension $R(t) < R_C$. The alternative “scaling law” $b^2 \ln |R| + 2bR \propto t$ (dashed purple line) for the early stage P1, where $b = 5$, is compared to the original scaling law for the two phase model $R \propto t^{\frac{1}{2}}$ (full blue line). These two “scaling laws” have been compared both on a regular plot on the left and on a double logarithmic plot on the right.

Taking a closer look at $b^2 \ln |R| + 2bR \propto t$, there are some restrictions as to which units R can be measured. Since $t > 0$, R should be measured in units where $b^2 \ln |R| + 2bR > 0$ for all t in the lag-time adjusted data. For endothelial cells, R can safely be measured in μm .

The alternative “scaling law” for the early phase, P1, will be compared to the one proposed by Cuvelier *et al.* in Section 6.6

The later stage, P2, in the two phase model for $R(t) > R_C$

The later stage, P2, is defined as the stage of active spreading, i.e., when the radius of the adhesion area exceeds the initial radius of the cell, $R > R_C$. At this stage, the cell spreads actively by forming lamellipodia. Lamellipodia formation requires active actin polymerization, so the cell is explicitly directing energy at enhancing adhesion. Cuvelier and his

collaborators propose a different model from the early phase ($R \leq R_C$) to reflect this. In the later stage $R > R_C$, the cell is no longer modeled as “a membrane-bound viscous shell that encloses a liquid cytoplasm”, but instead as “an entirely viscous drop”. The assumption is that when the cell begins to spread out actively, the viscous dissipation that accommodates the spreading will occur in the entire cell [76].

The power of adhesive energy is still the same for this new cell model

$$P_{\text{adhesive}} = J \frac{dA}{dt} = 2\pi R J \frac{dR}{dt} \quad ,$$

where J is the adhesion energy per unit area, and the rate of change for the adhesion area, $\frac{dA}{dt}$, is still denoted using the radius of the adhesion area, R , as $\frac{dA}{dt} = 2\pi R \frac{dR}{dt}$.

The power of viscous, dissipative energy is also still given as

$$P_{\text{dissipative}} = \int \eta (\nabla u)^2 dv \quad .$$

However, since the membrane and the cytoplasm are now modeled as one entity, and the viscous dissipation is assumed to occur in the entire cell, the viscosity η and the characteristic volume is different from the previous cell model in the early phase. Here, η_C and w_C denote the viscosity and the width of the cell as an entity, respectively [76]. The characteristic volume in which dissipation occurs is now the entire cell, which Cuvelier *et al.* approximate to $w_C \cdot \pi R^2$ (they assume that the cell has the shape of a small, fat cylinder). The power of viscous, dissipative energy becomes

$$P_{\text{dissipative}} = \eta_C \left(\frac{dR}{dt} \frac{1}{w_C} \right)^2 \cdot w_C \pi R^2 \quad .$$

The balancing of the adhesive and viscous power then leads to the following scaling law:

$$\begin{aligned} P_{\text{dissipative}} &\propto P_{\text{adhesive}} \\ \Downarrow & \eta_C \left(\frac{dR}{dt} \frac{1}{w_C} \right)^2 \cdot w_C \pi R^2 \propto 2\pi R J \frac{dR}{dt} \\ \Downarrow & \eta_C \left(\frac{dR}{dt} \frac{1}{w_C} \right)^2 \cdot w_C \pi R^2 \cdot \frac{4}{3} \pi R_C^3 \propto 2\pi R J \frac{dR}{dt} \cdot \frac{4}{3} \pi R_C^3 \end{aligned}$$

An extension of $\frac{4}{3} \pi R_C^3$ at this stage will make a different scaling law appear. The cell is assumed to be of a conserved volume throughout the adhesion process, so if w_C is the height of the spreading cell and R_C is the radius of the initial, spherical cell, it then follows that the approximate volume of the cell is $w_C \cdot \pi R^2 = \frac{4}{3} \pi R_C^3$.

$$\begin{aligned} \Downarrow & \eta_C \left(\frac{dR}{dt} \frac{1}{w_C} \right)^2 \cdot w_C \pi R^2 \cdot w_C \pi R^2 \propto 2\pi R J \frac{dR}{dt} \cdot \frac{4}{3} \pi R_C^3 \\ \Downarrow & R^3 \frac{dR}{dt} \propto \frac{J \cdot R_C^3}{\eta_C} \\ \Downarrow & \int R^3 dR \propto \int \frac{J \cdot R_C^3}{3\eta_C} dt \\ \Downarrow & R^4 \propto \frac{J \cdot R_C^3}{\eta_C} \cdot t \\ \Downarrow & R \propto \left(\frac{J \cdot R_C^3}{\eta_C} \right)^{\frac{1}{4}} \cdot t^{\frac{1}{4}}, \quad \text{for } R > R_C. \end{aligned}$$

The model’s predictions for a scaling law for the saturated later active spreading of the cell (P2) becomes $R \propto t^{\frac{1}{4}}$ when $R > R_C$.

Comments on the later stage of the two phase model:

The different scaling laws in the early and later stages of the two phase model are only due to the “trick” of extending the equation with $\frac{4}{3}\pi R_C^3$. Otherwise, the later scaling law would have been $R \propto \left(\frac{Jw_C}{\eta_C}\right)^{\frac{1}{2}} \cdot t^{\frac{1}{2}}$, which is the same scaling law as in the early phase, P1. There is nothing wrong with extending the equation, and it may even be argued that the extension rightly introduces the issue of the cell’s conserved volume to the problem mathematically. *Two* alternative “scaling laws” will be proposed in the following, one which uses the conserved volume extension and one which does not, to investigate both options.

The derivation of the scaling law for the later phase of cell spreading assumes that the cell can be modeled as an entirely viscous drop. Though the actin meshwork has the same properties as an active gel, and such a model provides simple calculations, the membrane and the actin cytoskeleton are still two very distinct entities. A model that cannot incorporate and model both of these entities is not as convincing. If the cell is still modeled as a membrane-bound, viscous shell that encloses a liquid cytoplasm (as in the early phase), different assumptions for the way the cell directs energy explicitly at enhancing adhesion will have to be made. The power of adhesive energy could be:

$$P_{\text{adhesive}} = J \frac{dA}{dt} - P \frac{dA}{dt} = 2\pi R(J - P) \frac{dR}{dt} \quad \text{for } R > R_C \quad ,$$

where J is the adhesion energy per unit area, and P is the energy expense of actin polymerization per unit area. In Cuvelier *et al.*’s derivation for the later phase, the power of adhesive energy is, in my opinion, erroneously still the same as before since the energy expense of active spreading is not taken into account.

In Cuvelier *et al.*’s derivation, the volume of the spreading cell is assumed to be approximately $w_C \cdot \pi R^2$, i.e., the cell resembles a small, fat cylinder. The three dimensional shape of an actual spreading cell will later be seen to be much more like a fried egg (see Section 6.5). The volume of an “egg-white” radius of R , a fried egg with a “yolk radius” of r , an “egg-white” height of h , and a “yolk” height of $h+r$ is approximately $V \approx \pi R^2 h + \frac{1}{2} 2\pi^2 R h^2 + \frac{1}{2} \frac{4}{3} \pi r^3$. The surface area of the “fried egg” is approximately $A_{\text{surface}} \approx 2\pi R^2 - \pi r^2 + \frac{1}{2} 4\pi^2 R h + \frac{1}{2} 4\pi r^2$.

As in my objections to the derivation of the scaling law for the early phase, I maintain that once a part of the cell has adhered, the cytoskeleton effectively pins the membrane to the substrate. The viscous dissipation would then occur primarily in the unattached part of the viscous shell, $V_{\text{affected}} = w \cdot (A_{\text{surface}} - \text{adhesion area}) \approx w \cdot ((2\pi R^2 - \pi r^2 + \frac{1}{2} 4\pi^2 R h + \frac{1}{2} 4\pi r^2) - \pi R^2) = w \cdot (\pi R^2 + 2\pi^2 R h + \pi r^2)$. The viscous power changes to

$$\begin{aligned} P_{\text{dissipative}} &= \int \eta (\nabla u)^2 dv \\ &= \eta \left(\frac{dR}{dt} \frac{1}{w} \right)^2 w \cdot (\pi R^2 + 2\pi^2 R h + \pi r^2), \end{aligned}$$

as a consequence of the newly defined affected characteristic volume of the viscous shell that experiences the characteristic strain.

Balancing the power of adhesive energy and the power of dissipative energy, the following relation between adhesion area and time appears:

$$\begin{aligned}
& P_{\text{dissipative}} \propto P_{\text{adhesive}} \\
\Downarrow & \quad \eta \left(\frac{dR}{dt} \frac{1}{w} \right)^2 w \cdot (\pi R^2 + 2\pi^2 Rh + \pi r^2) \propto \pi R (J - P) \frac{dR}{dt} \\
\Downarrow & \quad \frac{dR}{dt} (R^2 + 2\pi Rh + r^2) \frac{1}{R} \propto \frac{w(J-P)}{\eta} \\
\Downarrow & \quad \int (R^2 + 2\pi Rh + r^2) \frac{1}{R} dR \propto \int \frac{w(J-P)}{\eta} dt \\
\Downarrow & \quad \frac{1}{2} R^2 + 2\pi Rh + r^2 \ln |R| \propto \frac{w(J-P)}{\eta} \cdot t, \text{ for } R > R_C.
\end{aligned}$$

Another scaling law will appear if the equation is extended with the conserved volume of the cell $\frac{4}{3}\pi R_C^3$:

$$\begin{aligned}
& P_{\text{dissipative}} \propto P_{\text{adhesive}} \\
\Downarrow & \quad \eta \left(\frac{dR}{dt} \frac{1}{w} \right)^2 w \cdot (\pi R^2 + 2\pi^2 Rh + \pi r^2) \propto \pi R (J - P) \frac{dR}{dt} \\
\Downarrow & \quad \eta \left(\frac{dR}{dt} \frac{1}{w} \right)^2 w \cdot (\pi R^2 + 2\pi^2 Rh + \pi r^2) \cdot \frac{4}{3}\pi R_C^3 \propto \pi R (J - P) \frac{dR}{dt} \cdot \frac{4}{3}\pi R_C^3
\end{aligned}$$

The equation is extended with $\frac{4}{3}\pi R_C^3$ at this stage just as Cuvelier and his collaborators do, since this will make a different scaling law appear. The cell is still assumed to be of a conserved volume throughout the adhesion process, so $V \approx \pi R^2 h + \frac{1}{2} 2\pi^2 R h^2 + \frac{1}{2} \frac{4}{3} \pi r^3 = \pi R^2 h + \pi^2 R h^2 + \frac{2}{3} \pi r^3 = \frac{4}{3} \pi R_C^3$.

$$\begin{aligned}
& \eta \left(\frac{dR}{dt} \frac{1}{w} \right)^2 w (\pi R^2 + 2\pi^2 Rh + \pi r^2) (\pi R^2 h + \pi^2 R h^2 + \frac{2}{3} \pi r^3) \propto \pi R (J - P) \frac{dR}{dt} \frac{4}{3} \pi R_C^3 \\
\Downarrow & \quad \frac{dR}{dt} (hR^4 + (\pi h^2 + 2\pi h^2) R^3 + \\
& \quad (\frac{2}{3} r^3 + r^2 h + 2\pi^2 h^3) R^2 + (\frac{4}{3} \pi h r^3 + \pi h^2 r^2) R + \frac{2}{3} r^5) \frac{1}{R} \propto \frac{w(J-P)R_C^3}{\eta} \\
\Downarrow & \quad \int (hR^4 + (\pi h^2 + 2\pi h^2) R^3 + \\
& \quad (\frac{2}{3} r^3 + r^2 h + 2\pi^2 h^3) R^2 + (\frac{4}{3} \pi h r^3 + \pi h^2 r^2) R + \frac{2}{3} r^5) \frac{1}{R} dR \propto \int \frac{w(J-P)R_C^3}{\eta} dt \\
\Downarrow & \quad \frac{h}{4} R^4 + \frac{\pi h + 2\pi h^2}{3} R^3 + \\
& \quad \frac{\frac{2}{3} r^3 + r^2 h + 2\pi^2 h^3}{2} R^2 + (\frac{4}{3} \pi h r^3 + \pi h^2 r^2) R + \frac{2}{3} r^5 \ln |R| \propto \frac{w(J-P)R_C^3}{\eta} \cdot t, \text{ for } R > R_C.
\end{aligned}$$

This results in two alternative “scaling laws” for $R > R_C$: $\frac{1}{2} R^2 + 2\pi Rh + r^2 \ln |R| \propto \frac{w(J-P)}{\eta} \cdot t$ and $\frac{\frac{2}{3} r^3 + r^2 h + 2\pi^2 h^3}{2} R^2 + (\frac{4}{3} \pi h r^3 + \pi h^2 r^2) R + \frac{2}{3} r^5 \ln |R| \propto \frac{w(J-P)R_C^3}{\eta} \cdot t$.

$R(t)$ is also hard to derive analytically for these alternative “scaling laws” when the membrane shell *not* in contact with the substrate is the characteristic volume and not the entire cell as one entity. However, since $\frac{dR}{dt} > 0$ for $h, R, r, w, \eta, (J - P) > 0$, both equations are invertible. It is therefore possible to fit $R(t)$ to data without having an analytical expression for $R(t)$ by fitting $t(R)$ to data instead. The overall shape of the two resulting alternative “scaling laws” are compared to $R \propto t^{\frac{1}{4}}$ in Figure 6.7. In Section 6.6, the alternative “scaling laws” derived here, as well as the scaling laws of Cuvelier *et al.*, will be fitted to actual experimental data.

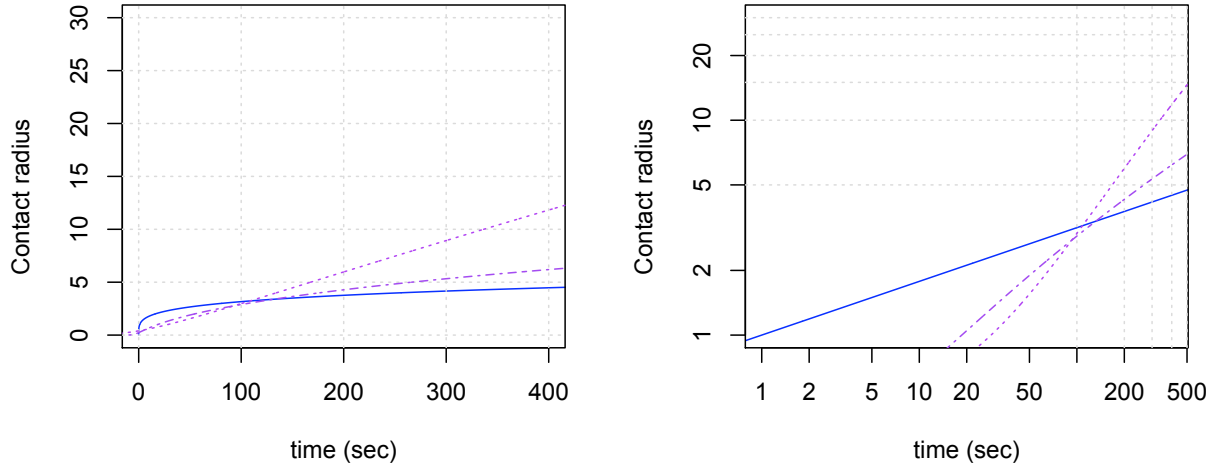


Figure 6.7: The shape of the two alternative “scaling laws” in the later stage, P2, where the radius of the adhesion area is smaller than the radius of the initial cell in suspension $R(t) > R_C$. The alternative “scaling laws” $\frac{1}{2}R^2 + 2\pi Rh + r^2 \ln |R| \propto \frac{w(J-P)}{\eta} \cdot t$ (dashed purple line) and $\frac{h}{4}R^4 + \frac{\pi h + 2\pi h^2}{3}R^3 + \frac{\frac{2}{3}r^3 + r^2 h + 2\pi^2 h^3}{2}R^2 + (\frac{4}{3}\pi h r^3 + \pi h^2 r^2)R + \frac{2}{3}r^5 \ln |R| \propto t$ (dashes-dotted purple line) for the later stage, P2, where $h = 9$ and $r = 5$ is compared to the original scaling law for the two phase model $R \propto t^{\frac{1}{4}}$ (full blue line). The “scaling laws” have been compared both on a regular plot on the left and on a double logarithmic plot on the right.

Summary of the original two phase model

Cuvelier and his collaborators’ two phase model gives rise to the following theoretical scaling laws:

$$\begin{aligned} \text{For P1 where } R(t) < R_C : & \quad R(t) \propto t^{\frac{1}{2}} \\ \text{and for P2 where } R(t) > R_C : & \quad R(t) \propto t^{\frac{1}{4}}. \end{aligned}$$

Since these scaling laws have been derived for angular isotropically spreading cells, $R = \sqrt{A/\pi}$, the scaling laws can also be expressed for the adhesion area, A , as:

$$\begin{aligned} \text{For P1 where } A(t) < A_C : & \quad A(t) \propto t^1 \\ \text{and for P2 where } A(t) > A_C : & \quad A(t) \propto t^{\frac{1}{2}}, \end{aligned}$$

where A_C is the cross-section of the initial cell in suspension. The exponential growth constant of the adhesion area, a_i , are then:

Model:	a_1 (P1)	a_2 (P2)
two phase with subtracted lag times	1.0	0.5

6.1.3 A mathematical model without phases

A third type of model was proposed by A. Bhattacharyay in 2008 [82]. The model is phenomenological and attempts only to fit a dynamical, mathematical model to the spreading dynamics previously seen in adhesion assays [65, 67, 71, 72, 73, 76, 77, 78]. The proposed dynamical model is composed of two coupled, partial differential equations:

$$\frac{\partial A}{\partial t} = \frac{1}{A} + pB - q \quad \text{and} \quad \frac{\partial B}{\partial t} = r - A \quad , \quad (6.1)$$

where A is the cell spreading area and B is the total polymerization rate of actin filaments or the rate at which the actin meshwork grows [82]. As observed in previous experiments, the dynamics resulting from these two coupled partial differential equations can be adjusted to resemble the entire temporal development of the adhesion area for a spreading cell. Figure 6.8 shows the temporal development of A in a double logarithmic plot for $p = 0.001$, $q = 0.5$ and $r = 10$. There is a likeness between the dynamics that can be modeled through these two coupled partial differential equations and the previously observed data in the three phase model.

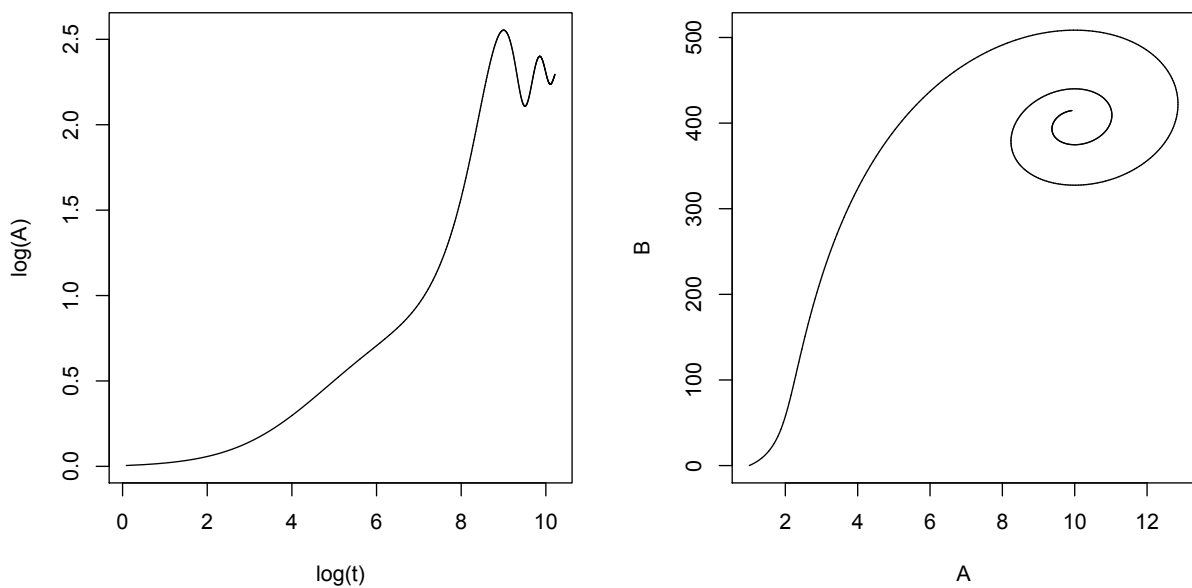


Figure 6.8: Left: Apparent dynamic phases shown by Bhattacharyay's model on a double logarithmic plot of adhesion area A and time t while spreading from an initial state given by $A_{\text{initial}} = 0.01$ and $B_{\text{initial}} = 0$. The parameter values are $p = 0.001$, $q = 0.5$ and $r = 10$. The adhesion area for one of the cells presented by Döbereiner *et al.* has been superimposed on the graph to illustrate the likeness. Right: Phase portrait showing the spiraling down to the fixed point (A_0, B_0) .

Bhattacharyay's dynamical system model has a unique fix point given by $A_0 = r$ and $B_0 = (q - 1/r)/p$. This point corresponds to the final state of a cell which has spread to the limit

where the rate of polymerization is equal to the rate of degradation of the actin filaments due to other forces [82]. If the system is perturbed, e.g., the cell was detached and brought into suspension, the phase trajectory should spiral down to the fix point (A_0, B_0) as long as $p > \frac{1}{4}r^4$ and the initial values of A and B are far from the fixed point. Figure 6.8 also shows the phase portrait for the dynamical system with the parameters $p = 0.001$, $q = 0.5$ and $r = 10$ that gave rise to the temporal development of A , which is also shown in this figure. The spiraling phase portrait gives rise to some characteristic oscillations in the adhesion area. Such oscillations have not been witnessed in the experiments presented here - not even in the hour-long adhesion assays. Since the mathematical model without phases does not reflect the experimental observations presented here, the model will not be described in more detail. However, it is important to mention that many have been perplexed by the inconsistency of the two and three phase models, and others have tried to solve this inconsistency.

6.1.4 The reconciled model

The three and two phase models both discuss the possibility of scaling laws governing the temporal development of the adhesion area in each phase. The scaling laws were in both models determined by fitting a piecewise linear function to the data on a double logarithmic plot. However, *double logarithmic plots do not always reveal a scaling law as a straight line*. This section is a brief detour that explains how the warning above should be heeded and proposes a reconciliation of the two and three phase models.

Double logarithmic plots can be used to reveal scaling laws. Since a scaling law is of the form

$$A(t) = c \cdot t^a \quad \Leftrightarrow \quad \ln(A(t)) = a \ln(t) + \ln(c)$$

The scaling law will appear as a straight line on a double logarithmic plot as long as an extrapolation of the data obeying the law passes through $\ln(c)$ for $t = 1$, i.e., $\ln(A(t = 1)) = \ln(c)$. This may seem obvious, but when the recoding of data has been initiated at arbitrary times compared to the initiation of cell adhesion it can become problematic.

Imagine that data did obey the scaling law, $A(t) = c \cdot t^a$, but that the recording of data was initiated either too late, $t_0 > 0$, or too early, $t_0 < 0$. The data would then be of the form:

$$A(t - t_0) = c \cdot (t - t_0)^b \quad \Leftrightarrow \quad \ln(A(t - t_0)) = b \ln(t - t_0) + \ln(c).$$

The exponential constants in the two scaling laws, a and b , are not the same. In fact, the scaling law above will not even appear linear on a double logarithmic plot. This can be shown by Taylor expanding the logarithmic function:

$$\ln(1 + x) = x - \frac{x^2}{2} + \frac{x^3}{3} - \frac{x^4}{4} + \frac{x^5}{5} - \dots \quad \text{for } -1 < x \leq 1$$

Applying this Taylor expansion to $\ln(A(t - t_0)) = b \ln(t - t_0) + \ln(c)$, the unadjusted scaling law becomes:

$$\begin{aligned}
 \ln(A(t - t_0)) &= b \ln(t - t_0) + \ln(c) \\
 &= b \ln\left(t\left(1 - \frac{t_0}{t}\right)\right) + \ln(c) \\
 &= b \ln(t) + b \ln\left(1 - \frac{t_0}{t}\right) + \ln(c) \\
 &= b \ln(t) + b \left(-\frac{t_0}{t} - \frac{1}{2} \left(\frac{t_0}{t}\right)^2 - \frac{1}{3} \left(\frac{t_0}{t}\right)^3 - \dots \right) + \ln(c) \quad \text{for } -t < t_0 < t.
 \end{aligned}$$

Though the series is convergent, the scaling law will no longer appear linear on a double logarithmic plot due to the many extra terms from the Taylor expansion. This non-linearity of the scaling law when data contains a lag-time, t_0 , is shown in Figure 6.9. The presence of a lag-time (either positive $t_0 > 0$ or negative $t_0 < 0$) does not have a drastic effect on analysis in a regular plot since it merely shifts the data. It is only when trying to reveal a scaling law by fitting a linear function to the data on a double logarithmic plot that lag-times poses a problem, so most pitfalls can be avoided by fitting a scaled function, $A(t) = c \cdot (t - t_0)^a$, to data on a regular plot, rather than fitting a linear function, $\ln(A(t)) = a \ln(t) + \ln(c)$, to data on a double logarithmic plot. Any lag-times in the data will manifest themselves as a bending of the expected linear growth on a double logarithmic plot. Fitting a linear function to such a non-linear data set will result in incorrect scaling laws.

By heeding the warning above, it is possible to reconcile the two and three phase models. The three phase model presented by Döbereiner and his collaborators in 2004 [67] is described in Section 6.1.1. In short the three phase model reported the existence of three distinct phases, each characterized by a specific scaling law, $A(t) \propto t^{a_i}$, where $i = \{1, 2, 3\}$ denoted the phases. The values for the exponential constant in the scaling laws for the increase in the adhesion area, a_i , found by Döbereiner and his collaborators in 2004 were:

Model:	a_0 (P0)	a_1 (P1)	a_2 (P2)
three phase	0.4 ± 0.2	1.6 ± 0.9	0.3 ± 0.2

Taking a closer look at their representative data in Figure 6.3 (also presented as a mock-up in Figure 6.10), it is clear that for the two representative cells' data has not been time adjusted to have their phase transition coincide temporally. Nothing in the temporal development of the adhesion area is aligned for the three phase model, neither the times of phase transitions, nor the times when the adhesion areas reach certain sizes. Döbereiner and his collaborators do not report any pre-analysis treatment of their data either, so it can be assumed that none was made. Some (lag-)time adjustments are necessary to compare data from different adhesion assays.

If cell adhesion is recorded at arbitrary times, then time adjustments are necessary for any meaningful comparison of data from different adhesion assays. To illustrate the effect that time adjustment of adhesion assay data can have on scaling laws, a mock-up of the data presented by Döbereiner *et al.* has been time adjusted in Figure 6.10. The mock-up is a replica of their data, which can be seen in Figure 6.3. The *unadjusted* data show three

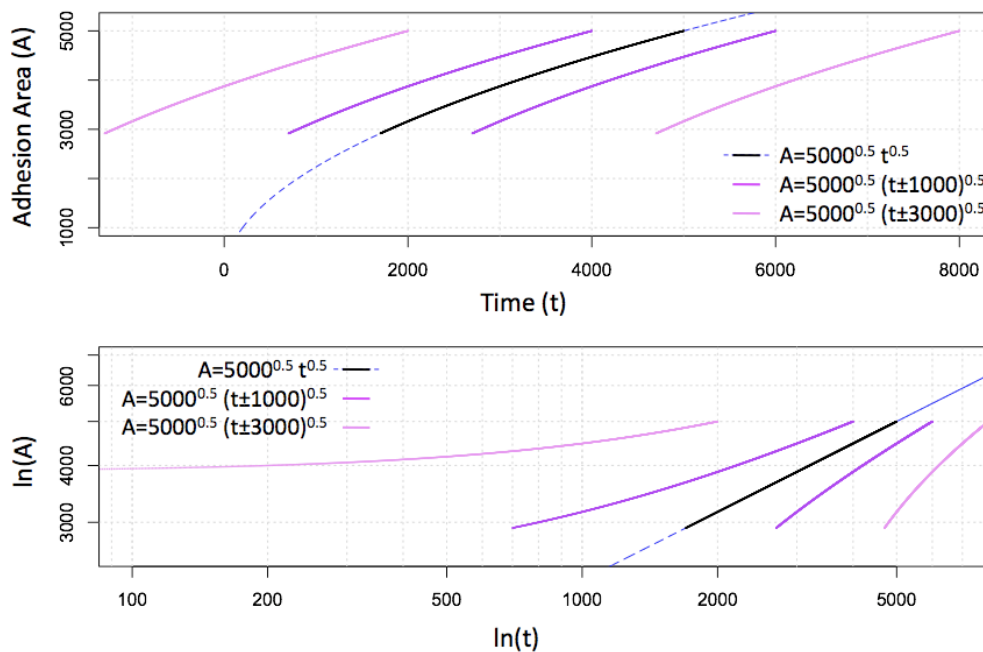


Figure 6.9: Graphic illustrations of what happens when lag-times or set-off areas are added to or subtracted from the data pre-analysis. Top: The subtraction of lag-times in a regular plot is only seen as a shift in the data points. The blue dashed line indicates the scaling law $A(t) = \sqrt{5000} \cdot t^{\frac{1}{2}}$. The black points are a fictional data set that obeys this scaling law. The purple points are the fictional data set with lag-times of $t_0 = 1000$ and $t_0 = -1000$ respectively, and the violet points are the fictional data set with lag-times of $t_0 = 3000$ and $t_0 = -3000$ respectively. Bottom: The subtraction of lag-times in a double logarithmic plot will cause the data set that does obey a scaling law to appear non-linear. The resulting scaling law will be incorrect if it is found by fitting a linear function to the data set with lag-times on a double logarithmic plot.

distinct phases on a double logarithmic plot, that each appear linear and have had a scaling law fitted to them. An inherent lag-time in the data will cause the scaling law to appear non-linear on a double logarithmic plot and attempting to fit a linear function to it would result in an erroneous exponential constant for the scaling law. Adjusting the data from Döbereiner *et al.* for a possible inherent lag-time, a different scaling law behavior is seen in the double logarithmic plot of Figure 6.10. The data was lag-time adjusted to have the phase transition from phase P1 to phase P2 occur at $t_1 = 400$ seconds or $6\frac{2}{3}$ minutes for both cells². The P1 to P2 phase transition is the easiest to identify, and it is linked to the physical observable transition from passive to active spreading when the adhesion area exceeds the bulk of the cell, $A < A_C$ to $A > A_C$. Figure 6.10 shows that the t_1 lag-time adjustment changes the appearance of the data for both cells. The two cells' adhesion area dynamics

²Time adjusting the data to make the phase transition from phase P1 to phase P2 occur at $t_1 = 400$ seconds, made the scaling law for phase P2 approximately, $A(t) \propto t^{\frac{1}{2}}$, illustrated by a black line in Figure 6.10. It should be mentioned that other scaling laws would have appeared for other values of t_1 . Here, $t_1 = 400$ seconds was chosen to reflect the subsequent analysis and make the three phase model comparable with the two phase model.

now appear similar, and the lag-phase P0 has disappeared altogether. The existence of a distinct phases P0 may be an artifact of plotting unadjusted data in a double logarithmic plot, and lag-time adjusting data so the phase transition, $A(t) = A_C$, coincide effectively make the three phase model a two phase model for the exemplary cell data. Access to all Döbereiner *et al.*'s data is needed to refit the scaling laws, $A(t) = c \cdot (t - t_0)^{a_i}$ for $i = \{1, 2\}$, and conclude the reconciliation in general.

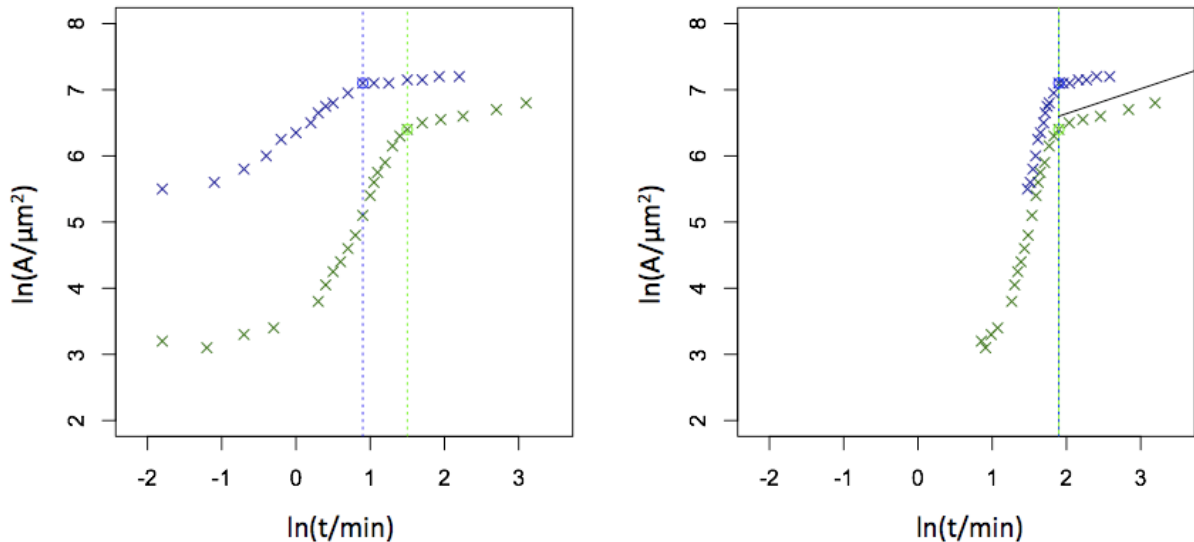


Figure 6.10: Left: A mock-up of Döbereiner *et al.*'s unadjusted data from 2004 [67], also seen in Figure 6.3. The phase transition from phase P1 to phase P2 is denoted with a dashed line for each data set. Neither phase transitions nor size of adhesion areas coincide temporally in this plot. Right: Döbereiner *et al.*'s data from 2004 [67] adjusted to have the phase transition from phase P1 to phase P2 occur at $t_1 = 400$ seconds or $6\frac{2}{3}$ minutes (the blue/green dashed line). The later, saturating phase P2 is still observable, and obeys a scaling law with a exponential constant of ≈ 0.5 (full, black line). No data points have been disregarded, but after lag-time adjusting the data, the lag-phase P0 seems to have disappeared. P0 may just have been an artifact plotting the data in a double logarithmic plot without taking lag-times into account. In fact, both the scaling laws are subject to change when the lag-time t_1 is altered.

Although the above supports the existence of two distinct phases in cell adhesion, there is still the matter of the value of the actual scaling law. If the scaling law is found by fitting a linear function to data on a double logarithmic plot, the scaling law is subject to change for different lag-time adjustments.

Not only did the scaling laws for Döbereiner *et al.*'s data change when the data was time adjusted (see Figure 6.10), the scaling laws also become more similar. This suggests that the large standard deviation that Döbereiner *et al.* report on the scaling laws, particular for the P1 phase $a_1 = 1.6 \pm 0.9$, may be due to unadjusted data. If this is the case, the separation of data into two groups, $A_1/A_0 < 5$ or $A_1/A_0 > 5$, depending on the relative growth in the P1 phase, is unnecessary. Much better statistics may be possible through the fitting of a scaled equation, $A(t) = c \cdot (t - t_0)^{a_i}$, to the data on a regular plot.

The disappearance of the lag-time phase P0 and the enhanced similarities between adhesion assay data sets when these have been lag-time adjusted, suggest that the three phase model may only be an artifact of the unadjusted data analysis on a double logarithmic plot. In the following comparison and analysis of the adhesion assays, no double logarithmic plot fittings will be used. Instead, scaled functions, $A(t) = c \cdot (t - t_0)^{a_i}$, will be fitted to data on regular plots.

The following section will describe the requisition of results and present the subsequent analysis of these results from the adhesion assays. The control experiments are endothelial cell adhesion assays on a Collagen IV substrate *without* arachidonic acid (AA) present in the media. The adhesion process for unaffected cell has to be characterized first to construct a standard with which to compare any changes in cell adhesion that the addition of arachidonic acid might cause.

6.2 Adhesion Assays: Materials and methods

Cell culture

The porcine aortic endothelial cells used in the adhesion assay experiments were from the strain used in the viability assays in Chapter 5. The cells were grown at the bottom of plastic wells (Multidish 6 wells from Nunclon™ Δ Surface) in a CO₂-dependent media consisting of D-MEM:F12 (1:1) + GlutaMAX medium supplemented with 10% heat inactivated fetal bovine serum (FBS), 100 U/mL penicillin and 100 μ g/mL streptomycin (all from Gibco, USA).

The cells were cultured in an ambient atmosphere with 5% CO₂ at 37°C and grown until confluence. When cells had reached confluence, they were passaged by gentle *trypsination*. As mentioned in Chapter 5, trypsination is the process of detaching the cells by severing the integrin bonds with which the cells adhere to the bottom of the plastic wells. The trypsination is halted and the cells brought into suspension by diluting the trypsinated cells with medium (1 μ L trypsin : 1 mL medium). The suspended cells can then be seeded in new plastic wells at any desired concentration or applied to an adhesion assay. Trypsination, dilution and seeding of the cells to grow in a new well constitutes *one* passage. Cells lose some of their endothelial characteristics every time they are passaged and should only be used until their 30th passage. In these experiments, cells were only used until their 15th passage, and the cells should still possess their endothelial characteristics.

Experimental samples

For experimentation, cultured, confluent endothelial cells were gently trypsinated and brought into suspension in CO₂-*independent* media, since the microscopic set-up cannot support an ambient atmosphere. The CO₂-independent media with the suspended endothelial cells were then transferred to a chamber consisting of *Collagen IV* coated glass slides. Collagen IV is an extracellular matrix protein usually found on mammalian cells. The glass slides were coated with Collagen IV to mimic the endothelial cells' *in vivo* environment as closely as possible.

In experimental adhesion studies, it is preferable to have the glass slides coated with an extracellular protein, such as collagen IV, to facilitate the adhesion of cells and thereby minimize the amount of biological noise. Figure 6.11 illustrates the experimental set-up of the glass slide chamber. The chambers were then sealed off and placed in a microscope, which was kept at a constant temperature of 37 °C. The process of adhesion to the collagen IV coated glass slides for an individual endothelial cell was recorded in the microscopic set-up.

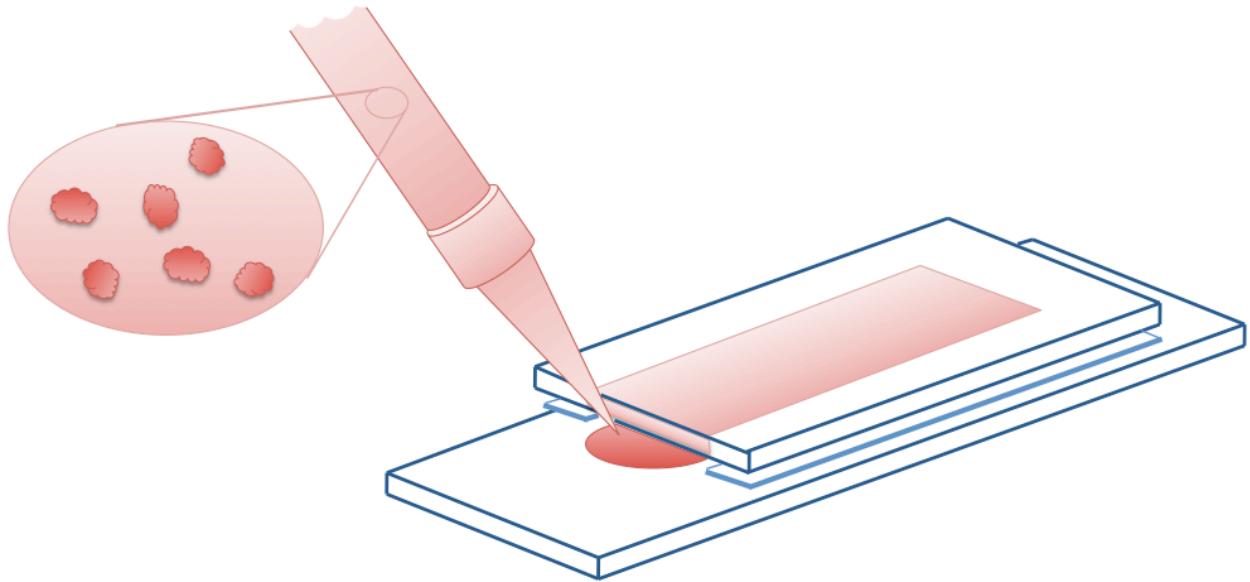


Figure 6.11: A schematic of the glass slide chambers used for the adhesion experiments.

Microscopes

The colorless and transparent internal structures of cells are notoriously difficult to study with regular, bright field microscopy. Two different types of microscopy were used to record the adhesion of individual endothelial cells: ¹⁾ Differential interference contrast (DIC) microscopy and ²⁾ confocal reflection interference contrast microscopy (C-RICM).

Differential interference contrast (DIC) microscopy increases the contrast of the image non-invasively by adding information about the optical density of the sample to the image. Denser materials induce a shift in the phase of the light. The phase of the light is invisible to the human eye, but DIC microscopy is one of the optical solutions that changes a difference in phase into a difference in light intensity. It does so by using a prism to split polarized light into two beams: an ordinary beam and an extraordinary beam. These two beams are slightly displaced³ and take slightly different paths through the sample. After passing through the specimen, the beams are reunited by a similar prism into one image.

³The displacement of the beams is less than the maximum resolution of the objective, so in a homogenous specimen, there is no observable difference between the two beams or their paths. There will be no added interference in the resulting image in a homogenous specimen.

If there is a refractive boundary, such as the nucleus within the cytoplasm or the cell's membrane in the media, the two displaced beams will experience a difference in their *optical paths*. The optical path is the product of the refractive index⁴ and the geometrical path length. A difference in the length of the optical path alters the phase of one of the beams relative to the other due to the delay experienced by the wave in the more optically-dense matter. When the two beams are reunited, the delay or difference in phase of one of the beams interferes with the other, and the contrast of the image is thus enhanced in areas of different optical density. The contrasts produced by the interference of the two beams with different optical path lengths appears as a three-dimensional physical relief corresponding to the variation of optical density of the sample (see Figure 6.12). The relief emphasizes lines and edges particularly, though the shape of the relief does not necessarily reflect the true three dimensional shape.

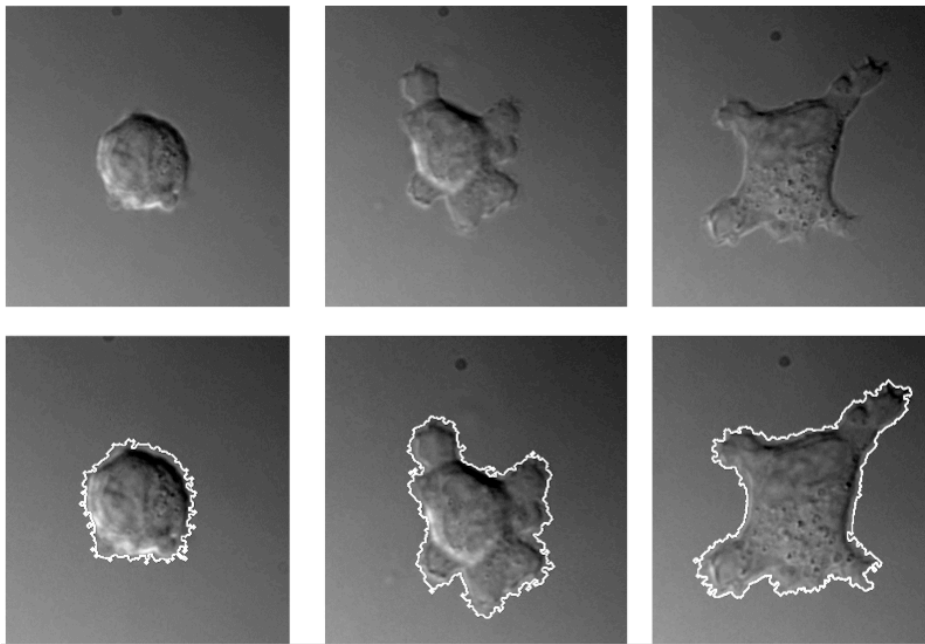


Figure 6.12: The adhesion area between an adhering endothelial cell and a Collagen IV coated glass slide as seen through a DIC microscope, and the outline identified by MatLab.

High resolution DIC has been used to characterize cell adhesion and local membrane dynamics [67]. A MatLab program was used to identify the leading edge of the observed adhesion area, and calculates the area, position, and length of the principal axis of the adhesion area. Examples of the adhesion areas identified by the MatLab program are also shown in Figure 6.12.

The advantages of using DIC microscopy when analyzing cell behavior are its emphasis on edges and its halogenic light source. Even over long exposures, halogen lamps are mostly harmless to cells. DIC microscopy has a broad focus, so much of the general behavior of the cell, such as apoptosis, can be readily seen. However, the broad focus is also a disadvantage

⁴The refractive index of a material is a measure of how much the speed of light is reduced inside the medium.

since the bulk of the cell is still discernible on images focused on the level of the cell-glass slide interface, i.e., the adhesion area. This implies that there is no immediate guarantee that the observed leading edge of a spreading cell is the leading edge of the actual adhesion area on the surface of the glass slide. The problem is illustrated in Figure 6.13 which shows three differently adhering cell conformations that all give rise to the same observed area.

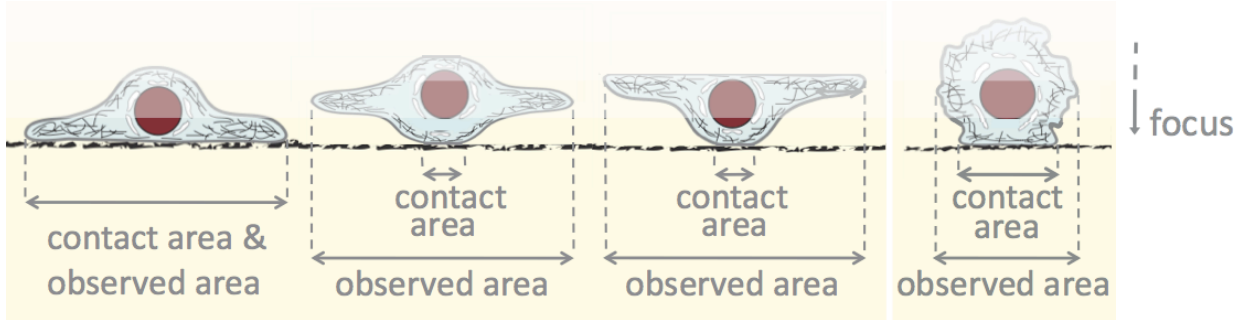


Figure 6.13: A schematic figure of what is observed through differential interference contrast (DIC) microscopy. Left: The same area would be perceived in the three instances shown and in any combination of those. Right: Even if our picture of adhesion of a cell spreading out directly on top of a glass slide is right, a DIC microscope would not be able to distinguish the cell-glass contact area from the cross section of the bulk of the cell.

Figure 6.13 also displays a fourth cell that illustrates another disadvantage of using DIC microscopy. When the adhesion area has not surpassed the cross section area of the cell bulk, $A < A_C$, the adhesion area cannot be adequately distinguished by the use of DIC microscopy. DIC microscopy can only be used for observing the later stage, P2, where the adhesion area exceeds the bulk of the cell, $A(t) > A_C$, and the cell is actively spreading. A microscopic technique with a narrower focus, such as confocal microscopy, is necessary to observe the stages before the adhesion area exceeds the bulk of the cell, $A(t) < A_C$, in which the cell spreads passively. Confocal microscopy can guarantee that the observed leading edge of the cell membrane is in fact the leading edge of the adhesion area and that the cell is in contact with the glass slide over the entire observed adhesion area (see Section 6.5).

Confocal reflection interference contrast microscopy (C-RICM) generates an image differently than the DIC microscope. A confocal microscope is a scanning probe microscope in which the sample is scanned by a fine beam, rather than illuminated using full sample illumination. Using a fine beam avoids the back scattering of out-of-focus light and gives the confocal microscope a slightly higher resolution and a much tighter focus of around $0.5\sim 1\ \mu\text{m}$. This narrow focus is much smaller than the height of a fully spread cell ($\approx 8\ \mu\text{m}$), so when a confocal microscope is focused on the surface of the glass, any observed adhesion area will be the actual adhesion area where the cell is in contact with the glass slide (see Figure 6.14). Due to its narrow focus, confocal microscopy is commonly used when the three dimensional structure of the specimen is important. In Section 6.5, the three dimensional structure of a spreading endothelial cell is shown to resemble fried eggs through the use of confocal microscopy.

The advantages of using confocal reflection interference contrast microscopy (C-RICM) are

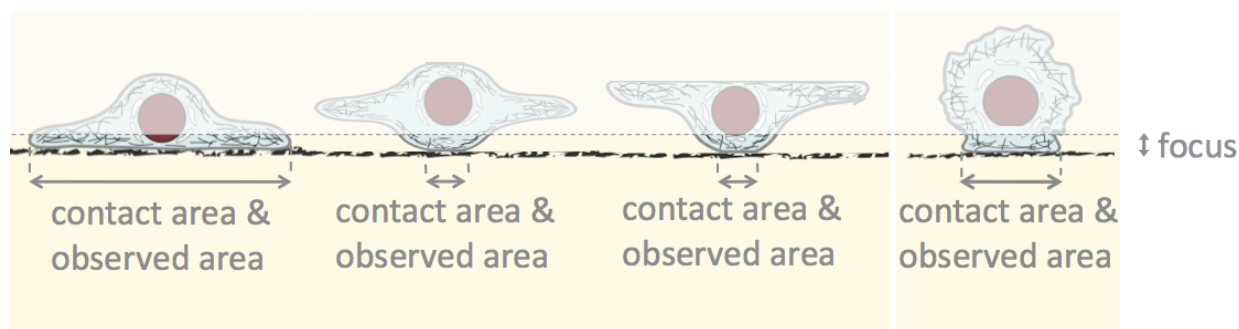


Figure 6.14: A schematic figure of what is observed through confocal microscopy.

its narrow focus, that can focus exclusively on the actual adhesion area, and its ability to bring the level of the interface between the medium and the glass slide into focus. Glass has a refractive index⁵ of $n_{\text{glass}} \approx 1.5$, and the aqueous medium has a refractive index of $n_{\text{medium}} \approx 1.3$. Light reflects partially from surfaces that have a refractive index different from that of their surroundings, so the scanning laser beam will be partially reflected by any part of the glass in direct contact with the aqueous media. C-RICM uses the reflected light of the laser to form an image⁶, so any glass-medium interface will appear light.

Fortunately, the refractive indices of the cell's components are close to that of the glass slide, $n_{\text{cell}} \approx 1.5$, so the scanning laser beam will not be reflected from any part of the glass that is in direct contact with a cell and such glass-cell interfaces will appear dark compared to glass-medium interfaces (see Figure 6.15) when observed through C-RICM. Figure 6.15 also shows examples of the adhesion areas identified with the MatLab program.

The disadvantage to using C-RICM is that the laser light used for illuminating the sample may be harmful to the cells. Different elements of cells are able to absorb light at different wavelengths, and the absorption of light is harmful to cells. The interval of 600-1300 nm is called the “optical window” for cells. As a rule of thumb, light with wavelengths in this interval should be avoided when studying cells. The halogen lamp used in DIC produces a continuous spectrum of light, from near ultraviolet to infrared, so there is an overlap with the optical window. However, the intensity at the harmful wavelengths is low in halogenic illumination, particularly compared to lasers which emit at a single wavelength rather than a continuous spectrum. Light at particular wavelengths is lethal to the cells, and the intensity of laser light could prove toxic to cells.

Laser light with a wavelength of 514 nm (outside the optical window for cells) and an effect of a few mW was used for the C-RICM investigations. A 514 nm wavelength is well outside the optical window for cells and does not harm the cells. However, the intensity of the laser light may still be harmful to the cells. Section 6.4 will test whether the C-RICM techniques used here were harmful to the cells, compared to the almost harmless halogen illumination of DIC microscopy.

⁵The refractive index of a material is a measure of how much the speed of light is reduced inside the medium.

⁶Normally the confocal microscope is used for fluorescent probes, but in the reflection mode, it can distinguish and focus on the glass-medium interface exactly.

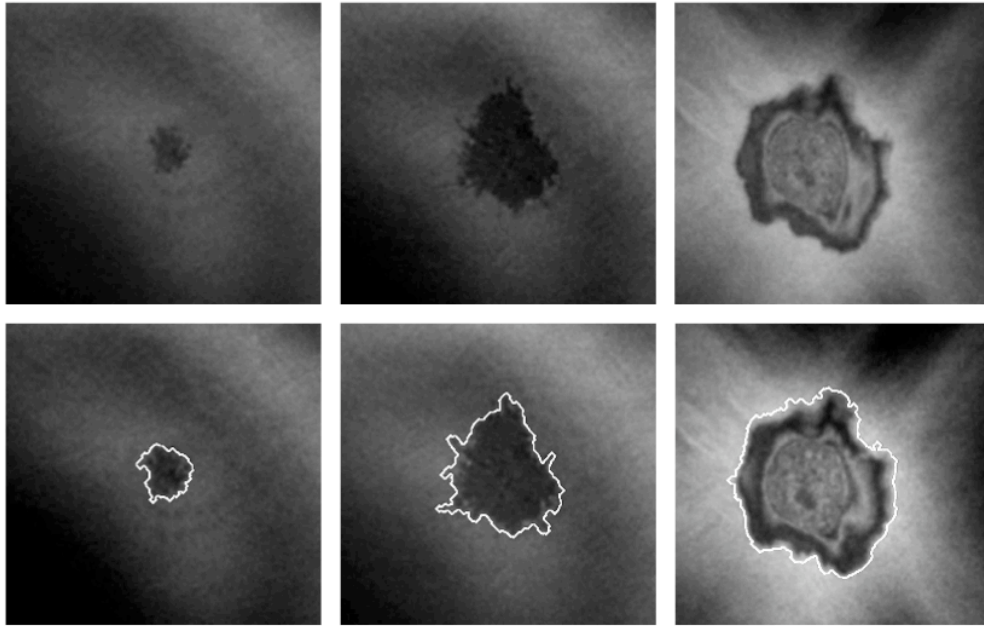


Figure 6.15: The adhesion area between an adhering endothelial cell and a Collagen IV coated glass slide as seen through a C-RICM, and the outline identified by MatLab.

6.3 Adhesion Assay Data for Regular Endothelial Cell Adhesion

Due to the advantages of a practically harmless illumination in differential interference contrast (DIC) microscopes, the 13 control experiments were conducted in a DIC microscope. Adhesion assays observed through DIC microscopes will only give information about the adhesion, when the adhesion area has exceeded the bulk of the cell, $A > A_C$, i.e., in the second phase P2. For the purpose of this thesis, the second phase of adhesion is the most interesting. In the second phase, the cell is actively spreading and the remodeling of the cytoskeleton can play a role. During the passive spreading of the first phase, P1, membrane proteins play the primarily role. To investigate the effect of arachidonic acid on cytoskeletal remodeling the second phase should show the effect most prominently.

The main adhesion data sets have been collected using a DIC microscope, but a couple of control experiments were conducted in a C-RICM as well. The purpose of these experiments was to ensure that the protrusions observed in the DIC microscope were in fact adhesive protrusions at the surface of the glass slide, and not membrane protrusions hovering above the surface. The general three dimensional shape of adhering cells is established using C-RICM in Section 6.5. If the laser light of the C-RICM harms the cell, the three dimensional shape of the cell may alter. It is necessary to first establish that the laser does not harm the cells in any measurable way before it is possible to trust the cell's three dimensional shape. So a test of any possible toxic effects of C-RICM's laser illumination is conducted in Section 6.4.

Once the it has been established that the C-RICM's laser does not harm the cells in any

measurable way (Section 6.4), the three dimensional shape of adhering cells is determined (Section 6.5) to ensure that the DIC microscope is identifying the actual adhesion area of the cells. The DIC data is then analyzed to establish a standard for endothelial cell adhesion on a Collagen IV substrate in the absence of arachidonic acid.

The broad focus of differential interference contrast (DIC) microscopy is unable to distinguish adequately between the bulk of the cell and the adhesion area of an adhering cell when the adhesion area is smaller than the bulk of the cell, $A < A_C$. It is therefore only applicable to observations of the later or final phase, P2, in the reconciled two phase model, $A > A_C$. Figure 6.16 shows the temporal development for the adhesion area of a representative endothelial cell observed through a DIC microscope. Figure 6.16 also shows some exemplary images of the adhering cell at different times during the adhesion to convey a sense of the time it takes for an endothelial cell to adhere to and spread out on a Collagen IV substrate. The temporal resolution for the DIC recordings were 18 frames per minute (fpm).

6.4 Toxicity Assay of the 514 nm Laser Illumination

The intense, single-wavelength illumination of the laser in confocal reflection interference contrast microscopy (C-RICM) may be harmful to the cell. It is possible to investigate how harmful C-RICM is compared to differential interference contrast (DIC) microscopy, by comparing the data from C-RICM to data from DIC microscopy which is practically harmless.

The cells were visually inspected and judged to be alive and healthy after each experiment, so the laser illumination is not lethal to the cells in the time span of these experiments. However, the laser may not have harmed the cells enough for visual detection but enough to affect the temporal development of the adhesion area. To ensure that the spreading cells observed through the confocal microscope were from healthy, unharmed samples, the temporal development of the adhesion area observed through a C-RICM was compared to the temporal development of the adhesion area as seen through a DIC microscope.

Figure 6.17 illustrates the close resemblance of the temporal development of the adhesion area between two representative spreading cells of approximately the same size⁷: one observed through DIC microscopy with halogenic illumination and one observed through confocal microscopy with laser illumination. The adhesion area can only be observed through the DIC microscope for $A > A_C$, so the two types of microscopy can only be compared in this interval.

Regarding Figure 6.17, it can be concluded that observations through a C-RICM coincide with the observations through a DIC microscope for $A > A_C$. Though Figure 6.17 only shows two representative cells, data observed through C-RICM was continuously compared to, and found to coincide with, the data from DIC for $A(t) > A_C$. In the following, it can be assumed that any toxic effect of the laser illumination is so small that it will not affect the outcome of the adhesion assays, and that the three dimensional shape found through

⁷Endothelial cells vary slightly in size, and the size of the cell is directly related to the cross-section of the bulk of the cell in suspension, A_C . The representative cells chosen for this toxicity test were of approximately the same size to facilitate the comparison.

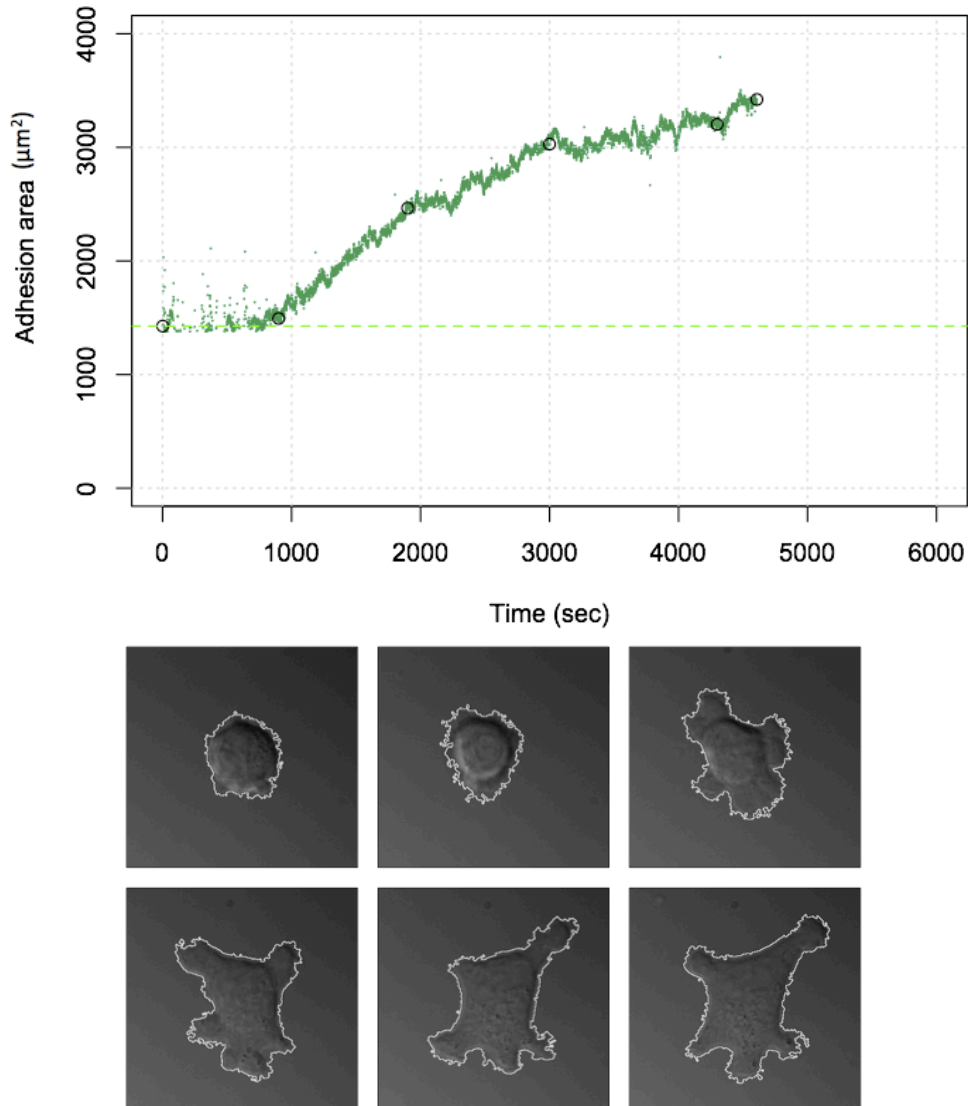


Figure 6.16: Exemplary data showing the temporal development of the adhesion area between a spreading, representative endothelial cell on a Collagen IV substrate as seen through a DIC microscope. Top: The adhesion area as a function of time on a regular plot. Bottom: Six DIC images of the spreading cell at different points in time, which are all marked in the regular plots above with black circles.

the use of C-RICM reflects the three dimensional shape of a healthy, adhering cell in a DIC microscope.

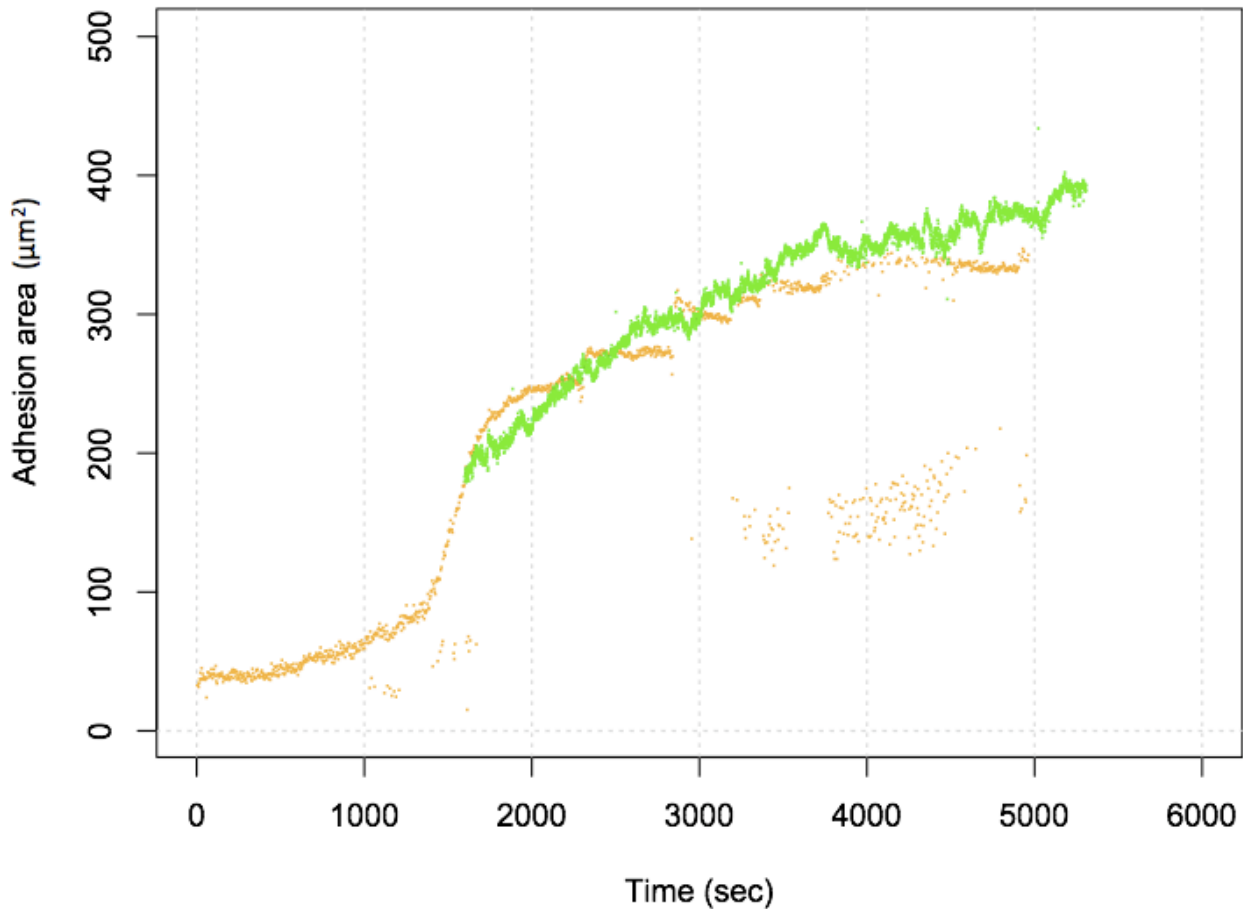


Figure 6.17: Exemplary data showing the temporal development of the adhesion area of three representative spreading cells on a Collagen IV substrate. The adhesion area as it is seen through a differential interference contrast (DIC) microscope (green points) and confocal microscope with reflective laser illumination (C-RICM) (orange points). The close resemblance suggests that any photo toxic effect of the reflective laser illumination or the laser induced fluorescence is too small to be noticed on a adhesion or spreading assay.

6.5 The Three-Dimensional Shape of Regularly Spreading Endothelial Cells

There are several three-dimensional shapes that would give rise to the images seen through a DIC microscope (see Figure 6.16), such as: a fried egg, a flying saucer and an upside-down fried egg (these are the three examples illustrated in Figure 6.13). There are theoretical reasons why the three-dimensional shape of an adhering cell should resemble a fried egg. It requires energy for a cell to deviate from a spherical configuration. The following equations

denote the energy required to form the shape of a fried egg (with a “yolk radius” of $2^{\frac{1}{3}}r$, an “egg-white” height of h , and a protrusion radius of R) and a flying saucer (with a protrusion thickness of the membrane protrusion at the saucer’s middle of h , the spherical part’s radius of r , and protrusion radius of R being the radius of the protrusion). With these parameters, the volume and surface are approximately the same for the fried egg and the flying saucer shapes, so the energy requirements should be comparable. The bending energy of the membrane is denoted using the shapes deviation from a spherical shape. For angularly isotropic shapes, the shape, or rather the shapes deviation from a sphere, is denoted with the dimensionless parameter $\rho = \frac{R}{r} \gg 1$ for the fried egg, and $\rho = \frac{R}{2^{\frac{1}{3}}r} \gg 1$ for the flying saucer.

$$\begin{aligned} \text{Fried Egg: } E_{\text{bend}} &\approx \pi\kappa_b(8 + \pi\rho) + 4\pi\kappa_G + 4\pi\kappa_b + 2\pi\kappa_G \\ \text{Flying Saucer: } E_{\text{bend}} &\approx \pi\kappa_b(8 + \pi\rho) + 2 \cdot (4\pi\kappa_G + 4\pi\kappa_b + 2\pi\kappa_G) \end{aligned}$$

where κ_b and κ_G are the harmonic and the gaussian bending modules, respectively [83]. The energy required for the shape resembling a fried egg is less than the energy required for the shape of a flying saucer. The lower energy requirements of a fried egg makes this configuration more likely. The cell adhesive energy increases through substrate attachment [76], so a larger adhesion area for the same configuration is more likely, favoring the rightside-up fried egg configuration rather than the upside-down. The shape resembling a fried egg is the most likely three dimensional shape for an adhering and spreading cell.

The three-dimensional shape of an adhering and spreading cell can be deciphered through regular confocal microscopy using fluorescent probes. Fluorescent probes are excitable through the absorption of high energy light. When the probes have been excited, they emit light of a different, lower frequency, and this effect is known as fluorescence. Fluorescence emission differs in wavelength from the excitation wavelength, so an image, of only the emitted light can display the location of the fluorescent probes. Alexa Fluor[®] 488 Hydrazide fluorescent probes were used to determine the three dimensional shape of spreading cells. Hydrazide probes are membrane impermeable and unable to penetrate the cells’ membranes and remain in the cells’ medium. In the resulting images, the interior of the cells will remain dark against the emitted light of the Alexa Fluor[®] 488 Hydrazide probes in the cell’s surrounding media.

A single $0.5 \mu\text{m}$ “slice” of the cell can be observed in the narrow focus of the confocal microscope. Figure 6.18 shows several such “slices” of a spreading cell taken at different heights using confocal microscopy with fluorescent probes in the media. It is apparent that the three dimensional shape of the spreading cell resembles a fried egg.

The three dimensional images in Figure 6.18 which were taken throughout the adhesion process confirms that a representative endothelial cell spread out on the substrate like a fried egg, as expected. The adhesion area observed through the broad focus of DIC microscopy can then be assumed to be the actual adhesion area between the cell and the substrate when the adhesion area exceeds the cross section area of the bulk of the cell.

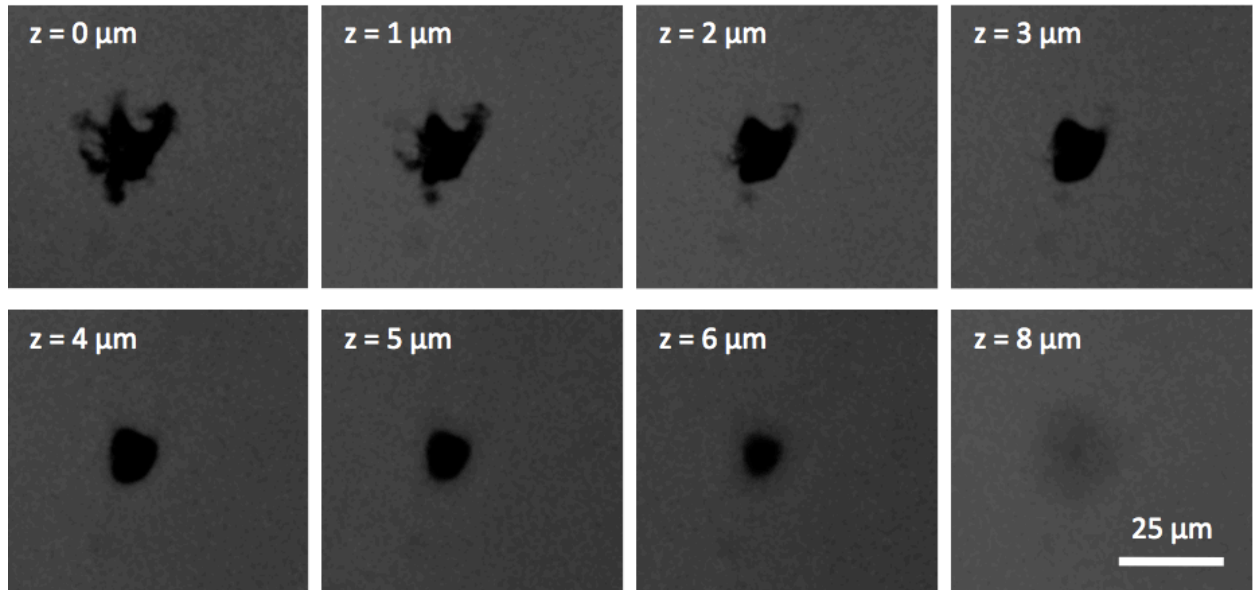


Figure 6.18: The images of an adhering cell as seen through a confocal microscope with membrane impermeable fluorescent probes in the media. The interior of the cell remains dark, while the probes in the media light up. The images are taken at different heights, z , above the surface of the glass slide. The image in the upper left corner, $z=0\mu\text{m}$, is the image of the adhesion area between the endothelial cell and the Collagen IV coated glass slide. The cell's three dimensional shape is clearly seen to resemble a fried egg closer than a flying saucer.

6.6 Standard for Regularly Adhering Endothelial Cells

According to the two tests above (Section 6.4 and 6.5), it can safely be assumed that the DIC microscopic observation will reflect the temporal development of the actual adhesion area. The temporal development of the adhesion area can then be used to establish a standard for endothelial cell adhesion.

Which model should be used for establishing the standard?

Several models describing the temporal development of the adhesion area were proposed in previous studies. Through a careful examination of the different models' data treatment and analysis methods, it was possible to reconcile the most prominent of the previous models: the two phase model and the three phase model (see Section 6.1.4). The reconciled model is a two phase model with a distinctly different temporal development in each phase. The first phase, P1, describes the passive spreading of the cell when the adhesion area has not yet exceeded the bulk of the cell, $A(t) < A_C$. The second phase, P2, describes the active spreading of the cell when the adhesion area exceeds the bulk of the cell, $A(t) > A_C$. The temporal developments in these two phases are both described as scaling laws, $A(t) = c_i \cdot (t - t_0)^{a_i}$ for

$i = \{1, 2\}$, but they are distinctly different, $a_1 \neq a_2$ and $c_1 \neq c_2$.

$$\begin{aligned} \text{For P1:} \quad A(t) &= c_1 \cdot (t - t_0)^{a_1} \\ \text{For P2:} \quad A(t) &= c_2 \cdot (t - t_0)^{a_2}. \end{aligned}$$

Cuvelier *et al.* propose a simple model for the cell, and through derivations based on assumptions of this model cell, they find the theoretical values for a_i to be: $a_1 = 1$ and $a_2 = \frac{1}{2}$ [76]. Section 6.1.4 also emphasized the importance of fitting a scaled function, $A(t) = c_i \cdot (t - t_0)^{a_i}$, to data on a regular plot, rather than fitting a linear function, $\ln(A(t)) = \ln(c_i) + a_i \cdot \ln(t)$, to data on a double logarithmic plot when identifying possible scaling laws. The later analysis method does not take the arbitrary initiations of the data recording into account.

Apart from the reconciled model, an alternative model was proposed in Section 6.1.2. The alternative model is also based on a simple model of the cell but with the cell's membrane and cytoskeleton modeled as two separate entities. Furthermore, the shape of the cell as it spreads out is assumed to resemble a fried egg, rather than a short, fat cylinder, and any viscous dissipation is assumed to occur in the part of the membrane which is not adhered to the substrate. This alternative model also has a distinctly different temporal development in each phase (two temporal developments are proposed for the second phase, P2):

$$\begin{aligned} \text{For P1:} \quad & b^2 \ln \left| \sqrt{\frac{A}{\pi}} \right| + 2b \sqrt{\frac{A}{\pi}} = k \cdot (t - t_0) \\ \text{For P2:} \quad & \frac{1}{2} \frac{A}{\pi} + 2\pi \sqrt{\frac{A}{\pi}} h + r^2 \ln \left| \sqrt{\frac{A}{\pi}} \right| = k \cdot (t - t_0) \\ \text{or} \quad & \frac{h}{4} \left(\frac{A}{\pi} \right)^2 + \frac{\pi h + 2\pi h^2}{3} \left(\frac{A}{\pi} \right)^{\frac{3}{2}} + \frac{\frac{2}{3}r^3 + r^2 h + 2\pi^2 h^3}{2} \frac{A}{\pi} + \\ & \left(\frac{4}{3} \pi h r^3 + \pi h^2 r^2 \right) \sqrt{\frac{A}{\pi}} + \frac{2}{3} r^5 \ln \left| \sqrt{\frac{A}{\pi}} \right| = k \cdot (t - t_0), \end{aligned}$$

since $R = \sqrt{A/\pi}$ for a spherical adhesion area. The endothelial cells have in the following been assumed to spread angularly isotropically (even though they do not) to enable the expression of the recorded adhesion area as the radius of the adhesion area, $R(t) = \sqrt{A(t)/\pi}$. The derivation of the models may not hold true for anisotropically spreading cells, but if the temporal development is similar to the one predicted by the model, the model still reflects a general, universal dynamic found in spreading cells.

To see which model describes the data best, the scaling laws of the reconciled model and the laws of the alternative model are fitted to each experimental data set by the program GNUplot, which uses "least-squares fitting". The "goodness of fit" for both models can be read from Table 6.1 in which both the weighted summed squared distance (WSSD) of the residuals and the degrees of freedom ($n - p$) have been noted for each fit. The WSSD of the residuals is a measure of the distance between the data points and the resulting fit or how well the fit describes data. The smaller the distance between the fit and the data points (WSSD) is, the better the resulting fit. WSSD is χ^2 distributed with $n - p$ degrees of freedom; n is the number of data points, and p is the number of parameters. The degrees

For P2 data set (DIC):	Reconciled		Alternative 1		Alternative 2	
	WSSD	$n - p$	WSSD	$n - p$	WSSD	$n - p$
Cell A	488.01	3627	519.936	3626	742.72	3626
Cell B	268.47	1234	268.56	1233	281.14	1233
Cell C	230.19	2319	299.96	2318	963.82	2318
Cell D	216.84	4447	350.76	4446	848.18	4446
Cell E	586.82	770	1851.14	769	609.82	769
Cell F	907.28	995	1932.00	994	2567.00	994
Cell G	578.82	1051	1523.43	1050	594.921	1050
Cell H	1226.09	808	2116.13	807	1260.87	807
Cell I	292.54	645	1091.64	644	298.05	644
Cell J	110.21	412	446.41	411	110.36	411
Cell K	315.26	1153	583.18	1152	323.04	1152
Cell L	80.61	993	227.122	992	83.27	992
Cell M	508.20	2067	1268.89	2066	535.50	2066

Table 6.1: The goodness of fit for the reconciled and both the alternative models for all the control cells. WSSD is the weighted summed squared distance and is χ^2 distributed with $n - p$ degrees of freedom.

of freedom have also been noted in Table 6.1 to convey a better sense of how good the fit (measured by WSSD) really is. A low WSSD for a data sets with more degrees of freedom is a better fit than a similar WSSD for a data set with fewer degrees of freedom. It is clear from Table 6.1 that, for all data sets, the reconciled model describes the data much better than the alternative model proposed in Section 6.1.2. This can also be seen in Figure 6.19, which shows the fitted reconciled model and the two fitted alternative model to an exemplary data set.

The objections that led to the proposal of the alternative model are still valid, but the failure of the alternative model to describe data better than the scaling laws of the reconciled model implies that there are other influences at play which either have not been taken into account or which have not been modeled correctly. The alternative model was proposed based on theoretical objections to the previous model's assumptions. The aim of this thesis is to investigate the effect of arachidonic acid on endothelial cell motility. Elucidating an alternative model falls outside the scope of this thesis.

A curious thing appeared when fitting the alternative model to data. In the alternative model, the shape of the spreading cell is described as a fried egg with an egg-white height, h , and a yolk radius, r , instead of as a short, fat cylinder. With almost no exceptions, the height of the egg-white was much larger than the radius of the yolk, $h \gg r$, in the best fit to data. This means that, even in the alternative model, the shape of the cell that fit the data best resembled a short, fat cylinder, rather than a fried egg, though, admittedly, the fit did not describe the data very well. However, in the cases where the second fit with the conserved volume extension described the data reasonable, e.g. Cell L which has a WSSD of 83.27, the parameters described the cell not only as a fried egg but as having dimensions that are close(r) to the actual observed shape of the adhering cell, $r = 0.42$ and $h = 0.66$ (see Section 6.5).

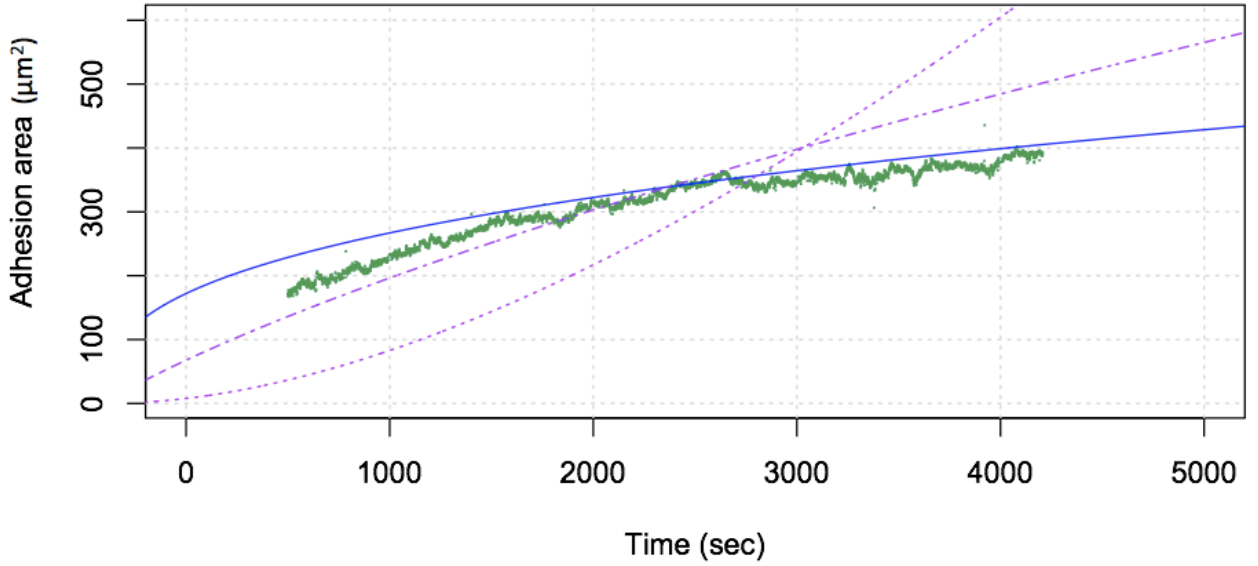


Figure 6.19: The adhesion area as a function of time for an exemplary data set (cell D) with the model fits. The model that best describe the data is the reconciled model (full blue line) with $c = 227$ and $a = 5.7039$. The two alternative models are also shown, but these fit the data less well (dashed and dashed-dotted purple lines).

Using the reconciled model to estimate the standard

The standard for regularly spreading endothelial cells on a Collagen IV coated glass slide with no arachidonic acid present in the media will be described through the parameters of the scaling laws provided by the reconciled model, since the reconciled two phase model describes the data better than the alternative model. The scaling laws of the reconciled model are:

$$\begin{aligned} \text{For P1:} \quad & A(t) = c_1 \cdot (t - t_0)^{a_1} \\ \text{and for P2:} \quad & A(t) = c_2 \cdot (t - t_0)^{a_2} . \end{aligned}$$

The parameters for the fitted laws of the reconciled model for each data set can be found in Table 6.2.

Another curious thing was found when fitting the scaling laws to data. Since the scaling laws were found by fitting a scaled function, $A = c_i \cdot (t - t_0)^{a_i}$, to the data on a regular plot, the fit is optimized for the lag-time parameter, t_0 , as well. It is worth noting that all the fitted values of t_0 that made the phase transition from the passive spreading phase, P1, to the active spreading phase, P2, coincide at approximately $t = 400$ seconds (see Figure 6.20). The adhesion area for one of the cells (blue) in Figure 6.20 illustrates the inability of DIC to capture the first phase. DIC cannot distinguish the adhesion area, so instead the area of the bulk of the cell is portrayed for the first phase, P1. This is seen as a horizontal accumulation of points at around $A = 150\mu\text{m}$, for $t < 400$. Cuvelier *et al.* lag-time adjust the data by subtracting a lag-time t_0 from their data before analyzing it [76]. The phase transition from P1 to P2 at $A = A_C$ coincided at $t = 400$ seconds for the lag-time adjusted

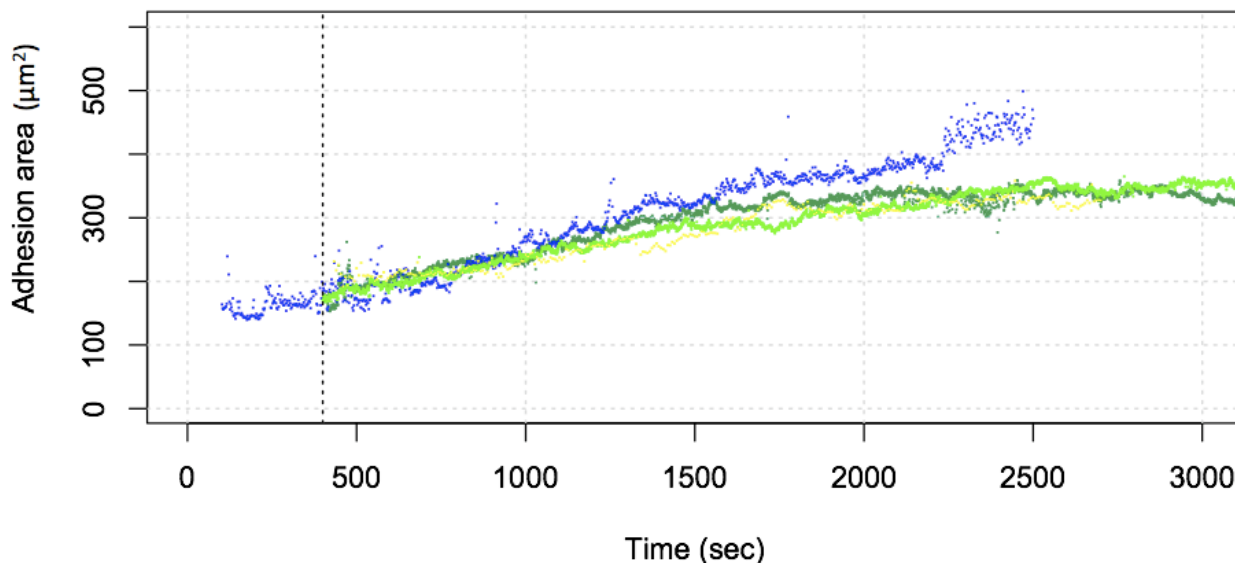


Figure 6.20: The best fit for the reconciled model gives a parameter for a possible lag-time t_0 . The temporal development for the adhesion area have been adjusted with the fitted value of t_0 and the phase transition from the passive spreading phase, P1, to the active spreading phase, P2, coincides at $t = 400$ seconds for almost all of them. Only four of exemplary cells (blue, dark green, green and yellow) are shown here to make the plot less cluttered. adjusts for lag-time in automatically Exemplary temporal developments of the adhesion area which have been fitted with the reconciled model.

data presented by Cuvelier *et al.* Data seems to be lag-time adjusted automatically when fitting a scaled function to data on a regular plot. This supports the hypothesis that the dynamics of a spreading cell have two distinct, naturally well-defined phases and that there is a sharp and fundamental transition between the two.

The standard for endothelial cell adhesion on a Collagen IV substrate *without* arachidonic acid is described by the parameter values of the scaling laws of the reconciled model. For the second, actively spreading phase ($A = c_2 \cdot (t - t_0)^{a_2}$) the parameters of Table 6.2 can be summarized to:

	no. of observations	mean of c_2	a_2
For P2 ($i = 2$)	13	31.92 ± 71.02	0.649 ± 0.239

These parameters differ⁸ from the theoretical values, $a_1 = 1$ and $a_2 = 0.5$, predicted by Cuvelier *et al.* [76]. These results for endothelial cells do not support their “universal” model. The disagreement between the theoretical parameter values and the parameter values found for endothelial cells may be due to some of the objectionable assumptions Cuvelier and his collaborators made to simplify their model or due to the presence of cell-type specific parameters, which were not part of the model.

⁸It is possible to make them similar to Cuvelier *et al.*’s theoretical values by lag-time adjusting data specifically to make the theoretical scaling laws appear on a double logarithmic plot. However, such a fit would not describe data accurately, as discussed in Section 6.1.4

data set:	c_2	t_0 (sec)	a_2
Cell A	144.98	0	0.365
Cell B	0.27	-800	0.793
Cell C	31.68	-1800	0.446
Cell D	227.39	800	0.351
Cell E	0.70	0	0.606
Cell F	0.49	2000	0.644
Cell G	1.546	100	0.552
Cell H	0.08	500	0.776
Cell I	0.61	-1100	0.592
Cell J	0.54	500	0.758
Cell K	0.09	-1600	0.890
Cell L	0.36	0	0.717
Cell M	0.03	-500	1.212

Table 6.2: The constants a_i and c_i of the scaling law $A(t) = c_i(t - t_0)^{a_i}$ for phase P2 found by fitting a scaled function to data on a regular plot. The first table contains observations from DIC microscopy, which can only observe the P2 phase. The second table contains observations from C-RICM microscopy, which can observe both phase P1 and P2.

The parameter t_0 describes the lag-time in the recording of data. In the context of Cuvelier *et al.*'s model, the parameter c has a physical interpretation, $c = k \cdot \frac{JR_C^3}{\eta_C}$, where k is a proportionality constant. The proportionality constant is the same for all data sets since it actually reflects the proportionality of the adhesive and dissipative energy, and this is the same for all data. Any variance in c will therefore be due to a variance in $\frac{JR_C^3}{\eta_C}$. The adhesion energy per unit area, J , and the viscosity of the cell, η_C , should be the same for all endothelial cells in the control experiments. The cells vary slightly in initial volume, R_C , but not nearly enough to account for the large deviation seen in the constant $c_2 = 31.92 \pm 71.02$. The large standard deviation of c_2 suggests that the theoretical assumptions behind Cuvelier *et al.*'s model do not describe the process of adhesion adequately.

Due to the practically harmless illumination of DIC microscopy the adhesion assays were recorded using DIC. This will admittedly only provide insights into arachidonic acid's effect on the active spreading that occurs in P2 and not the effect on the passive spreading in P1. Active spreading requires the remodeling of the cytoskeleton, and phase P2 is therefore excellently suited for answering the questions posed in the introduction to this chapter on adhesion assays: Does arachidonic acid affect endothelial cell migration through a regulation of the cytoskeletal behavior?

Deciphering the effect of arachidonic acid on the passive spreading in the first phase, P1, falls outside the scope of this thesis, since a cell's passive spreading is not a part of cell motility. The C-RICM observations are therefore only used to establish the existence of two distinct phases and to guarantee that the adhesion area observed through DIC microscopy is, in fact, the actual adhesion area.

6.7 Arachidonic Acid's Effect on Endothelial Cell Adhesion

The previous sections established a standard for the adhesion area's temporal development of an adhering and spreading endothelial cell in the absence of arachidonic acid. The standard describes a temporal development with two distinct phases: the first, passively spreading phase, P1, and the second, actively spreading phase, P2. The active spreading of an adhering cell is accommodated through cytoskeletal remodeling. An effect on the rate of adhesion when a cell is actively spreading is essentially an effect on the rate of the cytoskeletal remodeling. Cytoskeletal remodeling is also the process through which cells migrate, and by investigating arachidonic acid's effect on the rate of cytoskeletal remodeling, this section aims to elucidate the regulatory effect that arachidonic acid has on endothelial cell migration as observed by Jensen and his collaborators [35]. In this section, comparison with the standard is used to determine how the presence of arachidonic acid may affect the adhesion of endothelial cells.

Arachidonic acid is an amphiphilic compound, and when it is added to the cells' media, it will spontaneously incorporate itself into the cells' membranes to shield its hydrophobic tails. This incorporation of arachidonic acid in the membrane changes the membranes' composition and their physical properties. Four different concentrations of arachidonic acid were used in the following experiments to investigate its effect on endothelial cell adhesion: 20.53 μM , 41.06 μM , 61.59 μM and 82.11 μM .

The viability assays in Section 5 showed that arachidonic acid in concentrations of 82.11 μM or less do not harm the cells, so any observed change in adhesion behavior can be attributed to the harmless presence of arachidonic acid in the media. Arachidonic acid was added to the CO_2 -independent medium used for the adhesion assays from a 1 mM stock solution in ethanol. The amount of ethanol in the media never exceeded 0.1%, so it had no effect on the cells.

Methods

The confluent endothelial cells were trypsinated and brought into suspension using CO_2 -independent media containing 20.53, 41.06, 61.59 or 82.11 μM arachidonic acid, as in the control experiments described above. The suspended cells were then left to incubate in the media for 20 minutes with the arachidonic acid at 37°C to ensure that the arachidonic acid present in the media had been incorporated into the cells' membranes. The cells were stirred every few minutes during this incubation to keep the suspended cells from attaching. After the incubation, the suspended cells were transferred to chambers on Collagen IV coated glass slides for microscopic observations of their adhesion and spreading.

The adhesion assays were conducted through DIC microscopy, which can only distinguish an adhering cell's adhesion area once the area exceeds the bulk of the cell, $A(t) > A_C$. The adhesion area was observed as a function of time, and a scaled function, $A = c_2(t - t_0)^{a_2}$, was fitted to the data on a regular plot. The fitted parameters are then compared to the parameters of the reconciled two phase model which describes the standard for regular endothelial cell adhesion without arachidonic acid.

The second, actively spreading phase, P2, of the reconciled model is described by a scaling law, $A = c_2(t - t_0)^{a_2}$. The standard established in the previous section for adhering endothelial cells *without* arachidonic acid in the media is described through the value of its parameters:

$$c_2 = 31.92 \pm 71.02, \quad \text{and} \quad a_2 = 0.649 \pm 0.239.$$

Six cells were observed with 82 μM arachidonic acid in the media, five cells were observed with 62 μM arachidonic acid in the media, eight cells were observed with 41 μM arachidonic acid in the media and four cells were observed with 20 μM arachidonic acid in the media. A power law, $A(t) = c_2 \cdot (t - t_0)^{a_2}$, was fitted to each of the observations for the cells affected by arachidonic acid. The fitted values of a_2 and c_2 can be seen in Table 6.3. The results from Table 6.3 can be summarized as follows:

	no. of observations	c_2	a_2
0 (control)	17	29.668 ± 68.755	0.649 ± 0.239
20.53	5	0.216 ± 0.180	0.912 ± 0.121
41.06	8	1.575 ± 3.869	0.848 ± 0.185
61.59	5	1.060 ± 1.958	0.747 ± 0.315
82.11	6	161 ± 380.501	0.487 ± 0.101

The shape of a scaling law for the growth of the adhesion area is determined by the constant exponent a_2 . The exponential growth of the adhesion area with time described by the constant a_2 alters when the adhering cells have been affected by arachidonic acid. Figure 6.21 shows the fitted scaling laws' exponential constant a_2 as a function of the arachidonic acid concentration in the media. The lower concentrations (20, 41 and 62 μM) seem to enhance the growth of the adhesion area/speed up the spreading of the cell, since they have bigger exponential growths compared to the standard for endothelial cell adhesion without arachidonic acid. In contrast the highest concentration (82 μM) limits the growth of the adhesion area/slow down the spreading of the cell, since it has a lower exponential growth $a_2 = 0.487 \pm 0.101$ compared to the control, where $a_2 = 0.649 \pm 0.239$. These values can all be seen in Table 6.3 as well.

Even with the limited number of observations for each concentration of arachidonic acid, there are statistically significant deviations on a 5% level from the standard for the low (20.53 μM) and high concentrations (82.11 μM), and Figure 6.21 displays a distinct trend. This trend is reflected in arachidonic acid's effect on endothelial cell migration as previously observed by Jensen *et al.* [35]. The p-values from student's T-test are denoted in the table below where any p-values < 0.05 are highlighted in blue:

p-values (a_2)	control	20 μM AA	41 μM AA	62 μM AA	82 μM AA
control	-	0.014	0.056	0.487	0.054
20.53 μM AA	0.014	-	0.512	0.252	0.001
41.06 μM AA	0.056	0.512	-	0.482	0.001
61.59 μM AA	0.487	0.252	0.482	-	0.076
82.11 μM AA	0.054	0.001	0.001	0.076	-

data set (DIC):	Concentration:	c_2	t_0 (seconds)	a_2
cell a	20.53	0.115 ± 0.007	0	0.925 ± 0.010
cell b	20.53	0.169 ± 0.007	0	0.875 ± 0.006
cell c	20.53	0.483 ± 0.108	0	0.778 ± 0.025
cell d	20.53	0.098 ± 0.007	0	1.068 ± 0.016
cell e	41.06	0.132 ± 0.007	-200	0.793 ± 0.007
cell f	41.06	0.120 ± 0.007	-200	0.941 ± 0.010
cell g	41.06	10.349 ± 1.372	-200	0.549 ± 0.007
cell h	41.06	0.170 ± 0.031	0	0.809 ± 0.024
cell i	41.06	0.053 ± 0.004	0	1.114 ± 0.020
cell j	41.06	0.151 ± 0.046	0	0.742 ± 0.035
cell k	41.06	0.049 ± 0.003	0	0.990 ± 0.012
cell l	61.59	0.390 ± 0.478	-2300	0.597 ± 0.098
cell m	61.59	1.630 ± 0.166	-100	0.497 ± 0.006
cell n	61.59	5.298 ± 0.770	-500	0.477 ± 0.007
cell o	61.59	0.036 ± 0.002	0	1.223 ± 0.014
cell p	61.59	0.026 ± 0.008	-100	0.645 ± 0.039
cell q	61.59	0.0182 ± 0.001	0	0.617 ± 0.010
cell r	61.59	0.023 ± 0.002	0	1.175 ± 0.031
cell s	82.11	0.607 ± 0.172	-400	0.591 ± 0.021
cell t	82.11	1.139 ± 0.262	800	0.567 ± 0.046
cell u	82.11	938.063 ± 296	0	0.309 ± 0.006
cell v	82.11	1.987 ± 0.744	-500	0.494 ± 0.021
cell w	82.11	8.719 ± 5.755	2200	0.512 ± 0.034
cell x	82.11	18.445 ± 2.124	-500	0.450 ± 0.005

Table 6.3: The constants a_i and c_i of the scaling law $A(t) = c_i(t - t_0)^{a_i}$ for phase P2 found by fitting a scaled function to data on a regular plot. The first table contains observations from DIC microscopy, which can only observe the P2 phase. The second table contains observations from C-RICM microscopy, which can observe both phase P1 and P2.

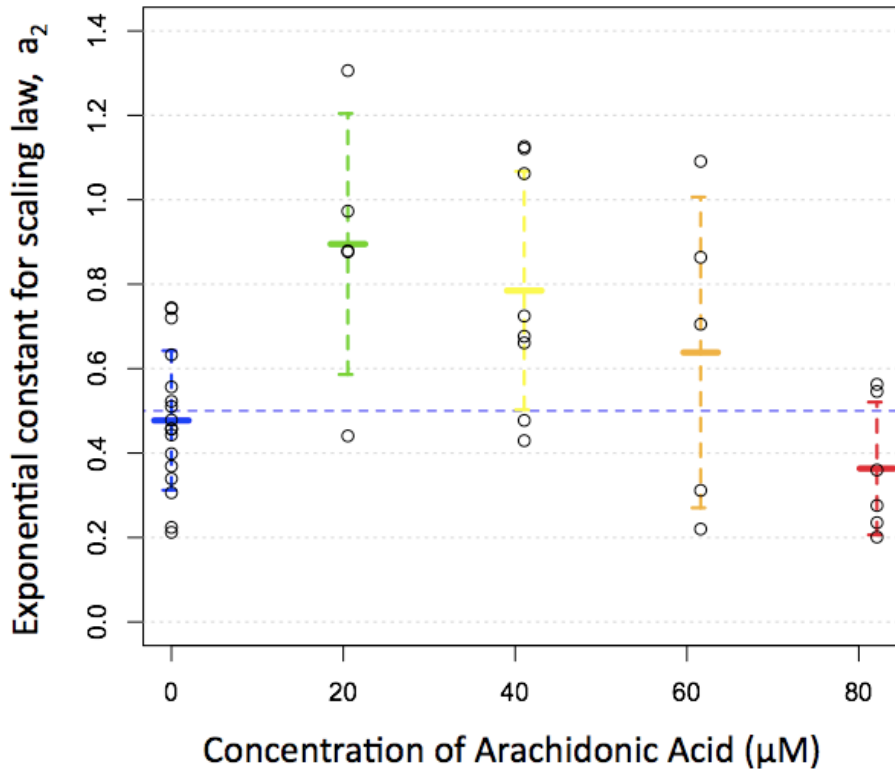


Figure 6.21: The exponential constant, a_2 , from the scaling law, $A(t) = c_2 t^{a_2}$, fitted to each experimental data set. The exponential constants, a_2 , are plotted as a function of the concentration of arachidonic acid (AA) in the medium of the adhering cell. The scaling law for the later phase in the two phase model as predicted by Cuvelier *et al.* is illustrated by a dashed, blue line at $a_2 = 0.5$. The mean and standard deviation for the control experiments and the experiments with different AA concentrations have been denoted with different colors: control with 0 μM AA (blue), 20.53 μM AA (green), 41.06 μM AA (yellow), 61.59 μM AA (orange), 82.11 μM AA (green). The mean and standard deviation for each set of experiments is shown by a thick, full line and by dashed lines respectively.

Though the number of observations for each concentration is limited, Figure 6.21 shows a clear trend in arachidonic acid's effect on endothelial cell adhesion. At lower concentrations, arachidonic acid enhances spreading, and at higher concentrations, it limits spreading. A similar trend can be seen for arachidonic acid's effect on endothelial cell migration. The previous results of AA's effect on migration from Jensen *et al* are also shown in Figure 6.22. Though the small number of observation makes the experimental data less statistically robust, the deviation from the standard for endothelial cell adhesion without arachidonic acid is statistically significant, and the resemblance to previous studies results of arachidonic acid's effect on endothelial migration makes the results presented here remarkable.

Jensen *et al* succeeded in pinpointing the metabolites of arachidonic acid as the source of AA's dual ability to both enhance and inhibit migration. It would be very interesting, and a natural progression of these studies, to investigate the arachidonic acid's metabolites for a similar regulation of cell adhesion.

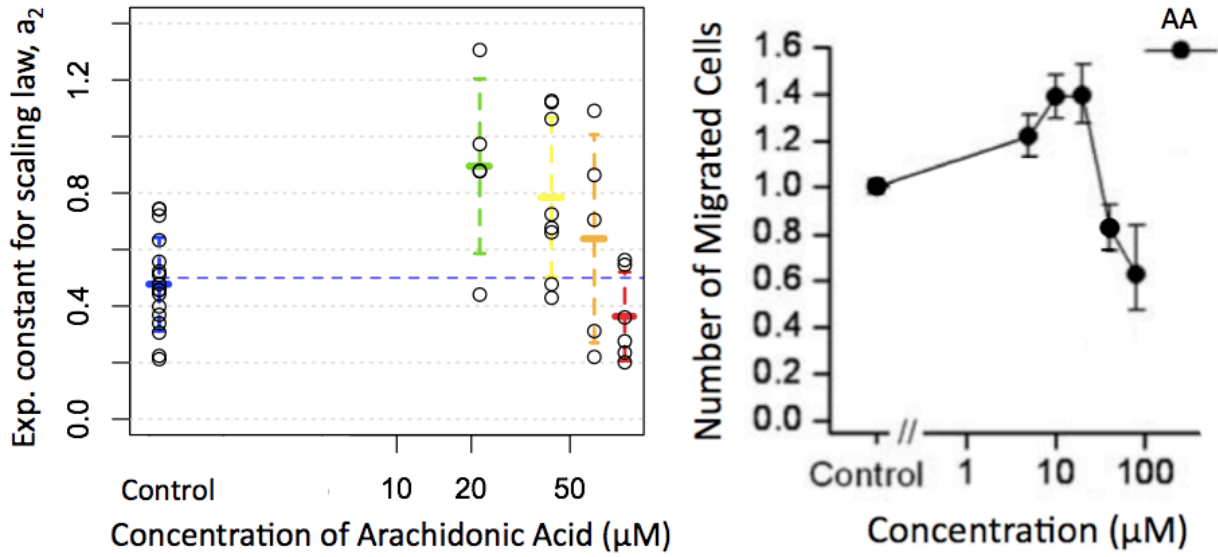


Figure 6.22: The exponential constant, a_2 , from the scaling law, $A(t) = c_2 t^{a_2}$, fitted to each experimental data set compared to previous results by Jensen *et al.* 2007. Left: The exponential constants, a_2 , are plotted as a function of the concentration of arachidonic acid (AA) in the medium of the adhering cell on a logarithmic scale for easier comparison. The colors and values are the same as in Figure 6.21. Right: The Number of Migrated Cells (NMC) as a function of the concentration of arachidonic acid (AA) in the medium of the migrating cell on a logarithmic scale (from Jensen *et al.* 2007). The general trend in the two plots is strikingly similar, particularly since they portray data from two such different assays, i.e., adhesion/spreading assays and migration assays. At lower concentrations, arachidonic acid (AA) enhances both the spreading and the migration of endothelial cells, whereas the spreading and the migration are both inhibited by high concentrations of AA.

The two phase model as presented by Cuvelier *et al.* [76] predicts the following scaling law for the later phase

$$A \propto \left(\frac{J \cdot R_C^3}{\eta_C} \right)^{\frac{1}{2}} \cdot t^{\frac{1}{2}} \quad \text{for } R > R_C .$$

The membrane's viscosity, η_C , acts as a scalar in this power law, and altering the viscosity will not change the scaling law's growth exponents, a_2 , only the scaling constant, c_2 . However, the data presented here show that altering the microviscosity does change the scaling law's growth exponent, a_2 . This suggests that Cuvelier *et al.*'s model does not describe the process of adhesion adequately with respect to induced changes in the membrane's physical properties.

6.8 Conclusion to Endothelial Cell Adhesion

Amphiphilic compounds were shown to affect the migration of endothelial cells in previous studies [34, 35]. Eukaryotic cell migration is very complex and it is difficult to discern, analyze and understand the myriad of biophysical processes that gives rise to this migration. It is possible to simplify the complex process of migration in an adhesion assay [65]. The adhesion assay isolate the cytoskeletal behavior from the myriad of other processes, since the most pronounced process during cell adhesion and spreading is the remodeling of the cytoskeleton. Using adhesion assays, it is possible to investigate whether the addition of amphiphilic compounds to the cells media affect the cytoskeletal regulation.

The adhesion was analyzed as a function of time using the reconciled model proposed in this chapter. The reconciled model is a two phase model which also models an inherent lag-time in the data and analyzes it in a specific way. A lag-time is introduced in the scaling laws that describe the temporal development of the adhesion area in each phase, $A = c_i(t - t_0)^{a_i}$, with the phase index $i = \{1, 2\}$. The remodeling of the cytoskeleton is a prominent feature both in endothelial cell adhesion and migration, but the remodeling of the cytoskeleton only occurs at in the second phase of adhesion in which the cell is actively spreading. The second phase of adhesion was investigated to discern the affect that arachidonic acid may have on cytoskeletal remodeling using a differential interference contrast (DIC) microscope. DIC microscopes can only be used for the inspection of the adhesion area in the second, actively spreading phase, but through the use of confocal microscopy it was determined that the observation of membrane protrusions through the DIC microscope was in fact adhesive protrusion on the Collagen IV coated glass slide.

The adhesion assays show that the presence of arachidonic acid have an effect on the second phase of endothelial cell adhesion in which the cell is actively spreading. The adhesion area increases at a higher rate, $a_2 = 0.912 \pm 0.121$, for a low concentration (20.53 μM) of arachidonic acid, than it does for control cells with no arachidonic acid in the media where the rate is $a_2 = 0.649 \pm 0.239$. The higher rate of adhesion area increase suggests an increased responsiveness in the remodeling of the cytoskeleton. In the previous studies by Jensen and his collaborators, the migration of endothelial cells were seen to be enhanced at this concentration of arachidonic acid.

For a high concentration (82.11 μM) of arachidonic acid the adhesion area increase occurred at a much lower rate, $a_2 = 0.487 \pm 0.101$, suggesting that a less responsive regulation of the cytoskeletal remodeling. The previous studies of arachidonic acid's effect on endothelial cell migration reported that a similar concentration of arachidonic acid inhibits cell migration. This is as could be expected as cell migration would also be affected by a lessened responsiveness in the cytoskeletal remodeling.

Endothelial cell adhesion and migration are both mediated through the remodeling of the cytoskeleton, and the accordance between the results for the effect of arachidonic acid on adhesion assays in this thesis with the previous results on migration assays is remarkable.

Chapter 7

Endothelial Cell Migration

Endothelial cell migration plays a significant role in many pathologies, so there is a large incentive to investigate, understand and possibly regulate cell migration. Migration studies can be conducted both *in vivo* and *in vitro*. *In vivo* studies most closely resemble naturally occurring cell pathologies, but the multiple biological factors of each individual test-animal are difficult to take into account. *In vitro* studies offer a higher degree of control over the experimental set-up and still resemble natural cell migration, even though these studies are farther removed from the natural circumstances. The amount of nutrients, oxygen, waste-products and chemical compounds (such as arachidonic acid or chemotaxins), as well as the cell types present in a sample, can be controlled *in vitro*. The migration of endothelial cells mediates angiogenesis. To isolate and investigate the effect that arachidonic acid could have on endothelial cell migration, and therefore on angiogenesis, only porcine aortic endothelial cells will be present in the *in vitro* samples presented.

The migration process is difficult to characterize because of its complexity. The adhesion assays in Chapter 6 simplified the process of migration considerably and showed that the presence of arachidonic acid has an effect on endothelial cell adhesion. Only by remodeling the cytoskeleton are cells able to adhere and spread out across surfaces. Cytoskeletal remodeling is also one of the major mechanisms behind cell motility in general and behind cell migration specifically. An adhesion assay isolates the regulation of the cytoskeletal remodeling from the myriad of other biological processes in the cell's general motility, and the regulation of cytoskeletal remodeling is easier to investigate in adhesion assays than in migration assays. The investigation in Chapter 6 showed that the presence of arachidonic acid affected the rate of adhesion of endothelial cells. Smaller concentrations (20 μM) of arachidonic acid made the cells spread out much faster, i.e. the cytoskeletal remodeling occurred or responded much quicker than when *no* arachidonic acid was present in the media. A quicker remodeling of the cytoskeleton would, all other things equal, also speed up the process of migration, and similarly, small concentrations of AA have indeed been shown to promote the migration of endothelial cells by Jensen *et al.* [35]. Larger concentrations (82 μM) of arachidonic acid, however, caused the cells to spread out much more slowly, i.e. the cytoskeletal remodeling was less responsive than when *no* arachidonic acid was present in the media. Similarly, large concentrations of arachidonic acid have also been shown to inhibit the migration of endothelial cells [35], as would be expected by a cytoskeleton made less responsive to remodeling.

Migration assays are usually constructed as “razor wound” assays in which a confluent, confined monolayer of cells is presented with vacant space. The progression of the cells out into the vacant space is then analyzed through microscopic observation. Migration assays can last for hours or for days. Most migration assays are conducted as a comparison of the before-and-after shots after 24 hours of migration. This was also the case for the previous experiments by Jensen and his collaborators that showed the regulatory effect of arachidonic acid on endothelial cell migration. This chapter will further investigate the migratory behavior of endothelial cells *in vitro* by conducting migration assays with a continuous observation of migrating endothelial cells. The dynamics of the monolayer as a whole will be analyzed, as well as the progression of individual cells within the monolayer. It is hoped that a better understanding of endothelial cell migration, both collectively and at the single cell level, will be achieved by following single cells and comparing their motion with the collective dynamics of the monolayer.

It is possible to study the migration of single cells as well as a monolayer of cells. Single cell migration assays resemble adhesion assays in that a single isolated cell is observed, but their individual migration is monitored over a much longer period of time. There are a number of single cell migration studies in the literature with several proposed models as well. Unfortunately, single cell studies are not relevant to endothelial cells, since endothelial cells are never found as single cells in healthy physiology [54]. Only the collective migration of endothelial cells occurs under natural circumstances and is physiologically relevant. Nonetheless, some single cell migration assays were performed during the course of this thesis. The outcome of these assays will not be discussed at length here, but they displayed highly variable and erratic migratory behavior for the single endothelial cells. Several individual cells can be monitored within the same field of observation using a 10× magnification. In the same frame, some cells would move rapidly and erratically while others remained completely stationary over the course of 24 hours. Due to the physiological irrelevance of the behavior of single endothelial cells, this thesis will not go into more detail about their migratory behavior. It suffices to say that their migratory behavior was found to be highly variable and erratic and completely different from the behavior of cells within a monolayer, even in the absence of arachidonic acid.

Apart from characterizing the migratory behavior of a confluent, monolayer of endothelial cells, as well as the individual cells within the monolayer, this chapter also investigates the effects of adding arachidonic acid to the media of migrating endothelial cells. In Chapter 6, the adhesion of endothelial cells *without* arachidonic acid was characterized to establish a standard for endothelial cell adhesion behavior in the absence of arachidonic acid and *then* to establish the effect of arachidonic acid by comparison to this standard. This chapter contains studies of several variables using the same data sets, so the effect of adding arachidonic acid to the media will be addressed immediately in every analysis to make this chapter more readable.

7.1 Previous Studies of Endothelial Cell Migration

The vacant space can be presented to a confluent monolayer of cells by either removing some of the cells from the confluent monolayer or by removing/lifting a confinement. It does not

matter which method is used, since it has been shown for both epithelial and endothelial cells that the presence of vacant space next to a confluent monolayer triggers a migration of the cells out into the vacant space [66, 54]. However, when cells are removed from the confluent monolayer, as is the case in most “wound” assays, particularly razor wound assays¹, the removal process destroys the removed cells. The destroyed cells intracellular content and other cell debris is released into the medium, which can be quite traumatic for the cells on the newly formed border [66], so the debris and remnants of the dead cells should be washed away as soon as possible after the cell removal. Even when the debris is quickly washed away, the cells on the newly formed border can be slightly traumatized. They were adhered to the removed cells through cell-cell contact, and the tearing off these adhesive junctions leaves the cells on the newly formed border partially permeable [66]. It has been speculated that the sudden influx of medium into the border cells and/or chemical signaling from the destroyed cells initiates the border cell’s migration. It is possible that one or both initiate migration, but migration is also initiated in the absence of both by the simple presence of a vacant space next to a confluent monolayer [66, 54].

Most characterizations of the collective migration of a confluent monolayer of cells in the literature are qualitative, rather than quantitative. Even qualitative characterizations can be difficult, since different cell types display different types of migration when presented with a vacant surface. Some cell types, such as muscle cells, dissociate and explore the new surroundings individually. Other cell types, such as epithelial or endothelial cells, maintain cell-cell contacts while invading the vacant space and migrate collectively as a sheet [66]. The different migratory behavior reflects the physiology of the different cell types. The lining of skin is primarily constituted of epithelial cells, and the lining of blood vessels are primarily constituted of endothelial cells. Both skin and blood vessels are required to be impermeable to specific molecules and become pathological if their collective front is breached. These cells need to maintain complete cell-cell contact at all times, even during migration.

Epithelial cells are the darling subject for “wound” migration assays, since their migration mediates the actual healing of wounds inflicted on the skin. In 2007 Poujade and his collaborators studied the migration of epithelial cells in a migration assay, in which vacant, virgin space was presented to confluent monolayers of epithelial cells. The progression of these confluent, epithelial monolayers can be seen in Figure 7.1. The onset of migration out into vacant space depends significantly on the initial cell density of the monolayer [85]. Poujade *et al.* reports that, within a couple of hours of presenting the confluent epithelium with a vacant, virgin surface, the epithelial cells became progressively motile in the direction perpendicular to the free edge [66].

Qualitative description of epithelial cell migration

The progression of the free edges of the epithelial wound was highly non-linear. The nonlinearities were a result of a roughening of the edge due to the appearance of *leader cells*.

¹Beside scratching the monolayer with pipettes or razorblades, cells can also be removed by laser photoablation or by applying a voltage pulse to an electrode under the monolayer. Both of these removal techniques have been used successfully in migration assays, but they are more harmful to the remaining cells than the razor wound assay [84]

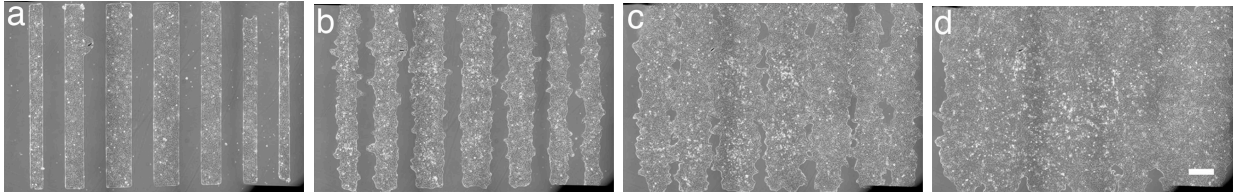


Figure 7.1: A sequence of micrographs showing the progression of several bands of different initial widths at different times: “a” is 1.5 hours (90 minutes) after the presentation of a vacant space, “b” is taken after 13 hours, “c” is taken after 25 hours, and “d” is taken after 37 hours. Each of the images (a-d) results from 18 acquisition fields stitched together, and the scale bar is $400 \mu\text{m}$ long (from Poujade *et al.* 2007 [66]).

Leader cells are distinct from the other epithelial cells of the border, since they are more spread out and more motile due to their development of a clear active ruffling lamellipodium [66]. The first leader cells typically appeared after 1 hour, both from the initial border and from the first, second and third rows of cells [66]. Apart from becoming larger and more motile, the leader cells also lose the sub-cortical actin and develop well-defined focal adhesions at their leading edge. Poujade *et al.* revealed the loss of these epithelial characteristics using fluorescence microscopy. The more motile leader cells maintain cell-cell contacts with their *followers* via the cadherin mediated adherens junction. Followers are less motile, regular epithelial cells with all their epithelial characteristics intact. The leader cells drag their followers into the vacant space, thereby forming “fingers”. These fingers can start at any point during the course of an experiment, so their numbers increase with time. This progression of fingers roughened the borders of the wound considerably. However, a quantitative evolution of the edge’s contour length revealed no universal behavior and this diversity in the observed behavior can be attributed to the fingering destabilization of the border [66]. The leader cells’ loss of epithelial characteristics was only transient because when the wound was closed, the leader cells regained their epithelial characteristics and became indiscernible from the other epithelial cells.

Quantitative analysis of epithelial cell migration

Having characterized the group migration of epithelial cells qualitatively by the description of the fingering instability, Poujade and his collaborators also made a few quantitative analyses:

- Typically, the average velocity of the free edge accelerated from 0 to $10 \pm 5 \mu\text{m}/\text{h}$ in 15 hours [66].
- The mean progression of the edge, $\langle s \rangle$, was fitted with a power law, $\langle s \rangle = a \cdot t^n$, and the exponential constant was $n = 1.8 \pm 0.4$ after a few hours [66]. Poujade *et al.* have no exact interpretation of this acceleration, but as the data seem to level off long term, they do not rule out the possibility of a slow transition toward a constant velocity regime ($n = 1$) after a latency time.
- The mean velocity of the border after 10 hours was $v_{\text{border}} \approx 10 \mu\text{m}/\text{h}$.

- The velocities of the leader cells were also measured and found to be $v_{\text{leader}} = 18 \pm 2 \mu\text{m}/\text{h}$, significantly higher than the mean velocity of the border. The leaders also had very high directionality, so once they took a direction they essentially kept it for the time-course of an experiment. For $\approx 70\%$ of the studied fingers, the direction of the leader cell was perpendicular to the initial border.
- The distribution of fingers along the border was very heterogeneous, but in some circumstances, Poujade *et al.* observed as many as five fingers per millimeter, i.e., one finger as often as every $200 \mu\text{m}$ or so.

Epithelial cell movement within a confluent monolayer

The above summarizes the characteristics of the migrating border of an epithelial “wound” assay. It has previously been observed that epithelial cells migrate actively *within* the confluent monolayer by developing active “cryptic” lamellipodia under the other cells [86]. Poujade *et al.* characterized the epithelial cell migration within the confluent monolayer using *particle image velocimetry* (PIV). Particle image velocimetry is a whole-field technique that can measure the local displacement vectors by cross-correlating successive images. The PIV technique is primarily used in hydrodynamics, but it can also be used to analyze the dynamics of cells if there is enough texture in the successive images. The displacement field in the migrating epithelium was found to be quite complex with a remarkable long-range correlation on the order of $100 \mu\text{m}$ [66]. It can be seen in Figure 7.2. The correlated flows of cells in the migrating epithelium were also not necessarily directed towards the free surface [66].

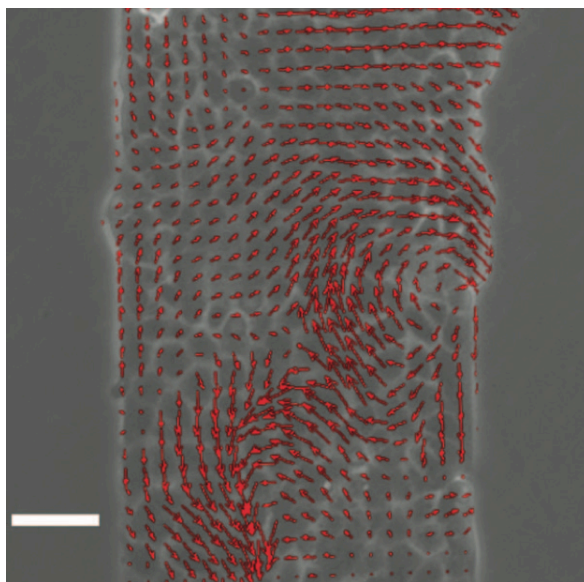


Figure 7.2: Snap shot of the velocity field 4 hours after presenting the confluent, epithelial monolayer with a vacant space on either side (Scale bar: $50 \mu\text{m}$). (from Poujade *et al.* 2007 [66]).

Arachidonic acid's effect on endothelial cell migration

Jensen *et al.* showed that arachidonic acid has a regulating effect on endothelial cells migration [35], and Ghosh *et al.* [34] showed that changing the microviscosity of endothelial cell membranes affect their migration. None of the authors above or their collaborator report a standard migration velocity for endothelial cells, instead they reported the relative change in migration by adding amphiphilic compounds to the media compared to the control. The speed or ease with which endothelial cells migrate is dependent on the substrate on which they migrate, as well as the medium, the temperature and the atmospheric composition. These dependencies makes comparison of quantitative measurements between experiments difficult. Adding amphiphilic compounds to the media of endothelial cells affects their migration, and the previous result has already be described in detail in Chapter 4. The following is a brief recap of the results of Jensen, Ghosh and their respective collaborators.

In a razor wound assay, the vacant space is created by carefully removing half the cells by pressing a sterile razor blade down to the glass and gently sweeping the cells to one side of the demarcation line off the glass slide. The progress of the cells' migration is then recorded as the number of migrated cells (NMC) that crossed the demarcation line in 24 hours. Figure 7.3 shows some typical observations of razor wound assays with arachidonic acid present in the media.

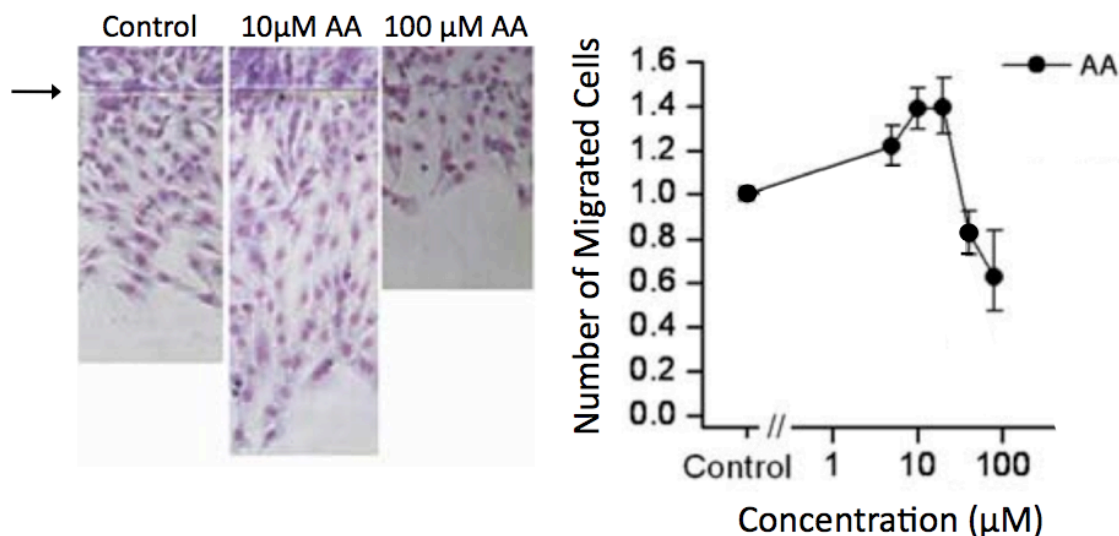


Figure 7.3: Left: Exemplary razor wound assays observed by Jensen *et al.*, both of a control assay and after adding 10 and 100 μM arachidonic acid (AA) to the media of the cells. Right: The number of migrated cells (NMC) when compared to the control razor wound assays as a function of the concentration of arachidonic acid added to the migration media (from Jensen *et al.* 2007 [35]). Arachidonic acid is an amphiphilic compound and its ability to both promote migration at low concentrations and inhibit migration at higher concentrations is clearly seen.

Arachidonic acid was the only amphiphilic compound tested by Jensen *et al.* that could promote, as well as inhibit, endothelial cell migration depending on the concentration with

which it was present in the cells' media. At low concentrations ($10 \mu\text{M}$), arachidonic acid promotes endothelial cell migration, whereas it inhibits migration at high concentrations ($100 \mu\text{M}$) [35], see Figure 7.3. Ghosh and his collaborators showed that the change in migration correlates particularly well with the change in the *microviscosity* of the membrane [34], as can be seen in Figure 7.4. Microviscosity is 1/fluidity of a lipid bilayer and refers to the rate of molecular motion within the bilayer. The rate of molecular motion is higher in a membrane with low microviscosity than in a membrane with high microviscosity. Jensen *et al.* showed a similar correlation between the change in endothelial cell migration and the change in the stiffness of the cells' membranes induced by the addition of arachidonic acid or other amphiphilic compounds [35].

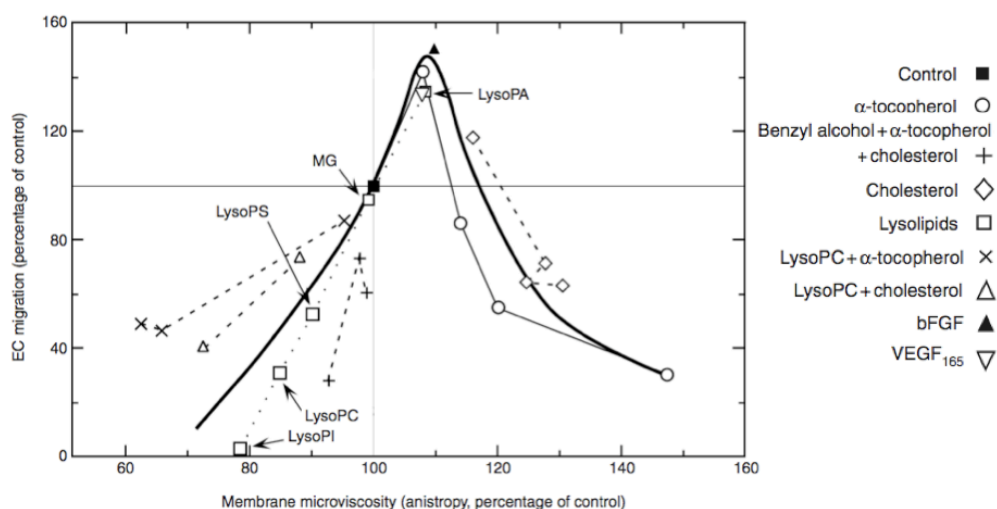


Figure 7.4: Endothelial cell migration plotted as a function of membrane microviscosity measured through membrane anisotropy. Several membrane-active agents were used, as indicated. All experiments were compared to the control experiments at (100%, 100%). The estimated fit for the biphasic relation between migration and microviscosity is shown as a broad solid line (from Ghosh *et al.* 2002).

In general the effect of amphiphilic compounds on the migration of endothelial cells correlates quantitatively with their effect on the physical properties of the membrane, such as microviscosity and stiffness. The close correlation between the change in physical properties of the membrane and the observed change in migration suggests that amphiphilic compounds affect the cells by their incorporation into the membrane and not by binding to specific receptors. Several amphiphilic compounds were tested by Jensen and his collaborators, and they found that the amphiphilic compounds induced similar changes in cell migration. The structural difference between all the amphiphilic compounds tested by Jensen *et al.* further support the claim of non-specific interaction.

It is the dual regulating properties of arachidonic acid that make it interesting compared to other amphiphilic compounds. In Chapter 6, arachidonic acid's effect on endothelial cell adhesion was investigated, and in this chapter, arachidonic acid's effect on endothelial cell migration will be further investigated, both in term of the collective dynamics of a monolayer of endothelial cells as well as at the individual cell level.

Poujade *et al.* used particle image velocimetry (PIV) to investigate the correlation between the individual cell in the monolayer, and Jensen, Ghosh and their respective collaborators counted the number of migrated cells (NMC) individually after 24 hours. However, PIV does not give the displacement vector of the individual cells but rather the displacement vectors of evenly distributed loci in the image, and the number of migrated cells (NMC) was only counted once, so only the final position of individual cells was analyzed, not the individual cells' progression toward these position.

No analysis of the migration of individual cells in group migration assays has been published (to my knowledge). This is probably because the existing software cannot identify the nucleus or outline of an individual living cell in a monolayer unless it has been immunostained. The lack of software means that all individual cell tracking has to be done by hand.

7.2 Migration Assays: Materials and methods

A razor wound assay is described briefly in Chapter 4. In these experiments, razor wound assays are performed on a Collagen IV coated glass slide as in the adhesion assays to facilitate a comparison of the results. Confluent, cultured endothelial cells are trypsinated, diluted and seeded onto these Collagen IV coated glass slides. The cells are then left to incubate with CO₂-dependent medium with FBS at 37°C in an ambient atmosphere of 5% CO₂ until the cells have grown to confluence, and there are no spaces between the individual cells. When the cells have grown confluent, a “wound” is created in the endothelial monolayer on the glass slide by gently pressing a sterile razor blade down and sweeping the cells to one side of the demarcation line off the glass slide, thereby vacating a large space into which the remaining cells can migrate (see Figure 7.5). The glass slide is then washed twice with CO₂-independent medium *without* FBS to remove any remnants of FBS, dead cells and other debris. A chamber consisting of several layers of parafilm, vacuumgrease and another glass slide is constructed around the razor wound, filled with CO₂-independent medium *without* FBS and sealed, see Figure 7.5. The chamber is constructed with several layers of parafilm to make is slightly larger than the ones used in adhesion assays. If the supply of media to the cells is altered during the course of the migration assay, the cells behavior is likely to be affected. The construction of the chambers in the razor wound assays should provide sufficient CO₂-independent medium for the cells to sustain them during the 24 hour migration assays.

Microscope

Due to the 24-hour observations of the migration assays, all experiments were conducted using a DIC microscope with a practically harmless halogenic light source. The migration of endothelial cells was recorded in a DIC microscope with 10 × magnification under constant halogenic illumination and with a sampling rate of 60 frame per minute. However, the analyses will be conducted with a lower temporal resolution, since the induced noise in the high temporal resolution hinders small scale observations.

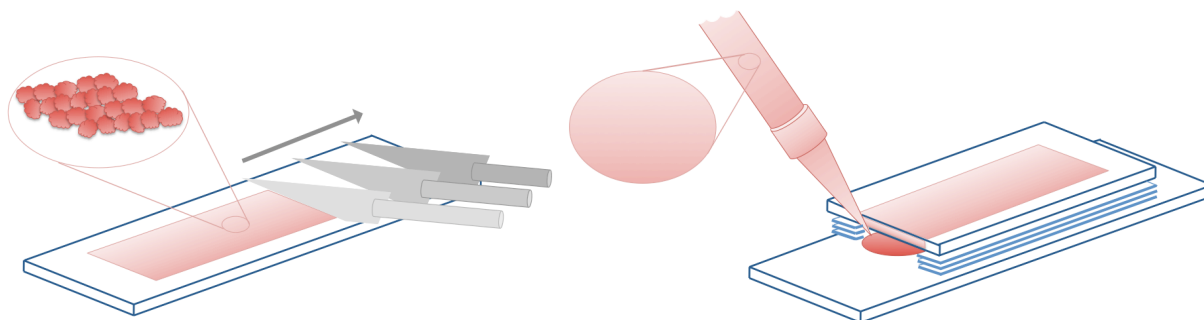


Figure 7.5: A schematic of the glass slide for razor wound assays and how a larger chamber is constructed with several layers of parafilm on these glass slides for use in the migration experiments.

7.3 Migration Assay Data

In vivo endothelial cells need to maintain complete cell-cell contact at all times to show a healthy physiology. These *in vitro* experiments try to mimic the *in vivo* circumstances as closely as possible. The data analyzed in this chapter are therefore from endothelial cell razor wound assays in which the cells within the monolayer maintained complete cell-cell contact at all times during the course of the experiment.

Some migration assays showed single leader cells at the edge of the monolayer which would lose contact with their followers. These cells would behave erratically when they lost contact with their followers. The erratic behavior can best be described as "running on the spot". It was clear that the cells were very motile, and they continuously made lamellipodial protrusions, but these lamellipods were retracted before the cell relocated to another position. When the erratically moving cells actually relocated to another position, the direction of these movements were completely random. This erratic behavior is similar to the one observed in the physiologically irrelevant single cell migration assays (not shown), but ceased once the disconnected leader cell regained cell-cell contact with its followers. The data sets presented and analyzed here contain no or few leader cells that disconnect.

Some data sets, which have been excluded from this analysis, showed discontinuity between the cells within the monolayer. Such discontinuity expresses a pathological state of the cells, and cannot be trusted to reflect the effect of arachidonic acid on endothelial cell migration. Arachidonic acid, in the concentrations used here, was shown to be harmless to the cells in Chapter 5, so the pathology observed in some samples through the discontinuity of cells within the monolayer should not be due to the arachidonic acid present in the media. Indeed, the migration assays displaying discontinuity within the monolayer were randomly distributed between migration assays with no arachidonic acid present and assays with arachidonic acid present in different concentrations. The monolayer in these migration assays had a high cell density when the razor wound was conducted, and conducting the razor wound assay when the cell density had not grown high yet (but the cells were still confluent) greatly improved the quality of the assays. *In vivo* there are natural internal regulations that keep the density of endothelial cells at the right level. The *in vitro* migration

assays fail to display a similar regulation and do not mimic the *in vivo* situation in this aspect. To reflect *in vivo* situation as closely as possible it is necessary to provide this cell density regulation externally by performing migration assay once the monolayer has reached confluence and before the cell density becomes too high.

Since the process of migration is so complex, and the influences many, a large effort was put into making the experimental conditions as similar as possible for the migrating endothelial cells, not only by making sure that the cell monolayer was confluent at all times, but also by disregarding the data sets in which the monolayer initially retracted from the demarcation line of a razor assay. If the monolayer retracts from the demarcation line, the interactions between the Collagen IV coated surface of the glass slide and many of the cells have been disrupted. The disruption of such focal adhesions takes time to reestablish. It has not been investigated how long it takes for the disrupted focal adhesions to reestablish here, so any data sets with a retracting edge has been left out of the analysis. This leaves only a few migration assays that resemble the *in vivo* conditions closely for the different concentrations of arachidonic acid. It would be much preferable to have more datasets for the analysis, but the few presented here are enough for a rough characterization of endothelial cell migration and the effect that arachidonic acid has on it, since all the described trends are statistically significant on a 5% level.

Figure 7.6 shows the progression of the confluent cell monolayer in a razor wound assay at six hour intervals. Movies of exemplary razor wound migration assays can also be viewed in the supplementary material. Endothelial cells are able to migrate a distance of at least 70 μm over 24 hours, when *no* arachidonic acid is present in the media.

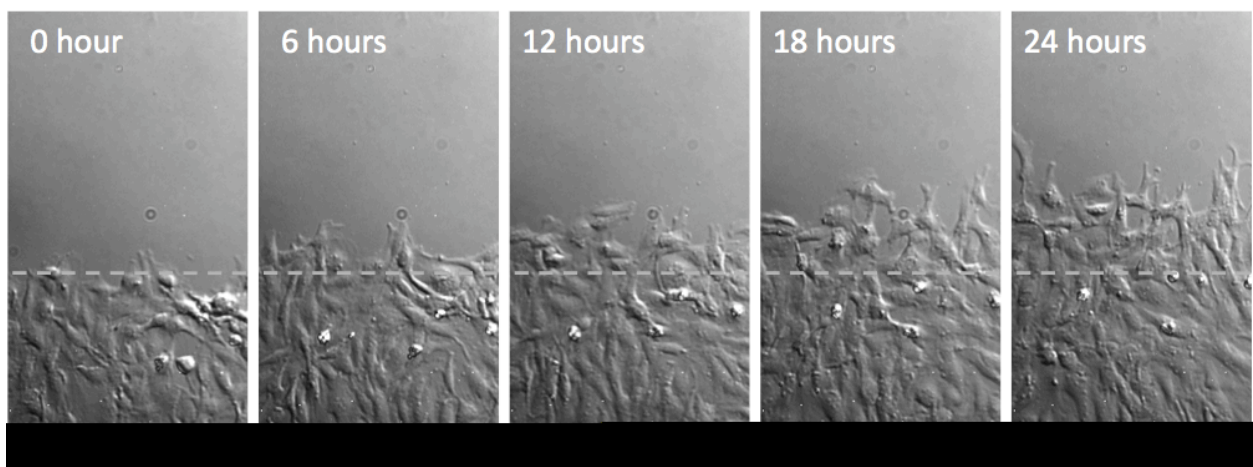


Figure 7.6: Exemplary data from a razor wound assay 0, 6, 12, 18 and 24 hours after the making of the demarcation line. The initial position of the demarcation line has been denoted with a grey dashed line in all 5 images. There is no arachidonic acid present in the media in this example, and the cells migrate at least 70 μm in 24 hours (length scale = 100 μm).

Figure 7.7 shows images of five different razor wound assays after 24 hours of migration. Each of these assays have had different concentrations of arachidonic acid in the media. It is clear from Figure 7.7 that adding arachidonic acid definitely has an effect on endothelial cell migration. From plain visual observations it appears that lower concentrations of arachidonic acid ($20\text{--}40\ \mu\text{M}$) enhance the endothelial cell migration, whereas higher concentrations ($20\text{--}40\ \mu\text{M}$) inhibit endothelial cell migration. Similar results were found in previous studies by Jensen *et al.*. However, this is only a qualitative observation, and the following section will investigate the effect of arachidonic acid on endothelial cell migration using quantitative studies that can be tested statistically.

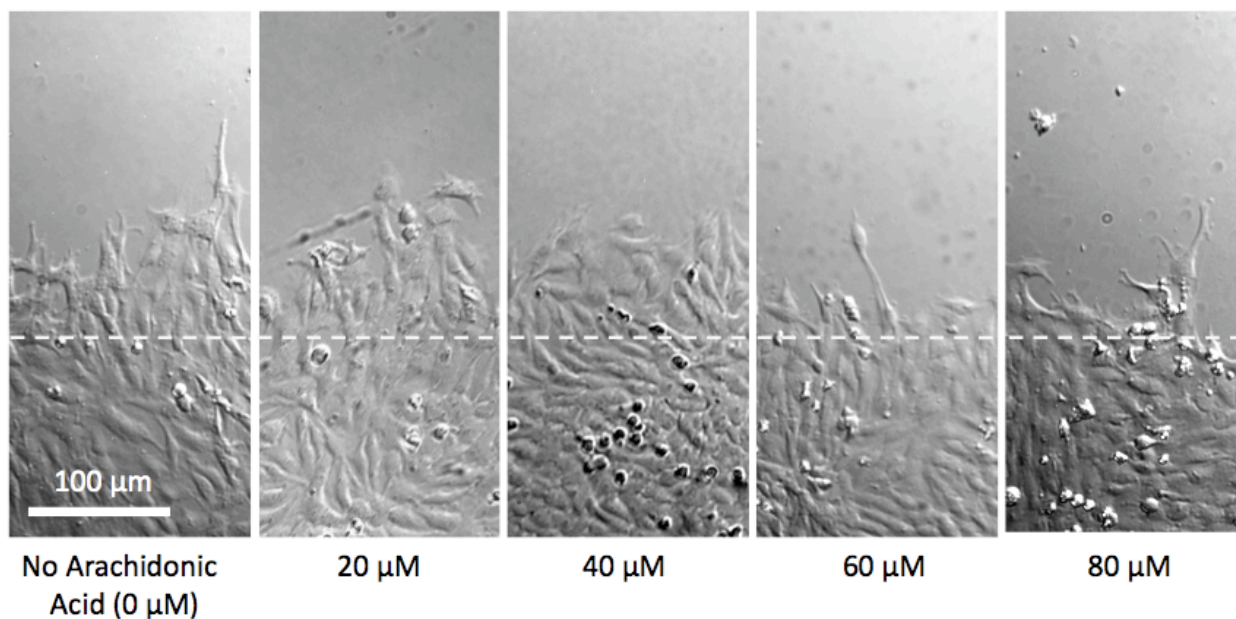


Figure 7.7: Exemplary data from a razor wound assays after 24 hours of migration for the control (no arachidonic acid) and the four different concentrations used in this study: 20.53 , 41.05 , 61.59 and $82.11\ \mu\text{M}$ arachidonic acid in the media. The initial position of the demarcation line has been denoted with a grey dashed line in all 5 images. It is clear that the presence of arachidonic acid affects the extent to which the endothelial cells have migrated in these examples (length scale = $100\ \mu\text{m}$).

For the quantitative studies, the cells were recorded throughout the 24 hour migration assay with a temporal resolution of 1 frame per second. The recorded images had a 1000×1000 pixel resolution. There are no programs available that can identify the outline or the position of the nucleus of individual cells in a migrating sheet of cells, so this was done by hand. Identifying the position of an individual cell in a migrating sheet of cells by hand, introduces a bit of error (a couple of pixels). A couple of pixels introduces a lot of noise with a temporal resolution of $60\ \text{fpm}$, since the movement of endothelial cells is much slower. The temporal resolution was optimized for the control assays with no arachidonic acid present, so that it was high enough to catch all the finer details of the cells migratory behavior that is reflected in the smaller step sizes and low enough not to induce too much noise that could break down the analysis. The optimal temporal resolution for cells with no arachidonic acid in the

media was 0.2 fpm (1 frame every 5 minutes). All the other assays were analyzed with this temporal resolution to enable a comparison of the analyzed assays. The temporal resolution in the study by Poujade and his collaborators [66] was 0.067 fpm (1 frame per 15 minutes), and they did not track the individual cells.

7.4 Collective Migration Behavior

The number of migrated cells (NMC) that crossed the demarcation line was used as a variable for detecting the effect of arachidonic acid on endothelial cell migration by both Jensen *et al.* [35] and Ghosh *et al.* [34]. The number of migrated cells were in these studies found through a comparison of the “before” and “after” images. The same type of analysis is possible for the data presented here, and the normalized number of migrated cells for each of the concentrations compared to the control can be seen in Figure 7.8.

Figure 7.8 shows that arachidonic acid limits the number of migrated cells at high concentrations (60-80 μM) compared to the control assays, just as previously reported by Jensen *et al.* However, at low concentrations (20 μM) the results presented here differ from the previously published. A larger reduction in the number of migrated cells is seen in Figure 7.8 when 20.56 μM arachidonic acid is added to the media. Such a reduction is highly unexpected when the previous migration results and the images in Figure 7.7 are taken into account. The images in Figure 7.7 show that the endothelial cells treated with 20.59 μM arachidonic acid migrated just as far as, if not further than, the control cells. The previous chapter showed that the addition of 20.11 μM to the media could increase the regulation rate of cytoskeletal remodeling, and, assuming that migration is purely an exercise in cytoskeletal remodeling, a low concentration of arachidonic acid in the media would be expected to enhance migration too. According to the number of migrated cells (NMC) that crossed the demarcation line in 24 hours, that is not the case. T-tests were performed to compare the number of migrated cells for different concentrations, and the p-values are listed in the table below (p-values < 0.05 are denoted in blue):

p-values (NMC)	control	20 μM AA	41 μM AA	62 μM AA	82 μM AA
control	-	0.013	0.672	0.025	0.007
20.53 μM AA	0.013	-	0.021	0.261	0.849
41.06 μM AA	0.672	0.021	-	0.052	0.020
61.59 μM AA	0.025	0.261	0.052	-	0.177
82.11 μM AA	0.007	0.849	0.020	0.177	-

The p-values above show that the number of migrated cells for 20.53 μM , 61.59 μM and 82.11 μM are significantly smaller than the number of migrated cells in the control assays. The inhibitory effect of higher concentrations of arachidonic acid is thus statistically significant on a 5% level, p-value < 0.05 . This is also the case for the low concentration of 20.53 μM arachidonic acid.

Since the cells migrating in medium with a low concentration of arachidonic acid appear to have migrated just as far as the controls in Figure 7.7, the number of migrated cells (NMC)

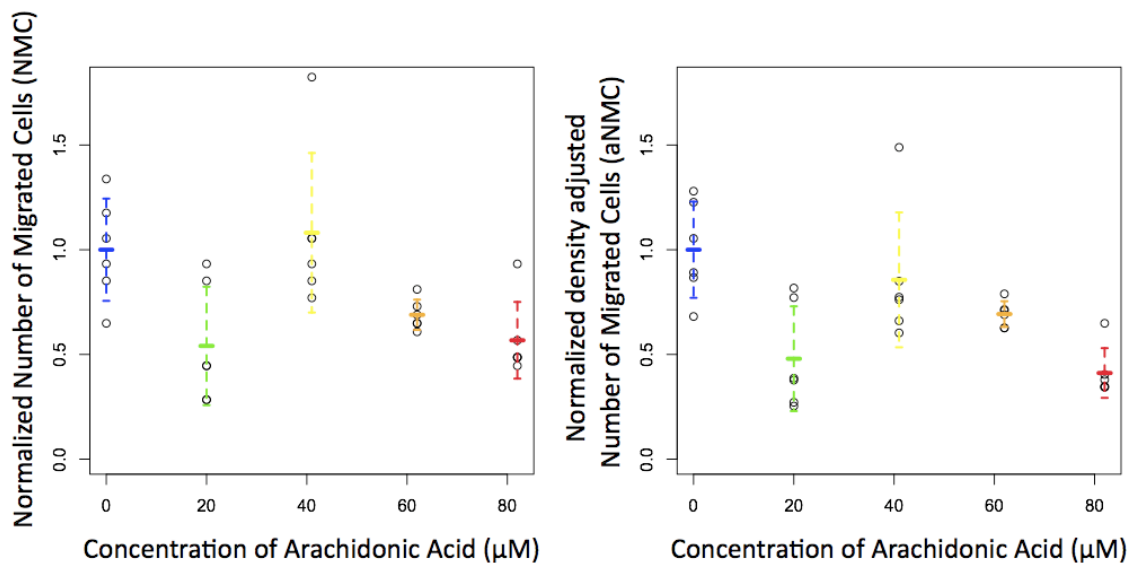


Figure 7.8: Left: The number of migrated cells (NMC) as a function of the concentration with which arachidonic acid (AA) is present in the media during the migration for the data presented here. Right: The density adjusted number of migrated cells (aNMC) as a function of the arachidonic acid concentration.

may not be the best variable to describe cell migration. It was previously noted that the cell density influences the maintenance of cell-cell contacts within the monolayer (in the omitted data sets) and the onset of migration out into vacant space [85]. When the cell density is high, the cells initiate migration into the vacant space much earlier than for low density monolayers [85]. The earlier the onset of migration is, the further the cells can migrate in 24 hours. To account for any possible head start that a sample with a high cell density may have had over other samples, a new variable for endothelial cell migration is presented here: The density-adjusted number of migrated cells (aNMC):

$$\text{aNMC} = \frac{1}{\rho_{\text{initial}}} \text{NMC}.$$

The density-adjusted number of migrated cells were also normalized to the mean of the aNMC of the control assays and have been plotted in Figure 7.8 as well. The density-adjusted number of cells does not offer much respite from the troubles of the unadjusted number of migrated cells. This is not completely unexpected since all the data sets in this analysis stem from samples which all maintained cell-cell contacts throughout the migration assay. The cell-density of these samples was high enough for the monolayer to be confluent and low enough for the cells to maintain cell-cell contact (if the cells did not maintain cell-cell contact, the data set was omitted from this analysis). The cell densities in this analysis is thus limited to a small window, and adjusting for such small differences does not affect the main result of the analysis. The density-adjusted number of migrated cells also decreases for higher (60-60 μM) concentrations, as well as the low concentration of 20.53 μM arachidonic acid. The trend is statistically significant on a 5% level, as can be seen from the following p-values of student's T-test.

p-values (aNMC)	control	20 μM AA	41 μM AA	62 μM AA	82 μM AA
control	-	0.004	0.396	0.021	0.001
20.53 μM AA	0.004	-	0.049	0.092	0.565
41.06 μM AA	0.396	0.049	-	0.273	0.018
61.59 μM AA	0.021	0.092	0.0273	-	0.001
82.11 μM AA	0.001	0.565	0.018	0.001	-

The only new contribution of using the density-adjusted number of migrated cells (aNMC) is that the aNMC for 82.11 μM arachidonic acid is now significantly lower than the aNMC for 61.59 μM , so the inhibitory effect of arachidonic acid for higher concentrations is more pronounced.

To facilitate the comparison of the effect of arachidonic acid on number of migrated cells reported here and the previously reported effect, the results in Figure 7.8 have been plotted on a logarithmic plot as in Jensen *et al.* in Figure 7.9. Comparing the results for the migration assays presented here with previously reported results [35], the effect of the higher concentrations of arachidonic acid on endothelial cell migration is similar. However, neither the normalized density-adjusted number of migrated cells nor the normalized number of migrated cells agree with the behavior reported by Jensen *et al.* for the low concentration (20.53 μM) of arachidonic acid.

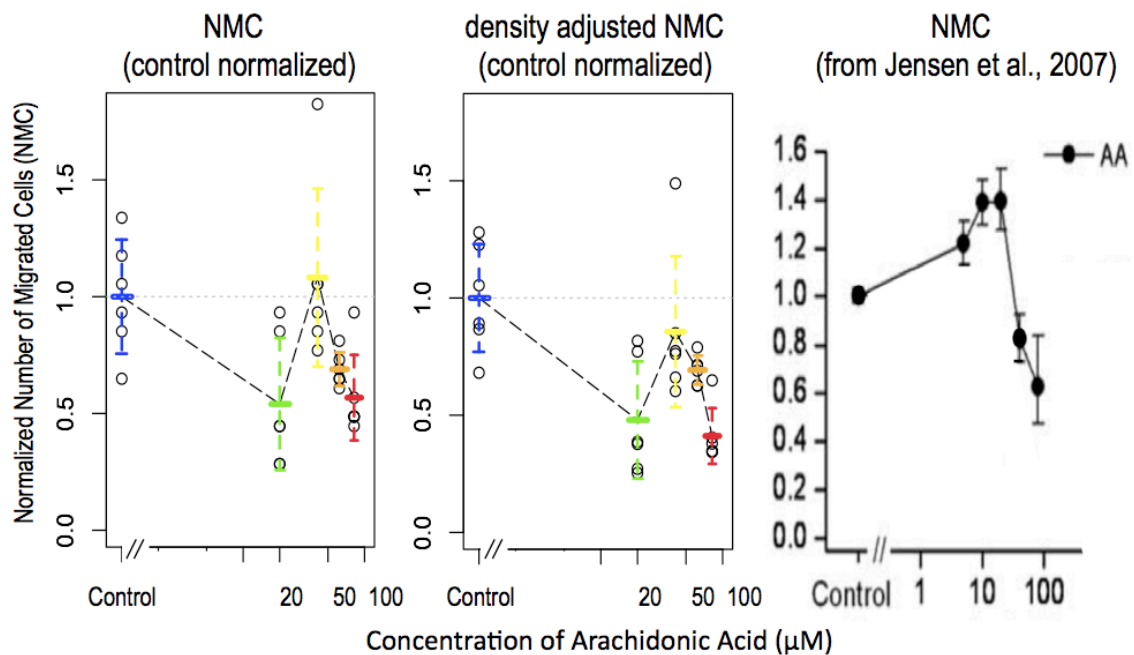


Figure 7.9: Left: The number of migrated cells (NMC) as a function of the concentration of arachidonic acid in the media during the migration for the data presented here. Middle: The density adjusted number of migrated cells (aNMC) as a function of the arachidonic acid concentration. Right: Previous results of arachidonic acid's effect on endothelial cell motility (from Jensen *et al.* 2007 [35]).

Jensen *et al.* hypothesized that the migration-enhancing ability of arachidonic acid was due to its metabolites [35], see Chapter 4. They were able to block the enhancing effect of low concentrations of arachidonic acids by blocking the major metabolic pathway for arachidonic acid with eicosatetraynoic acid. The presence of eicosatetraynoic acid in the media blocks the major metabolic pathways for arachidonic acid, and then arachidonic acid inhibits endothelial cell migration at low concentrations like most other amphiphilic compounds. Most amphiphilic compounds inhibit endothelial cell migration when present in the media [35]; the higher the concentration is the smaller the number of migrated cells. When the cells were incubated at an ambient atmosphere of 5% CO₂, they were incubated in the same medium used by Jensen and his collaborators. However, Jensen and his collaborators only needed to observe the cells twice: once before the cells initiated migration and once after 24 hours of migration. The cells are in these migration assays observed continuously for 24 hours in a microscope which cannot provide the cells with an ambient atmosphere of 5% CO₂. The cells' media was therefore changed to CO₂-*independent* media prior to experimentation. This media may have contained eicosatetraynoic acid or other compounds that block the metabolic pathway of arachidonic acid or the media may lack other compounds that are necessary for the metabolism of arachidonic acid. If either is the case, low concentrations would also be expected to have an inhibiting effect on endothelial cell motility based on previous results [35]. The inhibiting effect of 20.53 μ M arachidonic acid on endothelial cell migration is still much larger than that seen for higher concentrations, so the use of CO₂-*independent* media for experimentation can not explain the unexpected results entirely.

The endothelial cells are also migrating out into a space previously occupied by other endothelial cells. The glass slide was initially coated with Collagen IV and the removed cells may have coated the surface with some other extracellular matrix proteins as well before being removed by the sterile razor blade. The pressure with which the razor blade is pressed down could influence how much of the extracellular protein coating remains after the cell removal. Cells adhere more easily to glass already coated with an extra cellular protein, so removing the coating would also inhibit cell migration to some extent. The migration assays with low concentrations of arachidonic acid may have coincided with the assay in which the razor blade removed the extracellular protein and made it more difficult for the cells to move out into the (un-coated) vacant space. Further experiments should improve the statistics and could solve this inconsistency with previous results.

The number of migrated cells does not reflect the visual observations of arachidonic acid's effect on the extent of endothelial cell migration (see Figure 7.7). If there are fewer cells that have migrated across the demarcation line, but the distance or the extent to which the monolayer has migrated is approximately the same (which is the case for the control assays and the assays with a low concentration (20.53 μ M) of arachidonic acid), the cell density beyond the demarcation line must be affected. The density profiles of Figure 7.10 shows that this is indeed the case. The cell density profile is the normalized cell density as a function of the distance perpendicular to the demarcation line, and the profile has been plotted for six hour intervals: after 0 hours and after 6, 12, 18 and 24 hours of migration (the colors start dark and lightens as time passes).

Regarding the density profiles of Figure 7.10, the razor wound assays display the same kind of density profile as seen in diffusive mixing. The profile is initially a discrete stepwise function with a normalized density of 1.0 to one side of the demarcation line and 0.0 normalized

density of the other side. As time passes, the density profile becomes more and more sinusoidal in shape. This could suggest a diffusive behavior² of the cells rather than a directed walk (or march) into the vacant area. The density profile for a march of cells would have remained a discrete step from 1 to 0, which proceeds into the vacant area (to the right in Figure 7.10) as time passes. The migration of cells may be slightly diffusive in nature, but there is a definite flow, because the density profile for each time interval is slightly displaced to the right, i.e., the cells are not simply diffusing into the vacated space, but the monolayer also has an overall movement in that direction. The density profile of migrating endothelial cells display a behavior akin to diffusion with a flow in Figure 7.10, the extent of their diffusive nature can be determined through single cell observations.

7.5 Single Cell Tracking

In all the razor wound assays performed in this thesis, there is a general motion out towards the vacated space. A closer investigation of the cell-density profile revealed a possible diffusive nature in the cells' migration. Single cells at the leading edge of the monolayer were tracked to provide insight about such a diffusive behavior. The cells were tracked with a temporal resolution of 0.2 fpm, which is high enough to observe the finer details of cell migration and low enough to introduce a minimum amount of human error. The individually tracked cells were randomly chosen along the demarcation line to keep the analysis unbiased. Some sample tracks can be seen in Figure 7.11. Each track's initial position is denoted with a circle. The color of the circle reflects the concentration of arachidonic acid in the media: the control samples with no arachidonic acid have blue circles, the samples with 20.53 μM have green circles, the samples with 41.05 μM have yellow circles, the samples with 61.59 μM have orange circles, and the samples with 82.11 μM have red circles. The initial position of the tracks have been placed on an evenly spaced grid and do not reflect the actual initial position of the cells compared to the others. The demarcation line is horizontal on this plot (as in Figure 7.6) and an upward movement corresponds to a movement perpendicular to the demarcation line and into the vacated space. The cell tracks in Figure 7.11 are generally moving upward and into the vacated space as expected. The extent to which the cells at the edge (and the edge of the monolayer) migrate can also be discerned from these tracks. The tracks from cells with a high concentration of arachidonic acid in the media with orange (61.59 μM) and red (82.11 μM) circles are not as far outward as the tracks from the control cells with blue circles and no arachidonic acid in the media, indicating that the cell edge has not migrated as far out into the vacated space in these samples. The tracks for the individual cells display a general outward movement, but some also seem diffusive or random in their motion.

²A density profile of two initially separated liquids in a tube without flow would start discrete, turn sinusoidal and flatten out till the density of one liquid was evenly distributed. Without flow there would be no movement of the sinoidal curve over time just a flattening to horizontal.

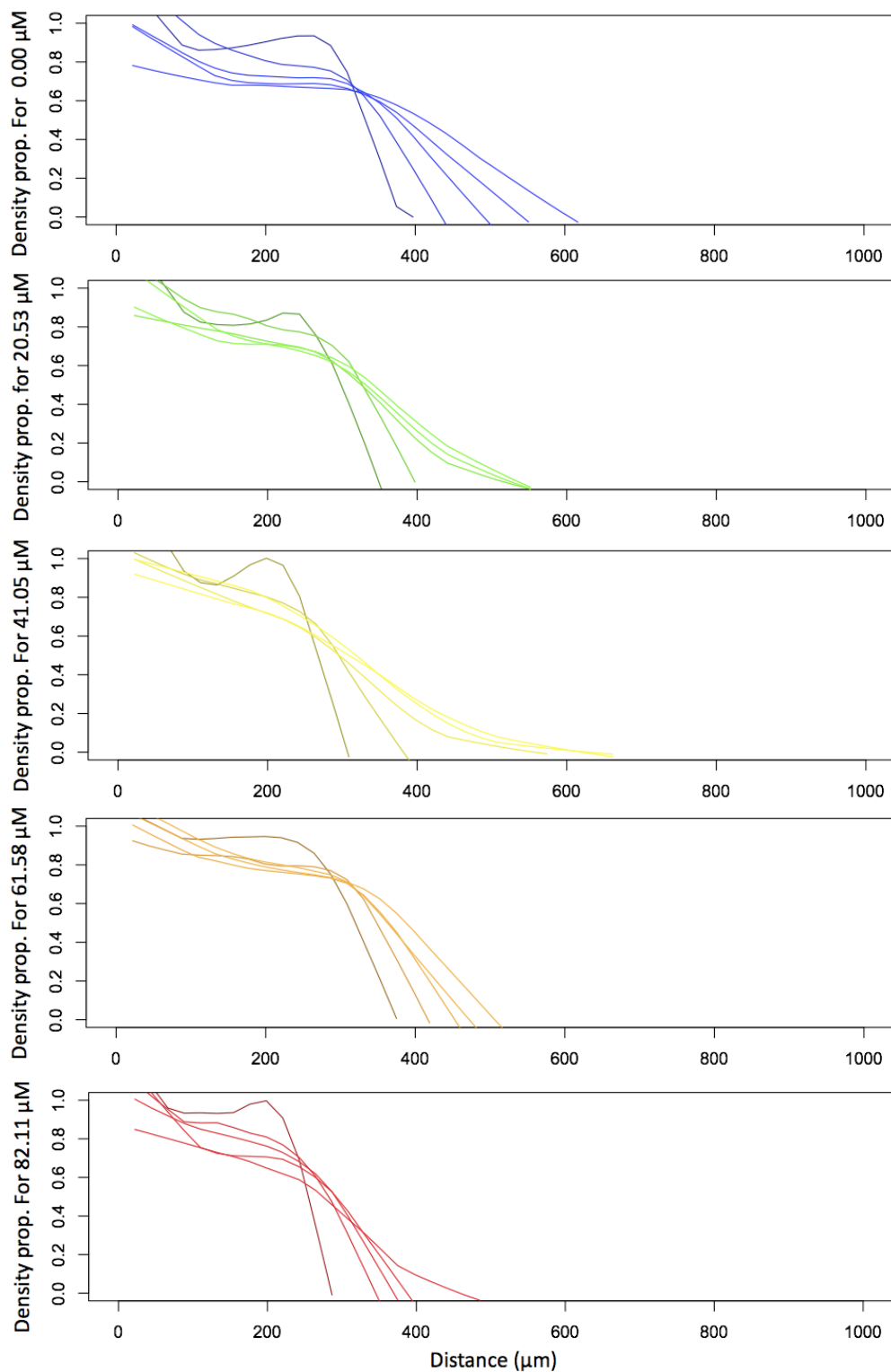


Figure 7.10: The cell-density profile as a function of the distance perpendicular to the demarcation line for the razor wound migration assays shown in Figure 7.7. The five graphs above show the density proportion of the control samples (blue) and the samples with 20.53 μM (green), 41.06 μM (yellow), 61.59 μM (orange), 82.11 μM (red) of arachidonic acid, respectively. The cell-density profiles are shown at six hour intervals. The first, at 0 hours, is a dark color, the next, after 6 hours of migration, is a lighter color, etc.

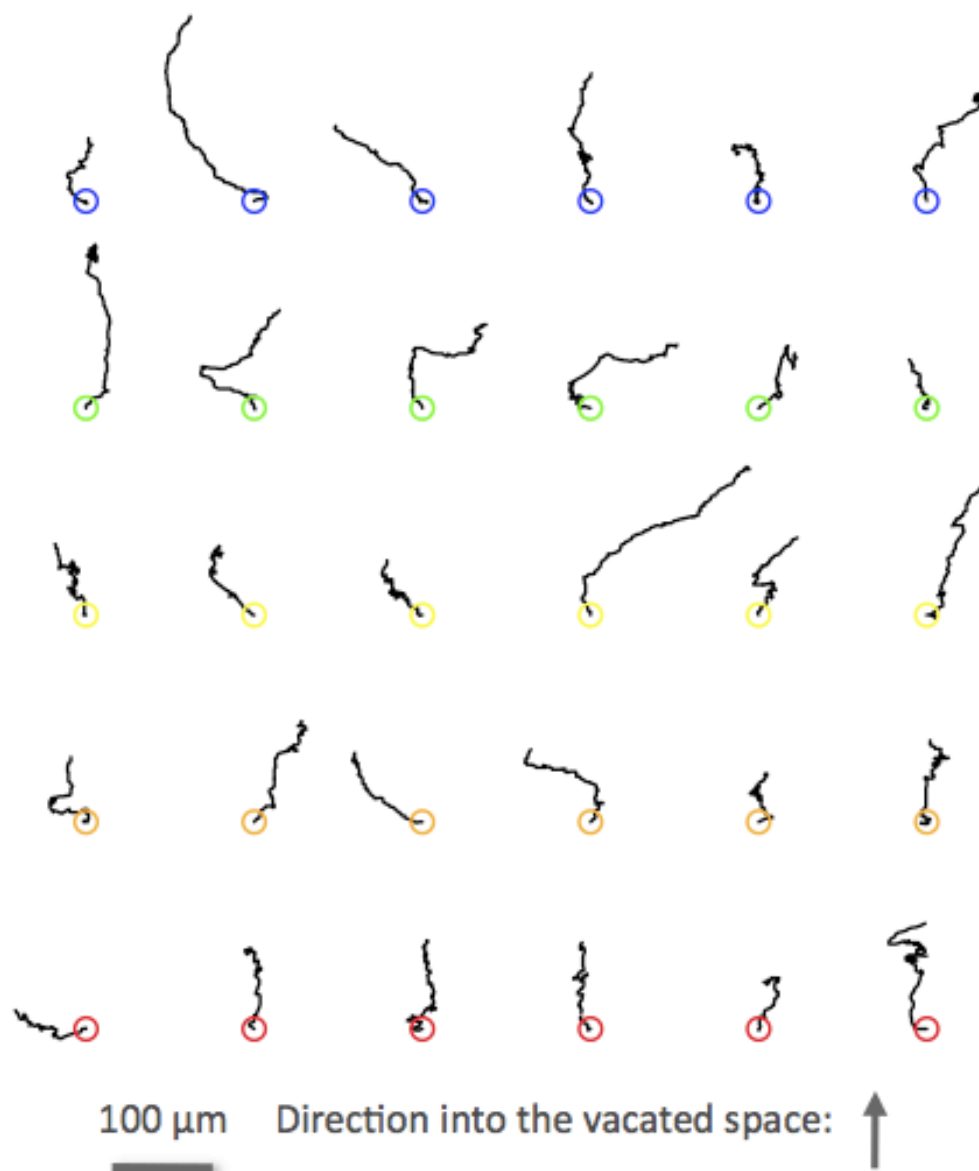


Figure 7.11: Individual cell tracks with their initial position spaced out on a grid. The initial positions of the cells are denoted with circles. The color of these circles reflect the concentration of arachidonic acid in the media for that particular sample: controls with no arachidonic acid have blue circles, 20.51 μM have green circles, 41.05 μM have yellow circles, 61.59 μM have orange circles and 82.11 μM have red circles. The cells were randomly chosen from the first line of cells at the demarcation line and their tracks positions above do not reflect their actual positions at the edge. All cells display a general outward movement into the vacated space, though some also seem slightly diffusive and random. The length scale is 100 μm and it is clear that the control cells migrate further than the cells with high concentrations (orange and red circles) of arachidonic acid.

Comparison to cells far from the edge

In razor wound assays, the cells are not only presented with different concentrations of arachidonic acid, but also with a vacated space. A control for the motion of cells without arachidonic acid and without a vacated space to migrate into is provided to shed light on how arachidonic acid affects the motion of individual cells at the edge of a razor wound assay. In the following analysis, the motion of the cells at the edge of a razor wound assay treated with arachidonic acid are not only compared to the cells at the edge of a control razor wound assay without arachidonic acid in the media, they are also compared to the motion of cells *far removed* ($\approx 10,000\mu\text{m}$) from the edge without arachidonic acid. Figure 7.12 shows the tracks of six control cells at the edge of a razor wound assay compared to tracks of six control cells far removed from any edge with no arachidonic acid in the media.

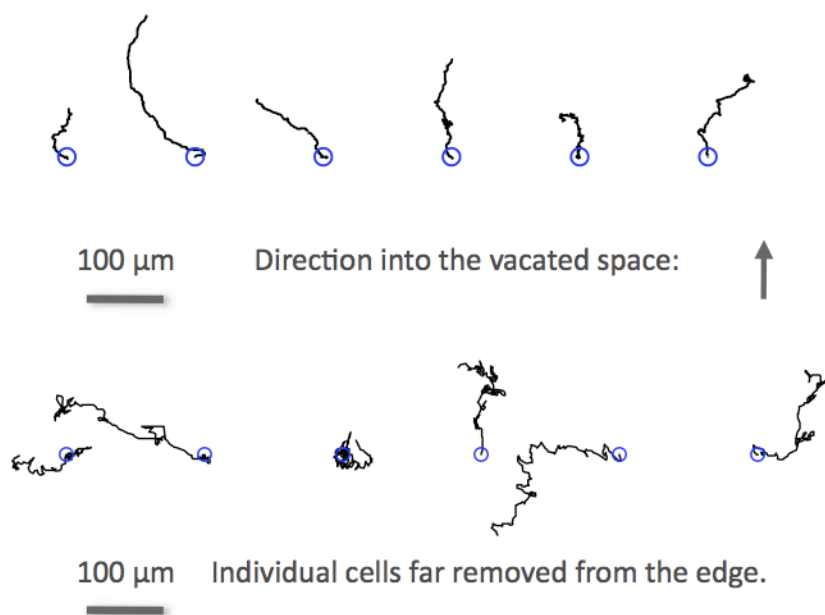


Figure 7.12: Individual cell tracks with their initial position spaced out on a grid. The initial positions of the cells are denoted with blue circles since there is no arachidonic acid in the media. The cells were chosen at random, and the initial positions above do not reflect their actual positions in the monolayer. The top row of cells are the control cells at the edge of a razor wound assay and the bottom row is the control cells far removed from any edges (length scale = $100\mu\text{m}$).

Two immediate conclusions can be drawn from comparing the movements of the control cells at the edge with the movements of the cells far from any edge (see Figure 7.12). Firstly, the cells far removed from any edge are motile, to the same extent that cells at the edge is - if not more. Endothelial cells thus migrate actively *within* the confluent monolayer. This has been noted to be true for epithelial cells as well [86], and it is possible that the endothelial cells migrate within the monolayer by developing active “cryptic” lamellipodia under the other cells as epithelial cells do. Secondly, the control cells at the edge have a general direction which the cells far removed from any edge lack.

Cell velocities

The velocity of the cells influences how far the cells are able to migrate in 24 hours. The velocity of all the individually tracked cells have been calculated as $v(t) = \frac{dr(t)}{dt} = \frac{r(t+\Delta t) - r(t)}{\Delta t}$, where $r(t)$ is the position of the cell at time t . Figure 7.13 shows an exemplary cell's velocity over the 24 hour migration experiment, and there appears to be no particular trend. The mean velocity that the cells have during all 24 hours was calculated and is also plotted in Figure 7.13 as a function of the arachidonic acid concentration. The velocities of the individual cells at the edge of a razor wound assay do not change with the amount of arachidonic acid present in the media, at least not on a statistically significant level, which can be seen in the table of p-values for a student's t-test below where none are below 0.05:

p-values (velocity)	control	20 μM AA	41 μM AA	62 μM AA	82 μM AA
control	-	0.910	0.614	0.289	0.687
20.53 μM AA	0.910	-	0.750	0.306	0.635
41.06 μM AA	0.614	0.750	-	0.051	0.320
61.59 μM AA	0.289	0.306	0.051	-	0.503
82.11 μM AA	0.687	0.635	0.320	0.503	-

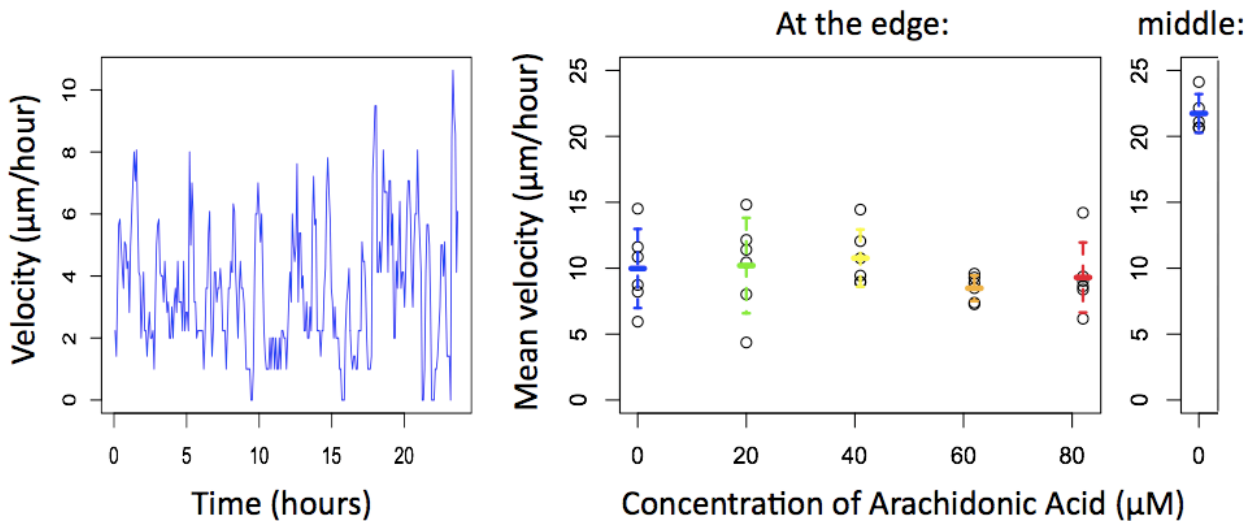


Figure 7.13: The velocity of individual cells. Left: The velocity of a single control cell with no arachidonic acid present in the media over the 24 hour duration of the migration assay. There is no trend to the velocity of the cell over time. Right: The mean velocity for each of the 36 individually tracked cells. The mean and standard deviation for each concentration is also shown on the plot. There is no statistically significant difference between the cells' velocity when affected with arachidonic acid.

The velocity of the cells far removed from any edge is also shown in Figure 7.13, and there can be no doubt that these cells move faster than their counterparts at the edge of the monolayer. This may be due to the extracellular matrix coating of the other cells that facilitate migration.

Squared displacement

Observations of the migratory motions (see Figure 7.11, 7.6, 7.7 and the movies in the supplemented material) leaves little doubt that the endothelial cells at the edge of a razor wound assay migrate out in the general direction of the newly vacated space. The density profile in Figure 7.10 in the previous section also indicated that the motions of the cells could be diffusive. It is possible to determine whether a trajectory is diffusive or directed by analyzing the squared *displacement*, r^2 . The displacement, r , at a given time $t = \tilde{t}$, is the distance from the cell's initial position at time $t = 0$ to its current position at time $t = \tilde{t}$, $r(\tilde{t}) = r(\tilde{t}) - r(t_0)$. An analysis of the squared displacement is made possible by the continuous observations of the razor wound migration, and has not been possible in the previous studies of endothelial cell migration that compare “before” and “after” images. The squared displacement analysis is based on the equations of motion for two different types of motion, diffusive and directed, both of which can be described by the squared displacement dependence on time.

Diffusive motion is characterized by the squared distance's linear dependence on time:

$$r^2 = Dt,$$

where D is the diffusion constant.

Directed motion is characterized by the distance traveled being proportional to the time, $r = v \cdot t$, where v is the velocity of the motion. The squared displacement as a function of time then becomes,

$$r^2 = v^2 t^2.$$

A motion analysis with the squared displacement, r^2 , is based on the general equation of motion, $r^2 = c \cdot t^d$, that can describe both diffusive and directed motion based on the value of the parameter d . The motion is diffusive if the exponent $d = 1$, and if $d = 2$ the motion is directed. If the motion is neither diffusive nor directed, and $1 < d < 2$, the higher the exponent d is (the closer to 2), the more the motion of the cell is governed by a directed motion. The general equation of motion, $r^2 = c \cdot t^d$, was fitted to each individually tracked cell's squared displacement by the program GNUplot, which uses “least-squares fitting”. The squared displacement of three exemplary control cells can be seen in Figure 7.14, and the figure also shows the fitted equations of motion.

The equation of motion, $r^2 = ct^d$, fitted to the data presented in Figure 7.14 has $d = \{1.515 \pm 0.024, 2.463 \pm 0.012, 1.887 \pm 0.063\}$. Since the exponents $d > 1$, the motion of the migrating cells are not completely diffusive. The analysis of the cell density profile of the razor wound assays (see Figure 7.10) hinted at a directionality in the motion of the cells because the density profile was more and more displaced as time progressed. However, for some of the cells $d < 2$, so these cells' motions are not completely directed either. This was also expected from the analysis of the cell density profile, since the discontinuous “step” function of the cell density at time $t = 0$ softened to look almost sinusoidal as time progressed - a clear indication of some diffusive behavior of the cells. The motion of migrating endothelial cells in the control razor wound assay cannot be characterized as strictly diffusive

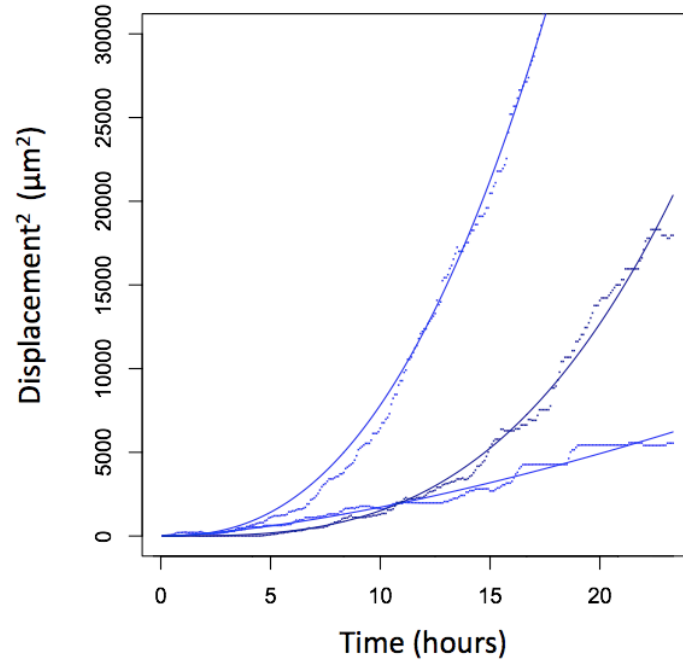


Figure 7.14: The squared displacement as a function of time for three exemplary control cells with no arachidonic acid in the media. The general equation of motion, $r^2 = c \cdot t^d$, has been fitted to the three cells' squared displacement, and these fits are shown as well.

or strictly directed, but as a diffusion with a directed flow where d describes the degree to which the underlying flow governs the motion of the cells.

The general equation of motion, $r^2 = c \cdot t^d$, was fitted to all the data sets, and the fitted values for the parameters c and d for all the analyzed cells can be found in Table 7.1. The results for the parameter d for all the different concentrations is shown graphically in Figure 7.15 and is summarized in the table below:

	no. of observations	d
0 (control)	6	2.126 ± 0.726
20.53	6	2.014 ± 0.539
41.06	6	1.475 ± 0.558
61.59	6	1.197 ± 0.260
82.11	6	1.282 ± 0.545
middle	6	2.157 ± 1.616

Figure 7.15 shows the resulting exponents d as a function of the concentration in which the arachidonic acid was present in the media during the 24 hours of migration. There is a distinct trend in the plot; the cells' motion at the edge becomes increasingly diffusive and random as the concentration of arachidonic acid increases.

The motion of the control cells is almost completely directed, $d \approx 2$. The cells motion becomes significantly more random than the control cells the higher the concentration of

Tracked at edge:	AA Concentration	c	d
Cell A	0	1.483 ± 0.191	1.515 ± 0.024
Cell B	0	0.072 ± 0.005	2.463 ± 0.012
Cell C	0	0.000773 ± 0.000123	3.067 ± 0.029
Cell D	0	0.00893 ± 0.00214	2.659 ± 0.043
Cell E	0	0.202 ± 0.070	1.887 ± 0.063
Cell F	0	44.774 ± 9.154	1.165 ± 0.038
Cell G	$20.53 \mu\text{M}$	0.113 ± 0.025	2.580 ± 0.044
Cell H	$20.53 \mu\text{M}$	1.494 ± 0.460	1.659 ± 0.057
Cell I	$20.53 \mu\text{M}$	5.228 ± 0.546	1.469 ± 0.019
Cell J	$20.53 \mu\text{M}$	0.012 ± 0.002	2.552 ± 0.032
Cell K	$20.53 \mu\text{M}$	0.085 ± 0.043	2.358 ± 0.106
Cell L	$20.53 \mu\text{M}$	1.540 ± 0.250	1.465 ± 0.030
Cell M	$41.05 \mu\text{M}$	25.842 ± 3.258	1.000 ± 0.237
Cell O	$41.05 \mu\text{M}$	174.025 ± 13.110	0.752 ± 0.014
Cell P	$41.05 \mu\text{M}$	2.464 ± 0.260	1.365 ± 0.020
Cell Q	$41.05 \mu\text{M}$	1.586 ± 0.136	1.917 ± 0.016
Cell R	$41.05 \mu\text{M}$	1.383 ± 0.293	1.570 ± 0.039
Cell S	$41.05 \mu\text{M}$	0.129 ± 0.013	2.246 ± 0.018
Cell T	$61.59 \mu\text{M}$	0.556 ± 0.236	1.600 ± 0.078
Cell U	$61.59 \mu\text{M}$	8.655 ± 0.744	1.408 ± 0.016
Cell V	$61.59 \mu\text{M}$	87.987 ± 6.253	0.926 ± 0.013
Cell W	$61.59 \mu\text{M}$	25.191 ± 2.181	1.126 ± 0.016
Cell X	$61.59 \mu\text{M}$	5.557 ± 1.081	1.155 ± 0.036
Cell Y	$61.59 \mu\text{M}$	52.648 ± 6.822	0.969 ± 0.024
Cell Z	$82.11 \mu\text{M}$	17.903 ± 1.801	1.100 ± 0.019
Cell AA	$82.11 \mu\text{M}$	271.498 ± 16.17	0.699 ± 0.011
Cell AB	$82.11 \mu\text{M}$	0.079 ± 0.007	2.144 ± 0.017
Cell AC	$82.11 \mu\text{M}$	3.462 ± 0.734	1.465 ± 0.039
Cell AD	$82.11 \mu\text{M}$	2.696 ± 0.328	1.524 ± 0.025
Cell AE	$82.11 \mu\text{M}$	273.957 ± 15.090	0.757 ± 0.010
Tracked in the middle:	AA Concentration	c	d
Cell a	0	0.00117 ± 0.000536	3.146 ± 0.094
Cell b	0	3.762 ± 0.994	1.713 ± 0.049
Cell c	0	$1.25 \cdot 10^{-9} \pm 1.97 \cdot 10^{-9}$	4.982 ± 0.280
Cell d	0	283.220 ± 27.600	0.761 ± 0.019
Cell e	0	53.855 ± 8.467	1.182 ± 0.029
Cell f	0	39.324 ± 9.755	1.156 ± 0.046

Table 7.1: The parameters for the fit of the general equation of motion, $r^2 = c \cdot t^d$, to the squared displacement as a function of time for each individually tracked cell's motion.

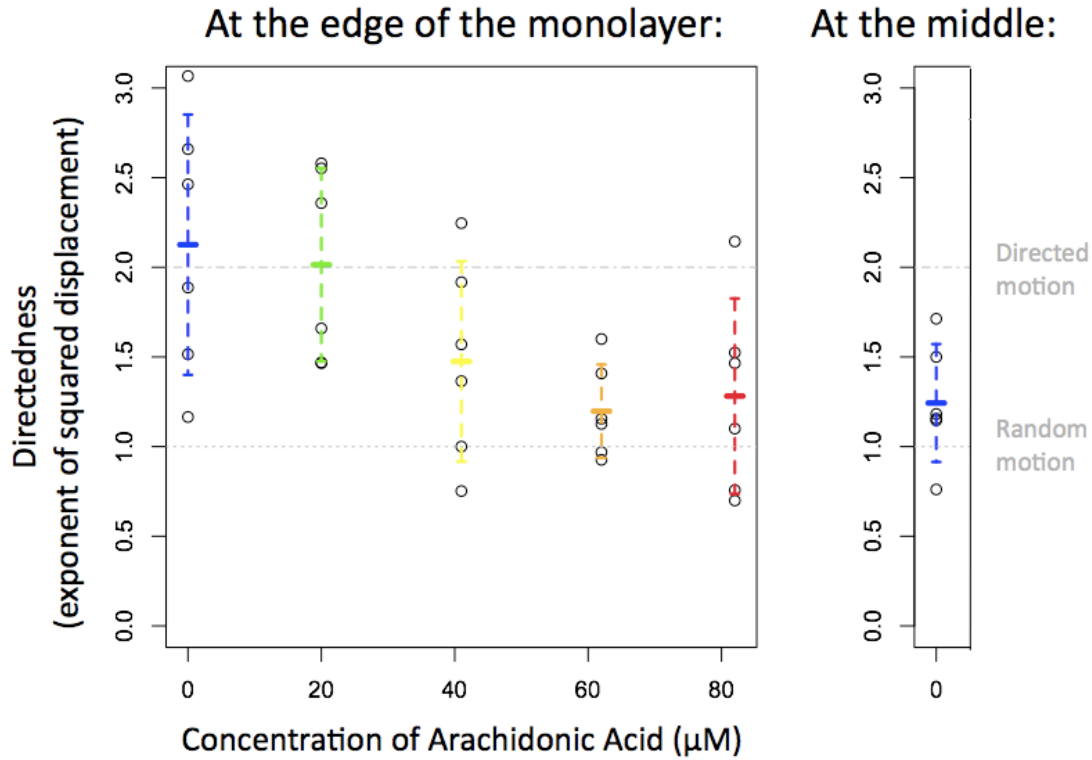


Figure 7.15: The directedness, d , from the equation of motion, $r^2 = c \cdot t^d$, for the individually tracked migrating endothelial cells as a function of the concentration of arachidonic acid in the media. The plot shows data for control cells (blue) both at the edge of a razor wound assay and in the middle of a monolayer. It is clear that the higher the concentration of arachidonic acid is in the media the less directed the motion of the individual cells become, until they at high concentrations are rendered in the same almost diffusive state as cells found in the middle of the monolayer far removed from the edge.

arachidonic acid is in the media. The p-values of student's t-test shows that this decrease in directedness is significant on a 5% level. The p-values for all of the t-test can be seen in the table below where all the p-values < 0.05 are denoted in blue.

p-values (edge)	control	20 μM AA	41 μM AA	62 μM AA	82 μM AA
control	-	0.768	0.114	0.024	0.047
20.53 μM AA	0.768	-	0.120	0.012	0.041
41.06 μM AA	0.114	0.120	-	0.305	0.557
61.59 μM AA	0.024	0.012	0.305	-	0.743
82.11 μM AA	0.047	0.041	0.557	0.743	-
p-values (middle)	0 μM AA (edge)	20 μM AA	41 μM AA	62 μM AA	82 μM AA
μM AA (middle)	0.030	0.017	0.406	0.795	0.886

The cells lose their sense of direction when affected by arachidonic acid. The higher the concentration is, the more random their motion. Such an analysis can not be seen if only before and after images are compared or using PIV.

From Figure 7.15 it is clear that the cells motion become more and more diffusive the higher the concentration of arachidonic acid is. A similar analysis of individual cell tracks for cells which are farther removed from the edge gives a sense of how diffusive the motion of normal cells are when no vacant space has been presented to them. Figure 7.15 also shows the directedness, $d = 1.282 \pm 0.545$, of cells moving in the middle of the monolayer far from the edge. Their motion is not directed nor random, but somewhere in between. Comparing the directness of the cells at the edge with higher concentration (61.59 μM and 82.11 μM) with the directedness of the cells at the edge with no arachidonic acid present, they are approximately the same. High concentrations of arachidonic acid in the media render the cells at the edge in a state that resembles the one they find themselves in when completely surrounded by other endothelial cells - their movements are not completely random, but they lack a general direction.

The physical interpretation of the parameter c varies with the value of d . If d is close to 1, the motion is primarily diffusive and c can be interpreted as the diffusion constant, D , but if d is closer to 2, the motion is more directed and c can be interpreted as the squared velocity, v^2 . The value of d is significantly different for the different concentrations of arachidonic acid, so the interpretation of c would differ for the different concentrations. The parameter c will not be further discussed, since it has different interpretations between the data sets.

Since the velocity of the cells is not significantly different when treated with arachidonic acid, the limited extent to which endothelial cells migrate when treated with high concentrations of arachidonic acid may well be due to the increasingly diffusive motion that the cells display when treated with higher concentrations of arachidonic acid.

An advantage to continuously recording, and not fixing and staining, the cells is that it is possible to make live observations even after the migration studies are over. The same is true for the type of viability assay described in Chapter 5. Migration and viability assay were periodically checked for up to 72 hours after the termination of a 24 hour assay. After 72 hours the cells still showed no sign of deterioration and had proliferated to such an extent that they no longer constituted a monolayer, but lay on top of each other as well. At that point the cells were hard to distinguish and no further check up was made thereafter. It is therefore reasonably safe to assume that cells were not harmed by the addition of arachidonic acid in the concentrations used in the experiments presented here.

7.6 Conclusion to Endothelial Cell Migration

All analyses in this chapter have been based on *in vitro* razor wound migration assays that reflect the *in vivo* environment as closely as possible. Any migration assays that failed to maintain complete cell-cell contact within the monolayer, or whose edge retracted from the demarcation line, have been omitted.

The study of collective cell migration through an analysis of the number of migrated cells that crossed the demarcation line revealed that high concentrations of arachidonic acid inhibit endothelial cell migration. Both the distance the cells at the edge had migrated and the number of migrated cells decreased in samples which had higher concentrations (61.59 μM and 82.11 μM) of arachidonic acid in the media. The inhibiting effect of arachidonic acid at high concentrations is similar to the effect observed by Jensen and his collaborators [35] in previous studies.

The analysis of the number of migrated cells also showed that a low concentration of 20.51 μM arachidonic acid in the media significantly lowered the number of migrated cells that crossed the demarcation line. This result was unexpected because the edge of the cell monolayer had migrated as far as it did in the control samples, and previous studies have shown the effect of low concentrations of arachidonic acid to enhance endothelial cell migration. The results from the analysis of the number of migrated cells at a low concentration of arachidonic acid presented here and the results of previous studies by Jensen *et al.* [35] could not be reconciled, even when the number of migrated cells were adjusted for differences in the initial cell-density of the confluent monolayer. The inconsistency can be speculated to originate in the media used for experimentation. A different, CO_2 -independent media was used in these migration assays, and the metabolism of arachidonic acid may have been blocked or hindered. The metabolites of arachidonic acid were hypothesized to induce the enhancing effect on endothelial cell migration in earlier studies [35].

Since a smaller number of migrated cells had crossed the demarcation line for the low concentration (20.51 μM) of arachidonic acid, but the edge of the monolayer had migrated the same distance as the monolayer in the control assays without arachidonic acid, the cell-density of the 20.51 μM sample was lower than in the control. This was clearly seen in the density profiles of the migration assays. The density profile offered no explanation for the smaller number of migrated cells at low concentrations, but it illustrated the possibility of a diffusive motion of the migrating cells.

Several cells, randomly chosen among those along the edge of the razor wound or in the middle of the monolayer far ($> 10,000\mu\text{m}$) from any edge, were tracked individually by hand. These individual tracks enabled the analysis of the cells' velocity and directedness.

The velocity of the individually tracked cells at the edge was not affected by the presence of arachidonic acid in the media. The velocity of cells at the edge of the razor wound assays were also compared to the velocity of cells in the middle of the monolayer. The cells at the edge move considerable slower than the cells within the monolayer. This may be due to the surplus of extracellular matrix proteins that coat the surfaces within and under the monolayer. The cells move more easily on pre-coated surfaces. This may explain the unexpected results for the low number of migrated cells with 20.53 μM arachidonic acid in the media. The analyses are based on a few successful migration assays which did not

retract or display discontinuities, and the razor blade may have been pressed too hard when removing the cells in a few of these assays, resulting in the removal of cells *and the underlying* Collagen IV coating. If the Collagen IV coating has been removed it is more difficult for the cells to migrate, and these assays may have coincided with the assays with 20.53 μM . Conducting more migration assays would not only improve the statistics but might solve this inconsistency with previous results.

The density profiles suggested a slightly diffusive behavior in endothelial cell migration out into a vacated area. A general equation of motion, $r^2 = c \cdot t^d$, that can describe both directed and diffusive motion depending on the value of the directness parameter, d , was fitted to the motion of the individual cells. The directedness parameter, d , was strongly affected by the amount of arachidonic acid in the media. The control cells at the edge with no arachidonic acid in the media had an almost completely directed motion with $d = 2.126 \pm 0.726$. The directness decreased from directed to almost diffusive with the concentration of arachidonic acid in the media. The higher the concentration of arachidonic acid was, the less directed and more diffusive the individual cells' motion became, and, already at 61.59 μM , the directedness has decreased to $d = 1.197 \pm 0.260$, rendering the cells' motion as diffusive as the motion for cells in the middle of the monolayer, which lack direction, $d = 2.157 \pm 1.616$.

Cells appear to be constantly moving within the monolayer, and the velocities of the cells are not affected by arachidonic acid. The only variable that seemed affected by arachidonic acid in a consistent way is the directedness of the individual cell's motion. The higher the concentration of arachidonic acid is, the less directed and more diffusive the cells become. When individual cell velocity is unchanged, the diffusiveness and lack of direction in the cell's motion at the edge may account for the lower number of migrated cells that cross the demarcation line. The effect of arachidonic acid on endothelial cell migration is that it induces a more diffusive and random motion of the individual cell, causing the monolayer as a whole to proceed at a slower rate.

The constant migration of cells within the monolayer may well induce a "pressure" from within that causes the endothelial cells at the edge to migrate outward into the newly vacated space as soon as the confinements to the monolayer are lifted. The cells may not be drawn to the vacant space or respond to an attractive or repelling chemotaxin signal but could be pushed out into the open space by the constant jostling and intermingling of cells in the monolayer.

Chapter 8

Conclusion

The aim of this thesis was to investigate arachidonic acid's effect on both endothelial cell adhesion and migration.

The adhesion assays successfully simplified the process of migration so that the effect of arachidonic acid on the cytoskeletal remodeling in the actively spreading phase of adhesion has been mirrored in the effect of arachidonic acid on cell migration seen in previous studies. For a low concentration (20.53 μM) of arachidonic acid, the adhesion area increases at a higher rate than it does for control cells with no arachidonic acid in the media. The higher rate of adhesion area increase suggests an increased responsiveness in the remodeling of the cytoskeleton. In accordance with the previous studies by Jensen and his collaborators, the migration of endothelial cells were seen to be enhanced at this concentration of arachidonic acid.

For a high concentration (82.11 μM) of arachidonic acid, the adhesion area increase occurred at a much lower rate, suggesting a less responsive regulation of the cytoskeletal remodeling. These results are in accordance with previous studies of arachidonic acid's effect on endothelial cell migration. The previous studies reported that a similar concentration of arachidonic acid inhibits cell migration. Cell migration would also be affected by a lessened responsiveness in the cytoskeletal remodeling. Endothelial cell adhesion and migration are both mediated through the remodeling of the cytoskeleton, and the similarity between the effect of arachidonic acid on these two types of motility is remarkable.

The study of collective cell migration through an analysis of the number of migrated cells that crossed the demarcation line revealed that high concentrations of arachidonic acid inhibit endothelial cell migration. The conducted migration assays replicated the previous results for high concentrations of arachidonic acid, but at low concentration of the results differed from the previous studies. The analysis of the number of migrated cells showed that a low concentration of 20.51 μM arachidonic acid in the media significantly lowered the number of migrated cells that crossed a demarcation line. This result was unexpected, because the edge of the cell monolayer had migrated just as far as in the control samples, and previous studies have shown the effect of low concentrations of arachidonic acid to enhance endothelial cell migration. The inconsistency with previous results for this concentration may be due to the unintentional removal of the extracellular matrix protein coating of the glass slide. It could

also be due to the CO₂-independent media used in these migration assays, which may have hindered the metabolism of arachidonic acid.

For the study of individual cell motion within the migrating monolayer, several cells were chosen at random along the edge of the razor wound for individual tracking. The motion of cells with different concentrations of arachidonic acid in the media were compared to the motion of control cells with no arachidonic acid in the media, both at the edge and in the middle of the monolayer. These individual tracks enabled the analysis of the cells' velocity and directedness.

The presence of arachidonic acid in the media does not affect the velocity of the individually tracked cells.

The directedness of the cells' motion was investigated because the cell-density profiles of the migration assays suggested a slightly diffusive behavior. The directedness of the cells' motion was strongly affected by the amount of arachidonic acid in the media. The control cells at the edge with no arachidonic acid in the media had an almost completely directed motion. The directness decreased from directed to almost diffusive with the concentration of arachidonic acid in the media. The higher the concentration of arachidonic acid, the less directed and more diffusive the individual cell's motion became. At 61.59 μM , the directedness decreased so much as to render the cells' motion as diffusive as the motion for cells in the middle of the monolayer, which have little direction.

Cells appear to be constantly moving within the monolayer, and the velocities of the cells are not affected by arachidonic acid. The only variable that seemed affected by arachidonic acid in a consistent way was the directedness of the individual cell's motion. The higher the concentration of the arachidonic acid in the media, the less directed and more diffusive the cells become.

When individual cell velocity is unchanged, the diffusiveness and lack of direction in the cell's motion at the edge may account for the lower number of migrated cells that cross the demarcation line. The effect of arachidonic acid on endothelial cell migration is that it induces a more diffusive and random motion of the individual cell which causes the monolayer as a whole to proceed at a slower rate.

The effect of arachidonic acid on endothelial cell adhesion and migration is not unambiguous, but there are similarities, particularly at high concentrations. At high concentrations, the remodeling of the cell's cytoskeleton is less responsive, and the number of endothelial cells that migrate out into a vacated area is inhibited. The inhibition is probably due to the diffusive behavior induced by the high concentrations of arachidonic acid. Though the migration of cells is mediated through the remodeling of the cytoskeleton, the short-time responsiveness does not seem to affect the migration, since the individual cell velocity is unaltered. The parallels between the cytoskeleton remodeling of adhesion and the diffusiveness of cell migration remain to be elucidated, but both effects are induced by the amphiphilic compound arachidonic acid, so the most probable explanation lies in the non-specific regulation of membrane proteins.

Acknowledgements

The optical tweezer group at the Niels Bohr Institute has not worked with mammalian cells before, and I would like to thank my supervisor Lene Oddershede, for not only welcoming me, but also these new organisms into her group. I would like to thank her for all the encouragement and advice she has so generously provided through the last nine months.

This project would not have been possible without the ideas, support and knowledge of my other supervisor Christine Selhuber-Unkel. I would like to thank her for making the first many months so enjoyable and for the many hours she spend with me in the laboratory establishing the cultivation of the new organism and setting up the initial experiments. I have missed her sorely since she moved this summer. I am also very thankful for the encouragements and advice she has kept providing, despite the great distance.

While working on this thesis I was fortunate to receive financial support through the Novo Nordisk Scholarship programme. This was possible through the support of Dr. Anker J. Hansen, and I am very grateful for this support and for his initial ideas which spawned the idea for this thesis. Anker also provided the endothelial cell strain investigated in this thesis along with unlimited advice about how to cultivate them. His colleague Pia Birn was also invaluable in the start up phase. I would like to thank both of them for their time, advice and of course the cell strain.

I would also like to thank all my fellow student and colleagues at the Niels Bohr Institute, for the laughs and insights we have shared, in particular Jan Valentin, Pia Cordsen and Anders Kyrsting.

Lastly, I would like to thank my family for their encouragement and support, my friends for being there, and Jacob for keeping a smile on my face through it all.

Bibliography

- [1] R. J. D'Amato *et al.* Thalidomide is an inhibitor of angiogenesis. *PNAS*, 91:4082–4085, 1994.
- [2] R. Auerbach *et al.* Angiogenesis assays: A critical overview. *Clin Chem*, 49:32–40, 2003.
- [3] N. Akhtar, E. B. Dickerson, and R. Auerbach. The sponge/matrigel angiogenesis assay. *Angiogenesis*, 5:75–80, 2002.
- [4] M. Kragh *et al.* *In vivo* chamber angiogenesis assay: An optimized matrigel plug assay for fast assessment of anti-angiogenic activity. *Int J Oncol*, 22:305–311, 2003.
- [5] J. Folkman. Tumor angiogenesis: Therapeutic implications. *N Engl J Med*, 285:1182–1186, 1971.
- [6] J. Folkman and M. Hochberg. Self-regulation of growth in three dimensions. *J Exp Med*, 138:745–753, 1983.
- [7] M. J. Folkman and F. F. Becker. Growth and metastasis of tumor in organ culture. *Cancer*, 16:453–467, 1963.
- [8] D. Artemov *et al.* Dynamics of prostate cancer cell invasion studied in vitro by NMR microscopy. *Magn Reson Med*, 42:277–282, 1999.
- [9] R. Neubert *et al.* Down-regulation of adhesion receptors on cells of primate embryos as a probable mechanism of the teratogenic action of thalidomide. *Life Sci*, 58:295–316, 1996.
- [10] T. D. Stephens, C. J. Bunde, and B. J. Fillmore. Mechanism of action in thalidomide teratogenesis. *Biochem Pharmacol*, 59:1489–1499, 2000.
- [11] U. Pilatus *et al.* Imaging prostate cancer invasion with multi-nuclear magnetic resonance methods: The metabolic boyden chamber. *Neoplasia*, 2, 2000.
- [12] S. Ostermann *et al.* Plasma and cerebrospinal fluid population pharmacokinetics of temozolomide in malignant glioma patients. *Clin Cancer Res*, 10:3728–3736, 2004.
- [13] S. B. Wedam *et al.* Antiangiogenic and antitumor effects of bevacizumab in patients with inflammatory and locally advanced breast cancer. *J Clin Oncol*, 24:769–777, 2006.

- [14] A. Gossmann *et al.* Dynamic contrast-enhanced magnetic resonance imaging as a surrogate marker of tumor response to anti-angiogenic therapy in a xenograft model of glioblastoma multiforme. *J Magn Reson Imaging*, 15:233–240, 2002.
- [15] John Hunter. *Treatise on the blood, inflammation and gunshot wounds*. Philadelphia, Thomas Bradford, 1794.
- [16] Domenico Ribatti. *History of Research on Tumor Angiogenesis*. Springer, 2009.
- [17] E. Goldman. The growth of malignant disease in man the lower animals with special reference to the vascular system. *Lancet*, ii:1236–1240, 1907.
- [18] W. H. Lewis. The vascular patterns of tumors. *John Hopkins Hosp Bull*, 41:156–162, 1927.
- [19] J. C. Sandison. Observations on growth of blood vessels as seen in transparent chamber introduced in rabbit's ear. *Am J Anat*, 41:475–496, 1928.
- [20] E. R. Clark, W. J. Hirschler, H. T. Kirby-Smith *et al.* General observations on the ingrowth of new blood vessels into standardized chambers in the rabbit's ear, and the subsequent changes in the newly grown vessels over a period of months. *Anat Rec*, 50:129–167, 1931.
- [21] E. R. Clark and E. I. Clark. Observations on the new growth of lymphatic vessels as seen in transparent chambers introduced into the rabbit's ear. *Am J Anat*, 51:49–87, 1932.
- [22] E. R. Clark and E. I. Clark. Microscopic observations on the new growth of capillaries in the living mammals. *Am J Anat*, 64:251–301, 1938.
- [23] A. G. Ide, N. H. Baker and S. L. Warren. Vascularization of the Brown-Pearce rabbit epithelioma transplant as seen in the transparent ear chambers. *Am J Roentg*, 32:891–899, 1939.
- [24] H. S. N. Green. Heterologous transplantation of mammalian tumors: I. The transfer of rabbit tumors to alien species. *J Exp Med*, 73:461–474, 1941.
- [25] G. H. Algire and H. W. Chalkley. Vascular reactions of normal and malignant tissue *in vivo*. *J Natl Cancer Inst*, 6:73–85, 1945.
- [26] R. M. Merwin and G. H. Algire. The role of graft and host vessels in vascularization of grafts of normal and neoplastic tissues. *J Natl Cancer Inst*, 17:23–33, 1956.
- [27] M. Greenblatt and P. Shubik. Tumor angiogenesis: Transfilter diffusion studied in the hamster by the transparent chamber technique. *J Natl Cancer Inst*, 41:111–124, 1968.
- [28] M. A. Gimbrone Jr., S. B. Leapman, R. S. Cotran *et al.* Tumor dormancy *in vivo* by prevention of neovascularization. *J Exp Med*, 136:261–276, 1972.

- [29] M. A. Gimbrone Jr., S. B. Leapman, R. S. Cotran *et al.* Tumor angiogenesis: Iris neovascularization at a distance from experimental intraocular tumors. *J Natl Cancer Inst*, 50:219–228, 1973.
- [30] N. Ferrara and W. J. Henzel. Pituitary follicular cells secrete a novel heparin-binding growth factor specific for vascular endothelial cells. *Biochem Biophys Res Commun*, 161:851–858, 1989.
- [31] K. J. Kim, B. Li, J. Winer, M. Armanini, N. Gillett, H. S. Phillips and N. Ferrara. Inhibition of vascular endothelial growth factor-induced angiogenesis suppresses tumour growth *in vivo*. *Nature*, 362 (6423):841–844, 1993.
- [32] J. M. Isner, A. Pieczek, R. Schadmfeld, R. Blair, L. Haley, T. Asahara, K. Rosenfield, S. Razvi, K. Walsh and J. F. Symes. Clinical evidence of angiogenesis after arterial gene transfer of phVEGF₁₂₁ in patient with ischemic limb. *Lancet*, 348:370–374, 1996.
- [33] M. Los, J. M. Roodhart, E. E. Voest. Target practice: Lessons from phase iii trials with bevacizumab and vatalanib in the treatment of advanced colorectal cancer. *The Oncologist*, 12 (4):443–450, 2007.
- [34] P. K. Ghosh, A. Vasanji, G. Murugesan, S. J. Eppell, L.M. Graham and P. L. Fox. Membrane microviscosity regulates endothelial cell motility. *Nature Cell Biology*, 11:894–900, 2002.
- [35] L. D. E. Jensen, A. J. Hansen and J. A. Lundbæk. Regulation of endothelial cell migration by amphiphiles - are changes in cell membrane physical properties involved? *Angiogenesis*, 10:13–22, 2007.
- [36] Geoffrey M. Copper and Robert E. Hausman. *The Cell: A Molecular Approach, third edition*. Washington D.C. ; ASM Press, 2004.
- [37] D. A. Lauffenburger and A. F. Horwitz. Cell migration: A physically integrated molecular process. *Cell*, 84:359–369, 1996.
- [38] M. Holt, D. Soong, J. Monypenny, I. Dobbir, D. Zicha and G. Dunn. *Cell Motility: From Molecules to Organism (Section 7: Using Bioprobes to follow Protein Dynamics in Living Cells)*. Chichester; John Wiley & Sons Ltd, 2004.
- [39] C. Ballestrem, N. Magid, J. Zonis, M. Shtutman and A. Berhadsky. *Cell Motility: From Molecules to Organism (Section 18: Cell Crawling, Cell Behaviour and Biomechanics during Convergence and Extension)*. Chichester; John Wiley & Sons Ltd, 2004.
- [40] C. Ballestrem, N. Magid, J. Zonis, M. Shtutman and A. Berhadsky. *Cell Motility: From Molecules to Organism (Section 5: Interplay between the Actin Cytoskeleton, Focal Adhesions and Microtubules)*. Chichester; John Wiley & Sons Ltd, 2004.
- [41] A. L. Bishop and A. Hall. Rho GTPases and their effector proteins. *Biochem. J.*, 348 (2):241–255, 2000.

- [42] S. Etienne-Manneville and A. Hall. Rho GTPases in cell biology. *Nature*, 420:629–635, 2002.
- [43] A. J. Ridley. Rho GTPases and cell migration. *J. Cell Sci.*, 114:2713–2722, 2001.
- [44] Thomas D. Pollard. *Cell Motility: From Molecules to Organism (Section 1: Molecular Mechanism Regulating Actin Filament Dynamics at the Leading Edge of Motile Cells)*. Chichester; John Wiley & Sons Ltd, 2004.
- [45] G. Gerisch. Chemotaxis in *Dictyostelium*. *Annu. Rev. Physiol.*, 44:535–552, 1982.
- [46] H. R. Bourne and O. Weiner. A chemical compass. *Nature*, 419:21, 2002.
- [47] L. A. Cary, D. C. Han and J. L. Guan. Integrin-mediated signal transduction pathways. *Histol. Histopathol*, 14:1001–1009, 1999.
- [48] S. P. Holly, M. K. Larson and L. V. Parise. Multiple roles of integrins in cell motility. *Exp. Cell Res.*, 261:69–74, 2000.
- [49] J. A. Lundbæk. Regulation of membrane protein function by lipid bilayer elasticity - a single molecule technology to measure the bilayer properties experienced by an embedded protein. *Journal of Physics - Condensed Matter*, 18:S1305–S1344, 2006.
- [50] J. A. Lundbæk. Lipid bilayer-mediated regulation of ion channel function by amphiphilic drugs. *J Gen Physiol*, 131:421–429, 2008.
- [51] M. J. Bruno, R. E. Koeppe and O. Andersen. Polyunsaturated fatty acids alter lipid bilayer elasticity. *Biophys J*, 90:1769, 2006.
- [52] P. D. Leeson and B. Springthorpe. The influence of drug-like concepts on decision-making in medical chemistry. *Nat Rev Drug Discov*, 6:881–890, 2007.
- [53] O. S. Andersen and R. E. Koeppe. Bilayer thickness and membrane protein function: An energetic perspective. *Annu Rev Biophys Biomol Struct*, 36:107–130, 2007.
- [54] R. van Horsen, N. Galjart, J. A. P. Rens, A. M. M. Eggermont and T. L. M. ten Hagen. Differential effects of matrix and growth factors on endothelial and fibroblast motility: Application of a modified cell migration assay. *J Cell Biochem*, 99 (6):1536–1552, 2006.
- [55] P. L. Yeagle, A. D. Albert, K. Boesze-Battaglia, J. Young and J. Frye. Cholesterol dynamics in membranes. *Biophys J*, 10:413–424, 1990.
- [56] J. V. Bonventre. Phospholipase A₂ and signal transduction. *J Am Soc Nephrol*, 3:128–150, 1992.
- [57] John W. Baynes and Marek H. Dominiczak. *Medical Biochemistry 2nd. Edition*. Elsevier Mosby, 2005.
- [58] M. A. Crawford and A. J. Sinclair. *Lipids, malnutrition and the developing brain (Nutritional influences in the evolution of the mammalian brain)*. Amsterdam, Elsevier, 1972.

- [59] T. Fukaya *et al.* Arachidonic acid preserves hippocampal neuron membrane fluidity in senescent rats. *Neurobiol Aging*, 28:1179–1186, 2007.
- [60] C. M. Wilborn, C. Roberts, M. Kerksick, L. Iosia and R. Kreider. Changes in whole blood and clinical safety markers over 50 days of concomitant arachidonic acid supplementation and resistance training. *Proceedings of the international society of sports nutrition (ISSN)*, 1, 2006.
- [61] G. J. Nelson, P. C. Schmidt, G. Bartolini, D. S. Kelley, S. D. Phinnet, D. Kyle, S. Silbermann and E. J. Schaefer. The effect of dietary arachidonic acid on plasma lipoprotein distributions, apoproteins, blood lipid levels, and tissue fatty acid composition in humans. *Lipids*, 32 (4):427–433, 1997.
- [62] D. S. Kelley, P. C. Taylor, G. J. Nelson, and B. E. Mackey. Arachidonic acid supplementation enhances synthesis of eicosanoids without suppressing immune functions in young healthy men. *Lipids*, 33 (2):125–130, 1998.
- [63] G. J. Nelson, P. C. Schmidt, G. Bartolini, D. S. Kelley and D. Kyle. The effect of dietary arachidonic acid on platelet fusion, platelet fatty acid composition, and blood coagulation in humans. *Lipids*, 32 (4):421–425, 1997.
- [64] B. I. Shraiman. Mechanical feedback as a possible regulator of tissue growth. *PNAS*, 102:3318–3323, 2005.
- [65] B. J. Dubin-Thaler, J. M. Hofman *et al.* Quantification of cell edge velocities and traction forces reveals distinct motility modules during cell spreading. *Plos One*, 2 (11):e3735, 2002.
- [66] M. Poujade, E. Graslnad-Mongrain, A. Hertzog, J. Jouanneau, P. Chavrier, B. Ladoux, A. Bugu Collective migration of an epithelial monolayer in response to a model wound. *PNAS*, 104:15988–15993, 2007.
- [67] H.-G. Döbereiner, B. J. Dubin-Thaler, G. Giannone, H. S. Xenias and M. P. Sheetz. Dynamic phase transitions in cell spreading. *Phys Rev Lett*, 93 (10):(108105)1–4, 2004.
- [68] J. L. McGrath. Cell spreading: The power to simplify. *Current Biology*, 17 (10):R357–R358, 2007.
- [69] L. S. Price, J. Leng, M. A. Schwartz and G. M. Bokoch. Activation of Rac and Cdc42 by integrins mediates cell spreading. *Mol Biol Cell*, 9:1863–1871, 1998.
- [70] C. L. de Hoog, L. J. Foster and M. Mann. RNA and RNA binding proteins participate in early stages of cell spreading through spreading initiation centers. *Cell*, 117:649–662, 2004.
- [71] K. Adamsky, J. Schilling, J. Garwood, A. Faissner and E. Peles. Glial tumor cell adhesion is mediated by binding of the FNIII domain of receptor protein tyrosine phosphatase beta (RPTPbeta) to tenascin C. *Oncogene*, 20:609–618, 2001.

- [72] M. Tamura, J. Gu, K. Matsumoto, S. Aota, *et al.* Inhibition of cell migration, spreading and focal adhesion by tumor suppressor PTEN. *Science*, 280:1614–1617, 1998.
- [73] G. von Wichert, G. Jiang, A. Kostic, *et al.* RPTP- α acts as a transducer of mechanical force on α/β 3-integrin-cytoskeleton linkages. *J Cell Biol*, 161:143–153, 2003.
- [74] Z. L. Bliokh and V. V. Smolianinov. [kinetics of fibroblast spreading]. *Biofizika*, 22:281–288, 1977.
- [75] J. Bereiter-Hahn, M. Luck, T. Miebach, H. K. Stelzer and M. Voth. Spreading of trypsinized cells: Cytoskeletal dynamics and energy requirements. *J Cell Sci*, 96:171–188, 1990.
- [76] D. Cuvelier *et al.* Universal dynamics of cell spreading. *Curr Biol*, 17:694–699, 2007.
- [77] F. Charmaraux, S. Fache, F. Bruckert and B. Fourcade. Kinetics of cell spreading. *Phys Rev Lett*, 94:158102(1–4), 2005.
- [78] C. A. Reinhart-King, M. Dembo and D. A. Hammer. The dynamics and mechanics of endothelial cell spreading. *Biophys J*, 89:676–689, 2005.
- [79] H.-G. Döbereiner, B. J. Dubin-Thaler, J. M. Hofman, T. N. Sims G. Giannone, H. S. Xenias, M. L. Dustin, C. H. Wiggins and M. P. Sheetz. Lateral membrane waves constitute a universal dynamic pattern of motile cells. *Phys Rev Lett*, 97(3):(038102)1–4, 2006.
- [80] B. J. Dubin-Thaler, G. Giannone, H.-G. Döbereiner and M. Sheetz. Nanometer analysis of cell spreading on matrix-coated surfaces reveals two distinct states and STEPs. *Biophysical J*, 286:1794–1806, 2004.
- [81] G. Giannone, B. J. Dubin-Thaler, H.-G. Döbereiner and M. Sheetz. Periodic lamellipodial contractions correlate with rearward actin waves. *Cell*, 116:431–443, 2004.
- [82] A. Bhattacharyay. A simple model for dynamic phase transition in cell spreading. *J Phys A: Math Theor*, 41:(055101–)1–7, 2008.
- [83] David Boal. *Mechanics of the cell*. Cambridge, Cambridge University Press, 2002.
- [84] C. R. Keese, J. Wegener, S. R. Walker and I Giaever. Electrical wound-healing assay for cells *in vitro*. *PNAS*, 101:1554–1559, 2004.
- [85] P. Rosen and D. S. Misfeldt. Cell density determines epithelial migration in culture. *PNAS*, 77:4760–4763, 1980.
- [86] R. Farooqui and G. Fenteany. Multiple rows of cells behind an epithelial wound edge extend cryptic lamellipodia to collectively drive cell-sheet movement. *J Cell Sci*, 118:51–63, 2005.
- [87] M. Théry, V. Racine, A. Pépin, M. Piel, Y. Chen, J.-B. Sibarita and M. Bornens. Anisotropy of cell adhesive microenvironment governs cell internal organization and orientation of polarity. *Nat Cell Biol*, 7:947–953, 2005.

- [88] H. Thiekele, Impidjati and G. R. Fuhr. Biopsy on living cells by ultra slow instrument movement. *J Phys Condens Matter*, 18:S627–S637, 2006.
- [89] J. M. Vasiliev. Spreading and locomotion of tissue cells: Factors controlling the distribution of pseudopodia. *Philos Trans R Soc Lond B Biol Sci*, 299:159–167, 1982.
- [90] A. Ponti, M. Machacek, S. L. Gupton, C. M. W-Storer and G. Danuser. Two distinct actin network drive the protrusion of migrating cells. *Science*, 305:1782, 2004.
- [91] A. P. Pathak, S. D. Rand and K. M. Schmainda. The effect of brain tumor angiogenesis on the *in vivo* relationship between the gradient-echo relaxation rate change (ΔR_2^*) and contrast agent (MION) dose. *J Magn Reson Imaging*, 18:397–403, 2003.
- [92] J. E. Maglione *et al.* Transgenic polyoma middle-T mice model premalignant mammary disease. *Cancer Res*, 61:8298–8305, 2001.
- [93] J. Folkman, R. Langer and R. Linhardt. Angiogenesis inhibition and tumor regression caused by heparin or a heparin fragment in the presence of cortisone. *Science*, 221:719–725, 1983.
- [94] J. Folkman. Angiogenesis in cancer, vascular, rheumatoid and other disease. *Nat Med*, 1:27–31, 1995.
- [95] R. A. Swerlick and T. J. Lawley. Role of microvascular endothelial cells in inflammation. *J Invest Dermatol*, 100(1):111S–115S, 1993.
- [96] L. Oddershede, J. K. Dreyer, S. Brown and K. Berg-Sørensen. The motion of a single molecule, the lambda-receptor, in the bacterial outer membrane. *Biophys. J.*, 83:3152–3161, 2002.
- [97] A. Shay-Salit, M. Shushy, E. Wolfovitz, H. Yahav, F. Breviario, E. Dejana and N. Resnick. VEGF receptor 2 and the adherens junction as a mechanical transducer in vascular endothelial cells. *PNAS*, 99:9462–9467, 2002.
- [98] T. Winther, L. Xu, K. Berg-Sørensen, S. Brown and L. B. Oddershede. Effect of energy metabolism on protein motility in bacterial outer membranes. *Biophysical Journal*, 97:1–8, 2009.
- [99] T. Winther and L. B. Oddershede. Effect of antibiotics and antimicrobial peptides on single protein motility. *Current Pharmaceutical Biotechnology*, 10:486–493, 2009.
- [100] T. M. Svitkina, A. B. Verkhovsky, K. M. McQuade and G. G. Borisy. Analysis of the actin-myosin ii system in fish epidermal keratocytes: mechanism of cell body translocation. *J. Cell Biol.*, 139:397–415, 1997.
- [101] L. Blanchoin and T. D. Pollard. Hydrolysis of bound ATP by polymerized actin depends on the bound divalent cation but not by profilin. *Biochemistry*, 41:597–602, 2002.

- [102] G. Borisy and T. M. Svitkina. Actin machinery: Pushing the envelope. *Curr. Opin. Cell Biol.*, 12:104–112, 2000.